UNIVERSITY OF VERONA

DEPARTMENT OF MEDICINE

GRADUATE SCHOOL FOR LIFE AND HEALTH SCIENCES

DOCTORAL PROGRAM IN BIOMOLECULAR MEDICINE

CURRICULUM IN CLINICAL GENOMICS AND PROTEOMICS

Cycle XXIX

Peroxiredoxin 2 Plays a Pivotal Role Against Oxidation in the Early Phase of Pulmonary Artery Hypertension

S.S.D. MED 09

Coordinator: Prof.ssa DE FRANCESCHI LUCIA

Tutor: Prof.ssa DE FRANCESCHI LUCIA

Doctoral Student: Dott.ssa FEDERTI ENRICA

Index

Abstract

Background. Peroxiredoxin 2 (Prx2) is a typical 2-cysteine (Cys) peroxiredoxin ubiquitously expressed. Prx2 is able to efficiently scavenge H_2O_2 and other hydro-peroxides to maintain intracellular redox balance. Prx2 has been largely studied in red cells, where it acts as antioxidant system and chaperone-like molecule. Although growing evidences indicate the important role of Prx2 in different cell models, much still remains to be investigated in complex disease scenario such as chronic lung disease or stress erythropoiesis.

Aim. The major aim of my work is to understand the functional role of Peroxiredoxin 2 in a mouse model of pulmonary artery hypertension.

Section 1. I focus on the functional role of peroxiredoxin-2 (Prx2) in lung homeostasis. Here, I studied the events related to the generation of pulmonary artery hypertension (PAH), a life threatening and highly invalidating chronic disorder. Hypoxia was used as trigger factor. I found that Prx2-/- mice displayed chronic lung inflammatory disease associated with (i) abnormal pulmonary vascular dysfunction; and (ii) increased markers of extracellular-matrix remodelling. Rescue experiments with in vivo the administration of fused-recombinant-PEP-Prx2 to hypoxic mice show a reduction in pulmonary inflammatory vasculopathy and down-regulation of autophagy. Thus, we propose Prx2 plays a pivotal role in the early stage of PAH as multimodal anti-oxidant system targeting oxidation, inflammatory vasculopathy and indirectly autophagy.

Section 2. I have studied the effect of iron-overload (IO) diet on Prx2-/- mouse erythropoiesis and its link with iron homeostasis. In Prx2-/- mice, IO displayed a potent cytotoxic effect on erythropoiesis and it was associated with lacking in liver STAT3 activation. This results in low hepcidin expression. Treatment with PEP Prx2 ameliorates IO-induced anemia and restored liver STAT3 activation, with adequate hepcidin expression in relation to IO. The importance of Prx2 on the axis between erythropoiesis and iron metabolism is also supported by the beneficial effects of PEP Prx2 on hepcidin levels a mouse model of β-thalassemia.

Section 3. I have studied a humanized mouse model for sickle cell disease (SCD, Tim Townes mouse model). Based on the revision of the literature, SCD and healthy mice were supplemented with ω-3 fatty acids. Hypoxia/reoxygenation stress was used to mimic SCD acute vaso-occlusive crisis. We found that ω-3 fatty supplementation reduces: (i) sickle cell related oxidative stress, (ii) systemic and local (lung and liver) inflammatory response, (iii) vascular endothelial activation and (iv) vascular dysfunction. Our data generate a rationale for ω-3 fatty supplementation in clinical management of SCD patients.

Abbreviations

PAH: pulmonary arthery hypertension
ALI: acute lung injury
ANP: atrial natriuretic peptide
ARE: anti-oxidant responsive element
ASK1: apoptosis signal-regulating kinase 1
Atg4: autophagy related 4
Atg7: autophagy related 7
BAFF: B cell-activating factor
Bax: BCL-2 like protein 4
Bcl-2: B-cell lymphoma 2
COPD: chronic obstructive pulmonary disease
Cu/Zn-SOD: copper/zinc - superoxide dismutase
DAMPs: damage-associated molecular pattern molecules
EC-SOD: extracellular superoxide dismutase
ET: ejection time
ET-1: endothelin 1
ERK: extracellular signal–regulated kinases
GAPDH: glyceraldehyde 3-phosphate dehydrogenase
Gpx: glutathione peroxidase
Grx: glutaredoxin
HIF: Hypoxia-inducible factor
HO-1: heme oxygenase 1
HSP: heat shock protein
ICAM-1: intercellular adhesion molecule 1
IL-23: interleukin 23
IL-1b: interleukin 1b
IL-6: interleukin 6
IL-10: interleukin 10
IPF: idiopathic pulmonary fibrosis
JNK: c-Jun N-terminal kinase
LC3 I/II: microtubule-associated protein 1A/1B-light chain 3
LPS: lipopolysaccharides
MAPK: mitogen-activated protein kinase
MEFs: mouse embryonic fibroblasts
MCP-1: monocyte chemoattractant protein-1

Mn-SOD: manganese - superoxide dismutase
NAC: N-acetyl-cysteine
NF-kB : nuclear factor kappa-light-chain-enhancer of activated B cells
Nrf2: nuclear factor-erythroid 2
6-OHDA: 6-hydroxydopamine
RBC: red blood cell
ROS: reactive oxygen species
RVSP: right ventricular systolic pressure
PAT: pulmonary acceleration time
PARP1:Poly [ADP-ribose] polymerase 1
PDGFR: platelet-derived growth factor receptors
PEP Prx2: Prx2 fused to cell penetrating carrier PEP1 peptide
Prx2: peroxiredoxin-2
SMCs: smooth muscle cells
SOD: superoxide dismutase
TGF-β: Transforming growth factor beta
TLR: Toll-Like Receptor
TNF-α: tumor necrosis factor alpha
TPA: 12-O-tetradecanoylphorbol-13-acetate
Trdx: Thioredoxin reductase
Ulk 1: Serine/threonine-protein kinase Ulk1
VCAM-1: vascular cell adhesion molecule 1
VEGF: vascular endothelial growth factor
VEGFR: vascular endothelial growth factor receptor

Introduction

Peroxiredoxin-2 (Prx2) plays a pivotal role as anti-oxidant system in cell homeostasis

Peroxiredoxin 2 (Prx2) is a typical two-cysteine peroxiredoxin and is ubiquitously expressed (1). Prx2 is able to reduce and detoxify H_2O_2 and other hydroperoxides based on its redox-active cysteine residue present in the catalytic site (Fig. 1). The second conserved cysteine, known as the resolving cysteine, reacts with the sulfenic acid to form a disulphide bridge, which is rapidly reduced by Thioredoxin (Trdx) (2, 3). Although peroxiredoxins have been involved in cellular defense mechanism against oxidative stress, recent reports suggest a possible role of peroxiredoxin(s) as molecular chaperone in cell proteostasis (4).

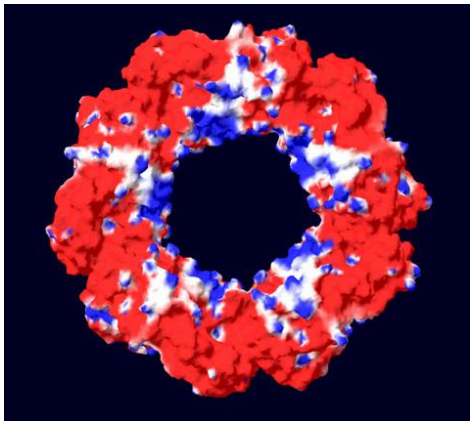

Fig. 1 Molecular surface analysis of the five-dimeric thoroid structure of Peroxiredoxin-2 (Prx2) (modified from Matté A et al. FRBM 2013 (5)). Regions negatively charged are represented in red. In blue positively charged regions are shown. The white areas represent regions without charge.

Prx2 is the third protein for abundance in red blood cells (RBCs), which have been used as cell model for Prx2 characterization. *In vitro* studies have shown that Prx2 is one of the key RBC antioxidant systems, facing low endogenous levels of H_2O_2 (2, 6). Although progresses have been made on the knowledge of Prx2, much

still remains to be investigated on its function in response to stress during red cell senescence and in pathological erythropoiesis.

The generation of a mouse genetically lacking Prx2 ($Prx2^{-/-}$) offers the possibility to functionally characterize Prx2. $Prx2^{-/-}$ mice display a mild hemolytic anemia with ineffective erythropoiesis and splenomegaly. An *in vitro* study has shown that $Prx2^{-/-}$ mouse red cells display a lower sensitivity to exogenous H_2O_2 or organic peroxides compared to RBCs lacking other antioxidant systems such as catalase or glutathione peroxidase 1 (Gpx1) (7). This finding suggests additional role for Prx2 in RBCs beside its anti-oxidant function. Indeed, Prx2 is also important in maintaining RBCs membrane features (5, 8). Recently, we have shown that Prx2 translocates to the RBC membrane in response to exogenous oxidative stresses (e.g. diamide) or hypoxia (9). Band 3 is the membrane-docking site for Prx2, which plays an important role as local cytoprotector of Band 3, the main RBC membrane integral protein (5). It is of note that hemichromes also bind to Band 3 and compete with Prx2 on Band 3 N-terminal cytoplasmic domain (10). Studies on RBCs have shown that membrane oxidation promotes Band 3 aggregation, which is linked to increase Band 3 tyrosine phosphorylation, mediated by Syk kinase activation (11-13). In $Prx2^{-/-}$ mouse erythrocytes, we found increased membrane oxidative damage and reduced RBC survival, which is associated with increased RBCs phagocytosis. Membrane translocation of heat shock proteins HSP70 and 27 is not enough to counteract the severe membrane oxidative damage of RBC lacking Prx2 (Fig. 2). The combination of severe oxidative stress and activation of Syk-mediate signaling results in increased vesciculation of $Prx2^{-/-}$ mouse RBCs to clear damage proteins and oxidized hemoglobin (Fig. 2) (8).

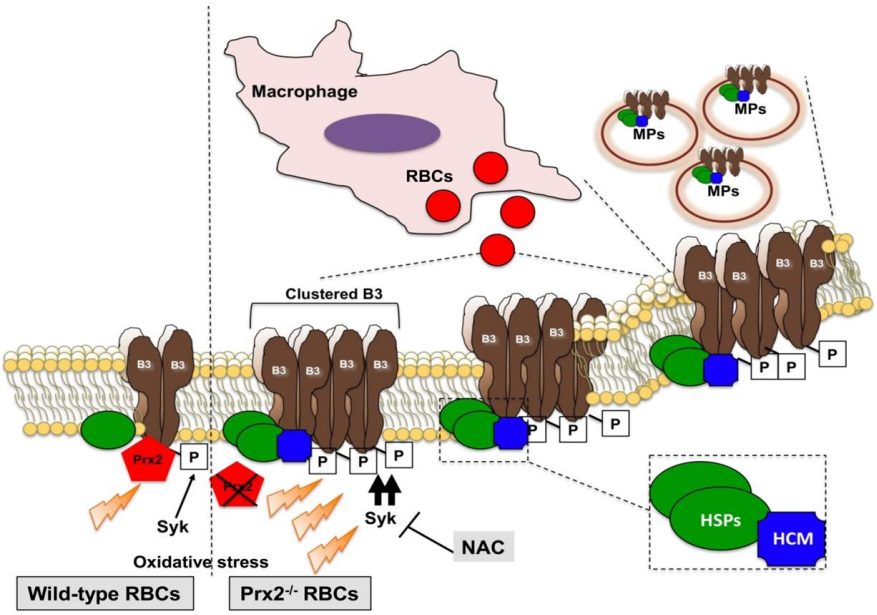

Fig. 2. Schematic diagram of the role of Prx2 in redox response to maintain red cell membrane proteostasis (modified from Matté A. et al. FRBM 2014 (8)). In wild-type mice, the oxidative stress induces translocation to the membrane of HSPs and Prx2, which limits membrane protein damage and the activation of Syk kinase, which phosphorylates Band 3. In $Prx2^{-/-}$ mice, the absence of Prx2 promotes membrane oxidative damage and translocation to the membrane of a high amount of HSPs, which are unable to counteract Band 3 oxidation and clusterization, favored by the high activation of Syk. This results in fast removal of prematurely damaged $Prx2^{-/-}$ RBCs by the macrophage system and increases the release of erythroid MPs that clear damaged proteins and oxidized hemoglobin. Prx2: peroxiredoxin 2; red blood cells (RBC); B3: Band 3; Syk: Src related Tyrosine Kinase; P: phosphorylation of Tyrosine residues on band 3; HMCs: hemichromes; HSPs: heat shock proteins; MPs: microparticles; NAC: N-Acetyl-Cysteine.

Li J. et al. have recently shown that Prx2 is highly expressed during normal human and mouse erythropoiesis, suggesting an important role of Prx2 during erythroid maturation (14). Indeed, mice genetically lacking Prx2 show ineffective erythropoiesis associated with extramedullary erythropoiesis similar to that observed in β-thalassemic mice (15). Increased ROS levels and apoptosis characterize $Prx2^{-/-}$ mouse erythropoiesis. This is associated with the activation of Nrf2, a redox-sensitive transcriptional factor, resulting in increased expression of ARE-related genes for anti-oxidant systems (15). To explore the role of Prx2 during stress erythropoiesis, we have backcrossed β-thalassemic mice ($Hbb^{th3/+}$) with $Prx2^{-/-}$ mice. We have observed that the absence of Prx2 worsens β-thalassemic ineffective erythropoiesis with increased ROS level and cell apoptosis compared to β-thalassemic mice. In $Prx2^{-/-}$ $Hbb^{th3/+}$, Nrf2 is activated as back-up mechanism against severe oxidation related to

the absence of Prx2. The functional interplay between Prx2 and Nrf2 is further supported by rescue experiments, using the fused recombinant protein PEP1-Prx2. $Hbb^{th3/+}$ and $Prx2^{-/-}Hbb^{th3/+}$ mice treated with PEP1-Prx2 show an amelioration of both hematologic phenotype and ineffective erythropoiesis. In addition, PEP1-Prx2 treated $Hbb^{th3/+}$ mice also display a significant reduction in liver iron-overload, supporting the key role of Prx2 in limiting β-thalassemic related organ damage (15). Collectively, these data highlight a new adaptive mechanism against oxidative stress involving Nrf2-Prx2 interplay in stress erythropoiesis. Our data also suggest the modulation of endogenous antioxidant systems as a new possible therapeutic option in pathologic erythropoiesis.

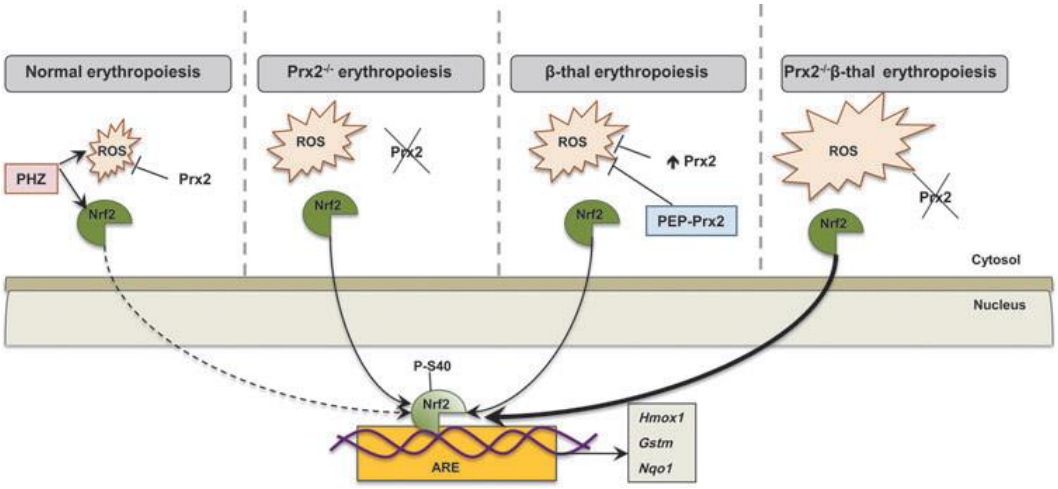

Fig. 3. Schematic diagram on the interplay between peroxiredoxin-2 (Prx2) and Nrf2 cooperating to limit oxidative damage in β-thalassemic erythropoiesis (modified from Matté A. et al. ARS 2015 (15))**.** In WT mice, the physiological generation of ROS during erythropoiesis is controlled by antioxidant systems such as Prx2 and Nrf2 is inactive. The acute oxidative stress induced by PHZ activates Nrf2, which upregulates ARE-genes of antioxidant systems (e.g. Hmox1, Gstm, or Nqo1). The absence of Prx2 promotes ineffective erythropoiesis and increases ROS levels with associated activation of Nrf2 as a backup mechanism to control oxidative stress. In β-thalassemic erythroid precursors, despite the upregulation of Prx2, oxidative stress promotes the activation of Nrf2. PEP1-Prx2 treatment ameliorates ineffective erythropoiesis and reduced ROS levels. In $Prx2^{-/-}Hbb^{th3/+}$ mice, the absence of Prx2 worsens β-thalassemic hematological phenotype and ineffective erythropoiesis with a further increase in ROS levels and further activation of Nrf2. PHZ: phenylhydrazine; ROS: reactive oxygen species; ARE: antioxidant responsive element; Hmox1: heme oxygenase 1; Gstm: Glutathione S-transferase Mu 1; Nqo1: NAD(P)H-quinone oxidoreductase 1.

We carried out a revision of the literature and we found that the contribution of Prx2 to cell homeostasis is not to be limited to erythroid cells. In fact, a study on $Prx2^{-/-}$ mice has shown an higher sensitivity of these animals to LPS-induced

endotoxic shock, possibly related to perturbation of innate inflammatory response (16). Platelets seem also to be affected by the absence of Prx2, which has been proposed to act as protective antioxidant enzyme against collagen-stimulated platelet activation and platelet-dependent thrombosis (17).

Peroxiredoxin-2 (Prx2) is protective against oxidative related organ damage

Since Prx2 is ubiquitously expressed, studies have been carried out to characterize Prx2 in different disease models, characterized by oxidative stress and inflammation, such as cardiovascular diseases, brain ischemia or acute lung injury (Table 1).

Prx2 and cardiovascular system (Table 1). Apo-$E^{-/-}$ mice, a known model for atherosclerosis, show accelerated arterial plaque formation in absence of Prx2 associated with an early development of atherosclerosis compared to wild-type mice (18). This has been related to enhanced activation of redox-depending signaling systems, involving p38 mitogen-activated protein kinase, that participates to endothelial vascular activation (e.g.: increased expression of Vascular cell adhesion molecule 1 (vCAM-1), Intercellular adhesion molecule 1 (ICAM-1) and Monocyte chemoattractant protein-1 (MCP-1) (18). The overexpression of Prx2 protects cardiomyocyte from oxidative stress (19, 20).

Prx2 and brain (Table 1). Ischemia followed by re-oxygenation is a strong pro-oxidant stimulus. In mouse model for post-ischemic brain injury, peroxiredoxins (Prx2 and 5) have been proposed to act as anti-oxidant system but also as DAMPs (damage-associated molecular pattern molecules), inducing IL-23 expression via TLR2 and TLR4. This modulates macrophages infiltration, regulating the local inflammatory response (21). Overexpression of Prx2 has been shown again to be protective against ischemic/reperfusion damage. The cytoprotective role of Prx2 has been also proposed to play a role in the response to either ischemic or age-linked neuronal cell damages in different brain areas (22-24).

Prx2 and lung (Table 1). Studies in $Prx2^{-/-}$ mice have highlighted the protective role of Prx2 against ovalbumin-induced mouse asthma, through the reduction of ROS (25). There are some evidences that Prx2 co-localizes with PDGFR and with markers of proliferating cells in the epithelium and lung parenchyma of patients with idiopathic pulmonary fibrosis (IPF) (26). In *in vitro*-cell based assay, epithelial cells overexpressing Prx2 are more resistant against formaldehyde-induced cell apoptosis (27).

Prx2 and skin (Table1). The absence of Prx2 has been shown to promote an accelerated cell aging in $Prx2^{-/-}$ mouse embryonic fibroblasts (MEFs). This involves (i) increased intracellular ROS production; (ii) cell cycle arrest in G2/M phase; and (iii) activation of p38 and ERK signaling pathway. *In vivo*, mice lacking Prx2 show accelerated skin aging and decreased dermis collagen mediated by the activation of ERK-JNK axis (28).

Table 1. Role of Peroxiredoxin-2 in different cell systems and disease models		
	Key results	**Refs**
In vitro		
Vascular cells	• In vascular endothelial cells (VECs), Prx2 acts as antioxidant regulator of VEGF-VEGFR2 signalling pathway. Prx2 protects VEGFR2 by blocking H_2O_2-dependent oxidation. • Cardiomyocytes overexpressing Prx2 are more resistant to H_2O_2-induced cell death and apoptosis. This has been related to increase expression of Bcl-2, and decrease expression of Bax and of active caspases 3, 9 and 12.	(29) (19)
Immune-related cells	• $CD8^+$ T cells genetically lacking Prx2 display increase ROS levels and decrease survival. • In BMDMs (bone marrow-derived macrophages), the anti-oxidant activity of Prx2 prevents the LPS-induced inflammatory gene expression and the activation of NF-kB, probably through the modulation of NADPH oxidase function. • Under inflammation, Prx2 is released from macrophages and it may act as cellular damage signal. Human recombinant Prx2 is able to induce macrophages release of TNF-α in absence of other stimuli.	(30) (16) (31)
Neuronal cells	• In neuronal differentiated MN9D DA cells, Prx2 protects against 6-OHDA neurotoxicity inhibiting ASK1 and JNK/p38 pro-death signalling pathway. • In neuronal cells, S-nitrosylation of endogenous Prx2 reduces its anti-oxidant power against oxidative stress, promoting neuronal cell death. • In cortical neuronal cells, overexpression of Prx2 is protective against oxidation (e.g.: cumene hydroperoxide) and in vitro ischemia (oxygen-glucose deprivation). • During neurogenesis, Prx2 protects ESC (embryonic stem cells) stemness against ROS injury.	(32) (33) (34) (35)
HeLa cells	• In hypoxic human HeLa cells, Prx2 and Prx4 interact with HIF-1α and HIF-2α. Prx2 is a direct HIF target gene and its expression is induced by prolonged hypoxia.	(36)
Lung epithelial cell line	• In lung epithelial cells treated with formaldehyde, the overexpression of Prx2 protects against cell apoptosis, through increased Bax activation and decreased Bcl-2, Caspase 3 and Caspase 9 function.	(37)
In vivo		
RBCs and erythropoiesis	• Prx2 is the third most abundant protein in RBCs and shows both cytosolic and membrane localization. It plays major roles against oxidative stress, preventing RBCs senescence. It scavenges low levels of hydrogen peroxide, maintains hemoglobin stability and prevents membrane oxidative damage. It is important in different red cell pathologies such as spherocytosis, sickle cell disease, β-thalassemia and chorea-acanthocytosis. • $Prx2^{-/-}$ mice display a mild hemolytic anaemia. • The absence of Prx2 promotes ineffective erythropoiesis similar to β-thalassemia. Prx2 plays an important role in preventing ROS mediated DNA damage inducing apoptosis and cell cycle arrest by p53 signalling pathway activation. $Prx2^{-/-}$ mice show activation of Nrf2 in orthochromatic erythroblasts, acting as back-up mechanism against severe oxidative stress.	(2) (3) (9) (38) (15) (8) (39) (40) (7) (41) (42) (43) (44)

Brain	• In hippocampus, Prx2 plays a role in age-associated physiological functions. It is required to preserve synaptic plasticity. • $Prx2^{-/-}$ mice show cognitive defects, linking Prx2 to age-dependent mitochondrial oxidative damage. Dietary vitamin E alleviated $Prx2^{-/-}$ neurologic phenotype. • Prx2 protects mice against ischemic/reperfusion brain injury through scavenging ROS, attenuating DNA damage and inhibiting different pro-death cascades (ASK1/JNK-, PARP1- and p53- dependent death pathways). • Mice overexpressing Prx2 are protected against 6-OHDA-induced degeneration (Parkinson's disease model).	(24) (22) (23) (32)
Skin	• Skin aging is accelerated in the absence of Prx2 through ERK and JNK activation. • In TPA-induced skin inflammation, anti-inflammatory effects of PEP-1-Prx2 local application have been reported. This involves modulation of NF-κB and MAPK function.	(28) (45)
Lung	• In ovalbumin-induced mouse asthma model, the absence of Prx2 increases the severity of asthma induction with a higher increase in bronchi thickness, mucus secretion and airway inflammation. Prx2 benefits asthma induction by reducing ROS levels, increasing BAFF expression and inhibiting TLR4 production. • In human idiopathic pulmonary fibrosis, Prx2 is weakly expressed in lung fibroblastic foci (FF) of IPF patients.	(25) (26)
Cardio-Vascular system	• in Apolipoprotein E–deficient ($ApoE^{-/-}$) mice, the absence of Prx2 accelerates plaque formation and is associated with the activation of redox-dependent signalling molecules (p65, c-Jun, JNKs and p38 MAPK). In endothelial cells, Prx2 deficiency results in increased expression of v-CAM-1 and I-CAM-1, accumulation of immune cells ($CD45^{+}$ cells, macrophages, and $CD4^{+}$ cells) and increase TNF-α production in atherosclerotic lesions. • Prx2 exerts a preventive effect against platelet-mediated plug formation in a mouse model of $FeCl_3$-induced carotid artery injury. $Prx2^{-/-}$ mice show a pro-thrombotic phenotype after $FeCl_3$-induced vascular injury.	(18) (17) (46)
Kidney	• In rat models of glomerulosclerosis, studies show that Prx2 is expressed in podocytes and contributes to modulation of angiotensin mediated cell apoptosis via Akt signalling. • Studies in human subjects with renal cell carcinoma correlate the expression of Prx2 with the disease progression.	(47) (48)
Thymus	• The absence of Prx2 is associated with thymus expansion, resulting in augmented number of thymocytes. This has been related to inefficient apoptosis, reduced number of $CD4^{+}/CD8^{+}$ T cells and increased level of ROS.	(49)
Immune response	• Prx2 modulates immune cell-response by the scavenging ROS. Cell number and responsiveness of $CD3^{+}$ T lymphocytes and dendritic cells are higher in the absence of Prx2.	(50)

VEGF: vascular endothelial growth factor; VEGFR: vascular endothelial growth factor receptor; Bcl-2: B-cell lymphoma 2; Bax: BCL-2 like protein 4; ROS: reactive oxygen species; LPS: lipopolysaccharide; NF-kB : nuclear factor kappa-light-chain-enhancer of activated B cells; TNF-α: tumor necrosis factor alpha; 6-OHDA: 6-hydroxydopamine; ASK1: apoptosis signal-regulating kinase 1; JNK: c-Jun N-terminal kinases; HIF: Hypoxia-inducible factor; RBCs: red blood cells; Prx2: peroxiredoxin-2; PARP1:Poly [ADP-ribose] polymerase 1; ERK: extracellular signal–regulated kinases; TPA: 12-O-tetradecanoylphorbol-13-acetate; MAPK: mitogen-activated protein kinase; BAFF: B cell-activating factor; TLR: Toll-Like Receptor; IPF: idiopathic pulmonary fibrosis; v-CAM-1: Vascular cell adhesion molecule 1; I-CAM-1: Intercellular adhesion molecule 1.

Oxidative stress and lung injury

Studies on both acute lung injury (e.g. ALI) and chronic lung disorders such as chronic obstructive pulmonary disease (COPD) or pulmonary hypertension (PAH) have identified oxidative stress as key hub in lung damage and in disease progression. Lung is exposed more than other organs to high oxidant-mediated stress due to the presence of high oxygen extraction and direct contact with extra-body environment (e.g. pollution). Oxidizing agents can be produced endogenously by metabolic reactions during inflammatory response (such as activation of phagocytes, mitochondrial electron transport, NADPH oxidase system) or exogenously by cigarette smoking, pollution, radiation or drugs. Therefore, lung requires efficient antioxidant systems to limit local oxidation.

In lung, different antioxidant systems are physiological expressed and required in lung homeostasis (Table 2). Among them, superoxide dismutase (SOD) has been widely investigated (Table 2). SOD efficiently scavenges $O2^{\bullet -}$ into H_2O_2. It is present in three forms: extracellular SOD (EC-SOD), copper/zinc-SOD (Cu/Zn-SOD) and manganese-SOD (Mn-SOD). Lack of SOD promotes oxidant-induced lung damage. The overexpression of SOD has been shown to be protective against (i) hypoxia-induced PAH; (ii) endotoxin-induced ALI; (iii) allergen induced lung injury. SOD seems to limit oxidation and inflammation, improving vascular dysfunction. Furthermore, SOD modulates extracellular matrix remodeling in models of chronic hypoxia-induced PAH and idiopathic pulmonary fibrosis (Table 2).

Other anti-oxidant systems such as catalase, glutathione peroxidase (Gpx), Peroxiredoxins (Prx1, 2, 3 and 6), thioredoxin and glutaredoxin (Grx) have been investigated in both acute or chronic lung injury (Table 2). These studies highlighted that (i) the absence of catalase promotes inflammation and fibrosis; (ii) Gpx and Grx levels are increased in various lung diseases (e.g. asthma, pulmonary sarcoidosis, allergic alveolitis, lung fibrosis); (iii) heme-oxygenase-1 (HO-1) degrades free heme and prevents heme-mediated severe local oxidation (Table 2). Finally, non-enzymatic molecules, such as vitamin C and E, glutathione and retinol have been reported to act as pulmonary antioxidants, scavenging oxygen free radicals (Table 2).

Table 2. Anti-oxidant systems involved in acute and/or chronic lung damage		
Anti-oxidant system	**Results**	**Refs**
Extracellular-SOD (EC-SOD)	• Scavenges superoxide anion ($O2^{\bullet-}$) • Prevents oxidant-induced extra-cellular matrix degradation, abolishing the release of pro-fibrotic cytokine and the activation of TGF-β. In idiopathic pulmonary fibrosis (IPF), EC-SOD is low in fibrotic areas. • In neonatal mouse model of bleomycin-induced bronchopulmonary dysplasia (BPD), the absence of EC-SOD worsens PAH, disrupting VEGF/NO signalling pathway. • Selective loss of vascular EC-SOD promotes hypoxia-induced PAH. • Mice overexpressing EC-SOD exposed to hyperoxia show reduced neo-angiogenesis by scavenging induced free radicals. • Overexpression of EC-SOD prevents the development of hypoxia induced PAH. • EC-SOD overexpression decreases the severity of endotoxin-induced acute lung injury (ALI). • EC-SOD overexpression attenuates chronic hypoxia-induced PAH, as supported by the reduction in vascular remodelling, small pulmonary vessels muscularization and collagen deposition.	(51) (52) (53) (54) (55) (56) (57) (58) (59)
copper/zinc-SOD (Cu/Zn-SOD)	• Scavenges superoxide anion ($O_2^{\bullet-}$) • In murine models of allergen-induced lung injury and asthma, Cu/Zn-SOD reduces lung injury. • Cu/Zn-SOD serum levels are increased in patients with idiopathic pulmonary fibrosis (IPF).	(58) (59) (60) (61) (57)
Manganese-SOD (Mn-SOD)	• Scavenges superoxide anion ($O_2^{\bullet-}$). • In extrinsic allergic alveolitis (EAA), pulmonary sarcoidosis and desquamative interstitial pneumonia (DIP), Mn-SOD reduces the local pulmonary damage. • Increased levels of Mn-SOD have been reported in alveolar epithelium from healthy smokers. • In rat lung, hyperoxia activates Mn-SOD and is associated with accumulation of inactive Mn-SOD.	(58) (59) (57) (62) (63) (64) (65)
Catalase	• Scavenge hydrogen peroxide. • The expression of catalase is increased in; (i) alveolar regions of usual interstitial pneumonia (UIP); (ii) granulomas of sarcoidosis; (iii) extrinsic allergic alveolitis. These suggest a protective role of catalase against oxidation and inflammation leading to disease progression. • In human pulmonary fibrosis, reduced expression and activity of catalase have been reported. Catalase seems to play a protective role in mice exposed to bleomycin-induced inflammation.	(58) (59) (63) (66)

Glutathione peroxidase (Gpx) and Glutathione	• Gpx protects alveolar epithelial cells against oxidative stress (e.g.: hyperoxia-induced lung damage). • Glutathione and glutathione peroxidase levels are increased in various granulomatous lung diseases (e.g.: chronic beryllium disease). • In sputum and plasma of IPF human subjects, glutathione content is reduced compared to healthy subjects.	(58) (59) (58) (67) (68)
Peroxiredoxin	• Increased expression of different peroxiredoxins (Prx1, 3 and 6) has been reported in lung cancer, alveolitis and hypoxia induce lung injury. • Peroxiredoxin-2 is expressed by alveolar type II cells and is associated with activation of PDGF signaling pathway and cell proliferation.	(58) (59) (69) (26)
Thioredoxin	• In patients with asthma attacks, thioredoxin serum level is increased compared to patients in remission. • Mice overexpressing thioredoxin and mice treated with human recombinant thioredoxin show decreased bleomycin-induced cellular infiltrates and fibrosis.	(58) (59) (70) (71) (72) (73)
Glutaredoxin	• In allergic alveolitis, lung fibrosis and pulmonary sarcoidosis, glutaredoxin expression is reduced.	(58) (59) (74) (75)
Heme Oxygenase-1 (HO-1)	• Converts heme to carbon monoxide and billiverdin. • It is upregulated in smokers and in patients with cystic fibrosis, asthma, acute lung injury, and it is downregulated in severe chronic obstructive pulmonary disease. • Protective effects of HO-1 have also been suggested in patients with asbestosis or silicosis. • HO-1 is decreased in macrophages of IPF patients.	(58) (59) (76) (77) (78)
Non-enzymatic antioxidants	• In lung, vitamin C, vitamin D, vitamin E, beta carotene and retinol act as scavenger for both protein and lipid peroxidation. The revised studies underline that supplementation with vitamins or beta carotene is associated with improvement acute and chronic lung diseases (e.g.: COPD) through still partially known mechanism(s).	(59) (79) (80) (81) (82) (83) (84) (85)

TGF-β: Transforming growth factor beta; PAH: pulmonary artery hypertension; VEGF: vascular endothelial growth factor; PDGF: platelet-derived growth factor; IPF: idiopathic pulmonary fibrosis; COPD: chronic obstructive pulmonary disease.

Exogenous anti-oxidant molecules (e.g.: quercetin, rutin) have been evaluated in both acute and chronic lung diseases (86-88). Studies on rat models of several lung injuries have shown that N-Acetylcysteine (NAC) have beneficial effects on (i) monocrotaline-induced pulmonary hypertension (89); (ii) endotoxin induced-ALI (90); (iii) silica-induced lung fibrosis (91); (iv) ischemia-reperfusion lung injury (92).

Chronic oxidative stress has been involved in the pathogenesis of two main chronic lung diseases such as chronic obstructive pulmonary disease (COPD) and pulmonary artery hypertension (PAH) (93, 94).

PAH is a chronic invalidating disorder, characterized by elevation of pulmonary arterial pressure combined with abnormality in vascular and extra matrix lung remodeling (95-97). Although in the last decade progresses have been made in the knowledge of PAH, much still remains to be investigated in the interplay between triggering factors and vascular dysfunctions in PAH. Three key factors have been identified to be important for development of PAH: (i) chronic inflammation, (ii) abnormal shear stress and (iii) hypoxia (98).

The combination of chronic inflammation and chronic hypoxia promotes structural changes in the pulmonary vascular bed such as pulmonary artery muscolarization, increased medial thickness and deposition of matrix components (e.g. collagen, elastan). The biocomplexity of PAH is further increased by the contribution of chronic inflammation plus abnormal shear stress that promote: (i) vascular endothelial cell damage; (ii) local reduction of vasodilator(s) (e.g. nitric oxide or prostacyclin); (iii) local increased of vasoactive mediators, promoting vascular remodeling (ET-1, PDGF, TGF-β, VEGF); and (iv) increased expression of vascular adhesion molecules (e.g. v-CAM-1, I-CAM-1) (98-102). Thus, these factors synergize and promote a high pro-oxidant environment, which requires efficient local anti-oxidant system to prevent or delay the development of PAH (103).

Previous studies have shown that the disruption of the local oxidant/antioxidant balance is a key step in development of severe chronic pulmonary damage (95). This is also supported by evidences in mouse models lacking

extracellular superoxide dismutase (EC-SOD), which displays hypoxia-induced severe pulmonary hypertension (54) (see also Table 2). Treatment with exogenous anti-oxidants such as NAC or quercetin or rutin has been proposed to limit oxidation that sustains the development of PAH. However, the beneficial effects of these anti-oxidants seem to be strictly dependent on the timing of the starting dose with respect to disease severity and to the possibility to affect the disease natural history.

In this scenario, autophagy is an efficient process used by stressed cells to clear intracellular damaged proteins and organelles. Growing evidences link oxidation to autophagy in different cell model. The slow removal of damaged proteins might drive cell to apoptosis (104, 105). Some of the autophagy related proteins (Atg) are redox-sensitive proteins and might be either directly modulated by ROS (e.g.: Atg4 or Atg7) or transcriptionally regulated by oxidative stress (e.g.: p62) (104, 106-108). The functional connection between ROS and autophagy is also supported by the improvement of autophagy promoted by exogenous anti-oxidants, such as NAC (104, 106).

The connection of autophagy with the development of pulmonary diseases is highlighted by data on mouse models lacking Atg proteins. $Atg7^{-/-}$ or $Atg5^{-/-}$ mice develop spontaneous lung inflammation characterized by increased lung inflammatory infiltrate and extracellular matrix remodeling with collagen deposition (109). In addition, it has been shown that the loss of Atg7 promotes endothelial-to-mesenchymal transition associated with upregulation of the pro-fibrotic TGFβ signaling pathway (110). *In vivo*, this results in increased lung collagen deposition and higher susceptibility to bleomycin-induced pulmonary fibrosis (110). Atg4b-deficient mice also display increased sensitivity to bleomycin-induced lung injury with (i) apoptosis of alveolar and bronchiolar epithelial cells, (ii) inflammation and (iii) extensive lung fibrosis (111). Collectively, these studies indicate that autophagy participates to lung protection against oxidation and inflammation.

Key References

1. S. Immenschuh and E. Baumgart-Vogt. Peroxiredoxins, Oxidative Stress, and Cell Proliferation. Antioxidants & Redox Signaling. May 2005, 7(5-6): 768-777.

2. Low FM, Hampton MB, Winterbourn CC. Peroxiredoxin 2 and peroxide metabolism in the erythrocyte. Antioxid Redox Signal. 2008 Sep; 10(9):1621-30.

3. Lee TH, Kim SU, Yu SL, Kim SH, Park DS, Moon HB, Dho SH, Kwon KS, Kwon HJ, Han YH, Jeong S, Kang SW, Shin HS, Lee KK, Rhee SG, Yu DY. Peroxiredoxin II is essential for sustaining life span of erythrocytes in mice. Blood. 2003 Jun 15;101(12):5033-8.

4. Lee W, Choi KS, Riddell J, Ip C, Ghosh D, Park JH, Park YM. Human peroxiredoxin 1 and 2 are not duplicate proteins: the unique presence of CYS83 in Prx1 underscores the structural and functional differences between Prx1 and Prx2. J Biol Chem. 2007 Jul 27;282(30):22011-22.

5. A. Matte, M. Bertoldi, N. Mohandas, X. An, A. Bugatti, A. M. Brunati, M. Rusnati, E. Tibaldi, A. Siciliano, F. Turrini, S. Perrotta, L. De Franceschi. Membrane association of peroxiredoxin-2 in red cells is mediated by the N-terminal cytoplasmic domain of band3. FRBM 55(2013)27–35.

6. Low FM, Hampton MB, Peskin AV, Winterbourn CC. Peroxiredoxin 2 functions as a noncatalytic scavenger of low-level hydrogen peroxide in the erythrocyte. Blood. 2007 Mar 15;109(6):2611-7.

7. R. M. Johnson, Y.-S. Ho, D.-Y. Yu, F. A. Kuypers, Y. Ravindranath, and G. W. Goyette. The Effect of Disruption of Genes for Peroxiredoxin-2, Glutathione Peroxidase-1 and Catalase on Erythrocyte Oxidative Metabolism. Free Radic Biol Med. 2010 Feb 15; 48(4): 519.

8. Mattè et all. The novel role of peroxiredoxin-2 in red cell membrane protein homeostasis and senescence. Free Radical Biology and Medicine Volume 76, November 2014, Pages 80–88.

9. Biondani A, Turrini F, Carta F, Matté A, Filippini A, Siciliano A, Beuzard Y, De Franceschi L. Heat-shock protein-27, -70 and peroxiredoxin-II show molecular chaperone function in sickle red cells: Evidence from transgenic sickle cell mouse model. Proteomics Clin Appl. 2008 May;2(5):706-19.

10. Lewis IA, Campanella ME, Markley JL, Low PS. Role of band 3 in regulating metabolic flux of red blood cells. Proc Natl Acad Sci U S A. 2009 Nov 3;106(44):18515-20. .

11. A. Pantaleo, E. Ferru, G. Giribaldi, F. Mannu, F. Carta, A. Matte, L. de Franceschi, F. Turrini. Oxidized and poorly glycosylated band 3 is selectively phosphorylated by Syk kinase

to form large membrane clusters in normal and G6PD-deficient red blood cells. Biochem. J., 418 (2009), pp. 359–367.

12. Bordin L1, Fiore C, Bragadin M, Brunati AM, Clari G. Regulation of membrane band 3 Tyr-phosphorylation by proteolysis of p72(Syk) and possible involvement in senescence process. Acta Biochim Biophys Sin (Shanghai). 2009 Oct;41(10):846-51.

13. E. Ferru, A. Pantaleo, F. Carta, F. Mannu, A. Khadjavi, V. Gallo, L. Ronzoni, G. Graziadei, M.D. Cappellini, F. Turrini. Thalassemic erythrocytes release microparticles loaded with hemichromes by redox activation of p72Syk kinase. Haematologica, 99 (2014), pp. 570–578.

14. Jie Li, John Hale, Pooja Bhagia, Fumin Xue, Lixiang Chen, Julie Jaffray, Hongxia Yan, Joseph Lane, Patrick G. Gallagher, Narla Mohandas, Jing Liu and Xiuli An. Isolation and transcriptome analyses of human erythroid progenitors: BFU-E and CFU-E. Blood 2014 :blood-2014-07-588806.

15. Mattè at all. The Interplay Between Peroxiredoxin-2 and Nuclear Factor-Erythroid 2 Is Important in Limiting Oxidative Mediated Dysfunction in β-Thalassemic Erythropoiesis. Antioxid Redox Signal. 2015 Dec 1; 23(16): 1284–1297.

16. Yang CS, Lee DS, Song CH, An SJ, Li S, Kim JM, Kim CS, Yoo DG, Jeon BH, Yang HY, Lee TH, Lee ZW, El-Benna J, Yu DY, Jo EK. Roles of peroxiredoxin II in the regulation of proinflammatory responses to LPS and protection against endotoxin-induced lethal shock. J Exp Med 204: 583-94, 2007.

17. Jang JY, Wang SB, Min JH, Chae YH, Baek JY, Yu DY, Chang TS. Peroxiredoxin II is an antioxidant enzyme that negatively regulates collagen-stimulated platelet function. J Biol Chem. 2015 May 1;290(18):11432-42.

18. Park JG, Yoo JY, Jeong SJ, Choi JH, Lee MR, Lee MN, Hwa Lee J, Kim HC, Jo H, Yu DY, Kang SW, Rhee SG, Lee MH, Oh GT. Peroxiredoxin 2 Deficiency Exacerbates Atherosclerosis in Apolipoprotein E-Deficient Mice. Circ Res. 2011 Sep 16; 109(7):739-49.

19. Zhao W, Fan GC, Zhang ZG, Bandyopadhyay A, Zhou X, Kranias EG. Protection of peroxiredoxin II on oxidative stress-induced cardiomyocyte death and apoptosis. Basic Res Cardiol. 2009 Jul; 104(4):377-89.

20. Cullingford TE, Wait R, Clerk A, Sugden PH. Effects of oxidative stress on the cardiac myocyte proteome: modifications to peroxiredoxins and small heat shock proteins. J Mol Cell Cardiol. 2006 Jan; 40(1):157-72.

21. Shichita T, Hasegawa E, Kimura A, Morita R, Sakaguchi R, Takada I, Sekiya T, Ooboshi H, Kitazono T, Yanagawa T, Ishii T, Takahashi H, Mori S, Nishibori M, Kuroda K, Akira S, Miyake K, Yoshimura A. Peroxiredoxin family proteins are key initiators of post-ischemic inflammation in the brain. Nat Med. 2012 Jun; 18(6):911-7.

22. Rehana K. Leak, Lili Zhang, Yumin Luo, Peiying Li, Haiping Zhao, Xiangrong Liu, Feng Ling, Jianping Jia, Jun Chen and Xunming Ji. Peroxiredoxin 2 battles PARP1- and p53-dependent pro-death pathways following ischemic injury. Stroke. 2013 Apr; 44(4): 1124–1134.

23. Yu Gan, Xunming Ji, Xiaoming Hu, Yumin Luo, Lili Zhang, Peiying Li, Xiangrong Liu, Feng Yan, Peter Vosler, Yanqin Gao, R. Anne Stetler, and Jun Chen. Transgenic Overexpression of Peroxiredoxin-2 Attenuates Ischemic Neuronal Injury Via Suppression of a Redox-Sensitive Pro-Death Signaling Pathway. Antioxid Redox Signal. 2012 Sep 1; 17(5): 719–732.

24. Kim SU, Jin MH, Kim YS, Lee SH, Cho YS, Cho KJ, Lee KS, Kim YI, Kim GW, Kim JM, Lee TH, Lee YH, Shong M, Kim HC, Chang KT, Yu DY, Lee DS. Peroxiredoxin II preserves cognitive function against age-linked hippocampal oxidative damage. Neurobiol Aging. 2011 Jun;32(6):1054-68.

25. Moon EY, Kang JS, Han SH, Yang KH, Pyo S, Lee MY, Lee HK, Yu DY. Differential role of peroxiredoxin II (PrxII) on the expression of toll-like receptor 4 (TLR4) and B-cell activating factor (BAFF). in ovalbumin (OVA)-induced mouse asthma. Int Immunopharmacol. 2008 Jun;8(6):935-44.

26. Vuorinen K, Ohlmeier S, Leppäranta O, Salmenkivi K, Myllärniemi M, Kinnula VL. Peroxiredoxin II expression and its association with oxidative stress and cell proliferation in human idiopathic pulmonary fibrosis. J Histochem Cytochem. 2008 Oct;56(10):951-9.

27. Lim SK1, Kim JC, Moon CJ, Kim GY, Han HJ, Park SH. Formaldehyde induces apoptosis through decreased Prx 2 via p38 MAPK in lung epithelial cells.Toxicology. 2010 May 27;271(3):100-6.

28. Han YH, Kim HS, Kim JM, Kim SK, Yu DY, Moon EY. Inhibitory role of peroxiredoxin II (Prx II) on cellular senescence. FEBS Lett. 2005 Aug 29;579(21):4897-902.

29. Kang DH, Lee DJ, Lee KW, Park YS, Lee JY, Lee SH, Koh YJ, Koh GY, Choi C, Yu DY, Kim J, Kang SW. Peroxiredoxin II is an essential antioxidant enzyme that prevents the oxidative inactivation of VEGF receptor-2 in vascular endothelial cells. Mol Cell. 2011 Nov 18;44(4):545-58.

30. Michalek RD, Crump KE, Weant AE, Hiltbold EM, Juneau DG, Moon EY, Yu DY, Poole LB, Grayson JM. Peroxiredoxin II regulates effector and secondary memory CD8+ T cell responses. J Virol. 2012 Dec;86(24):13629-41.

31. S. Salzano, P. Checconi, E.-M. Hanschmann, C. H. Lillig, L. D. Bowler, P. Chan, D. Vaudry, M. Mengozzi, L. Coppo, S. Sacre, K. R. Atkuri, B. Sahaf, L. A. Herzenberg, L. A. Herzenberg, L. Mullen and P. Ghezzia. Linkage of inflammation and oxidative stress via release of glutathionylated peroxiredoxin-2, which acts as a danger signal. Proc Natl Acad Sci U S A. 2014 Aug 19; 111(33): 12157–12162.

32. X. Hu, Z. Weng, C. T. Chu, L. Zhang, G. Cao, Y. Gao, A. Signore, J. Zhu, T. Hastings, J. T. Greenamyre and J. Chen. Peroxiredoxin-2 protects against 6-hydroxydopamine-induced dopaminergic neurodegeneration via attenuation of the ASK1 signaling cascade. J Neurosci. 2011 Jan 5; 31(1): 247–261.

33. J. Fang, T. Nakamura, D.-H. Cho, Z. Gu, and S. A. Lipton. S-nitrosylation of peroxiredoxin 2 promotes oxidative stress-induced neuronal cell death in Parkinson's disease. Proc Natl Acad Sci U S A. 2007 Nov 20; 104(47): 18742–18747.

34. Boulos S1, Meloni BP, Arthur PG, Bojarski C, Knuckey NW. Peroxiredoxin 2 overexpression protects cortical neuronal cultures from ischemic and oxidative injury but not glutamate excitotoxicity, whereas Cu/Zn superoxide dismutase 1 overexpression protects only against oxidative injury. J Neurosci Res. 2007 Nov 1;85(14):3089-97.

35. Kim SU, Park YH, Kim JM, Sun HN, Song IS, Huang SM, Lee SH, Chae JI, Hong S, Sik Choi S, Choi SC, Lee TH, Kang SW, Rhee SG, Chang KT, Lee SH, Yu DY, Lee DS. Dominant role of peroxiredoxin/JNK axis in stemness regulation during neurogenesis from embryonic stem cells. Stem Cells. 2014 Apr;32(4):998-1011.

36. Luo W, Chen I, Chen Y, Alkam D, Wang Y, Semenza GL. PRDX2 and PRDX4 are negative regulators of hypoxia-inducible factors under conditions of prolonged hypoxia. Oncotarget. 2016 Feb 9;7(6):6379-97.

37. Lim SK1, Kim JC, Moon CJ, Kim GY, Han HJ, Park SH. Formaldehyde induces apoptosis through decreased Prx 2 via p38 MAPK in lung epithelial cells. Toxicology. 2010 May 27;271(3):100-6.

38. A. Matté, M. Bertoldi, N. Mohandas, X. An, A. Bugatti, A. M. Brunati, M. Rusnati, E. Tibaldi, A. Siciliano, F. Turrini, S. Perrotta, L. D. Franceschi. Membrane association of peroxiredoxin-2 in red cells is mediated by the N-terminal cytoplasmic domain of band3. Free Radical Biology and Medicine 55 (2013) 27–35.

39. Han YH, Kim SU, Kwon TH, Lee DS, Ha HL, Park DS, Woo EJ, Lee SH, Kim JM, Chae HB, Lee SY, Kim BY, Yoon do Y, Rhee SG, Fibach E, Yu DY. Peroxiredoxin II is essential for preventing hemolytic anemia from oxidative stress through maintaining hemoglobin stability. Biochem Biophys Res Commun. 2012 Sep 28;426(3):427-32.

40. Nagababu E, Mohanty JG, Friedman JS, Rifkind JM. Role of peroxiredoxin-2 in protecting RBCs from hydrogen peroxide-induced oxidative stress. Free Radic Res. 2013 Mar;47(3):164-71.

41. Yang HY, Kwon J, Choi HI, Park SH, Yang U, Park HR, Ren L, Chung KJ, Kim YU, Park BJ, Jeong SH, Lee TH. In-depth analysis of cysteine oxidation by the RBC proteome: advantage of peroxiredoxin II knockout mice. Proteomics. 2012 Jan;12(1):101-12.

42. Rocha S, Vitorino RM, Lemos-Amado FM, Castro EB, Rocha-Pereira P, Barbot J, Cleto E, Ferreira F, Quintanilha A, Belo L, Santos-Silva A. Presence of cytosolic peroxiredoxin 2 in the erythrocyte membrane of patients with hereditary spherocytosis. Blood Cells Mol Dis. 2008 Jul-Aug;41(1):5-9.

43. A. Matte, P. S. Low, F. Turrini, M. Bertoldi, M. E. Campanella, D. Spano, A. Pantaleo, A. Siciliano, L. D. Franceschi. Peroxiredoxin-2 expression is increased in β-thalassemic mouse red cells but is displaced from the membrane as a marker of oxidative stress. Free Radical Biology & Medicine 49 (2010) 457– 466.

44. Kwon TH, Han YH, Hong SG, Lee DJ, Ha HL, Kang SW, Li W, Yoon DY, Yu DY. Reactive oxygen species mediated DNA damage is essential for abnormal erythropoiesis in peroxiredoxin II(-/-) mice. Biochem Biophys Res Commun. 2012 Jul 20;424(1):189-95.

45. H. J. Jeonga, M. Parka, D. W. Kimb, E. J. Ryua, J. I. Yonga, H. J. Chaa, S. J. Kima, H. J. Yeoa, J.-H. Jeongc, D.-S. Kimc, H. C. Kimd, E. J. Shind, E. Y. Parke, J. H. Parke, H. Y. Kwonf, J. Parka, W. S. Euma, S. Y. Choia. Down-regulation of MAPK/NF-κB signaling underlies anti-inflammatory response induced by transduced PEP-1-Prx2 proteins in LPS-induced Raw 264.7 and TPA-induced mouse ear edema model. Int Immunopharmacol. 2014 Dec;23(2):426-33.

46. W. Li, M. Febbraio, S. P. Reddy, D.-Y. Yu, M. Yamamoto, and R. L. Silverstein. CD36 participates in a signaling pathway that regulates ROS formation in murine VSMCs. J Clin Invest. 2010 Nov 1; 120(11): 3996–4006.

47. Hsu HH, Hoffmann S, Di Marco GS, Endlich N, Peter-Katalinić J, Weide T, Pavenstädt H. Downregulation of the antioxidant protein peroxiredoxin 2 contributes to angiotensin II-mediated podocyte apoptosis. Kidney Int. 2011 Nov;80(9):959-69. .

48. Y. Soinini et all. Oxidative/nitrosative stress and peroxiredoxin 2 are associated with grade and prognosis of human renal carcinoma. APMIS 114: 329–37, 2006 .

49. Moon EY, Han YH, Lee DS, Han YM, Yu DY. Reactive oxygen species induced by the deletion of peroxiredoxin II (PrxII) increases the number of thymocytes resulting in the enlargement of PrxII-null thymus. Eur J Immunol. 2004 Aug;34(8):2119-28.

50. Moon EY, Noh YW, Han YH, Kim SU, Kim JM, Yu DY, Lim JS. T lymphocytes and dendritic cells are activated by the deletion of peroxiredoxin II (Prx II) gene. Immunol Lett. 2006 Feb 15;102(2):184-90.

51. Gao F, Kinnula VL, Myllärniemi M, Oury TD. Extracellular superoxide dismutase in pulmonary fibrosis. Antioxid Redox Signal. 2008 Feb;10(2):343-54.

52. Kinnula VL, Hodgson UA, Lakari EK, Tan RJ, Sormunen RT, Soini YM, Kakko SJ, Laitinen TH, Oury TD, Pääkkö PK. Extracellular superoxide dismutase has a highly specific localization in idiopathic pulmonary fibrosis/usual interstitial pneumonia. Histopathology. 2006 Jul;49(1):66-74.

53. C. Delaney, R. H. Wright, J.-R. Tang, C. Woods, L. Villegas, L. Sherlock, R. C. Savani, S. H. Abman and E. Nozik-Grayck. Lack of EC-SOD worsens alveolar and vascular development in a neonatal mouse model of bleomycin-induced bronchopulmonary dysplasia. and pulmonary hypertension. Pediatric Research (2015) 78, 634–640

54. Nozik-Grayck E, Woods C, Taylor JM, Benninger RK, Johnson RD, Villegas LR, Stenmark KR, Harrison DG, Majka SM, Irwin D, Farrow KN. Selective depletion of vascular EC-SOD augments chronic hypoxic pulmonary hypertension. Am J Physiol Lung Cell Mol Physiol. 2014 Dec 1;307(11):L868-76.

55. Ahmed MN, Zhang Y, Codipilly C, Zaghloul N, Patel D, Wolin M, Miller EJ. Extracellular superoxide dismutase overexpression can reverse the course of hypoxia-induced pulmonary hypertension. Mol Med. 2012 Feb 10;18:38-46.

56. Hassett P, Curley GF, Contreras M, Masterson C, Higgins BD, O'Brien T, Devaney J, O'Toole D, Laffey JG. Overexpression of pulmonary extracellular superoxide dismutase attenuates endotoxin-induced acute lung injury. Intensive Care Med. 2011 Oct;37(10):16.

57. Kinnula VL, Crapo JD. Superoxide dismutases in the lung and human lung diseases. Am J Respir Crit Care Med. 2003 Jun 15;167(12):1600-19.

58. Rahman I, Biswas SK, Kode A. Oxidant and antioxidant balance in the airways and airway diseases. Eur J Pharmacol. 2006 Mar 8;533(1-3):222-39. Epub 2006 Feb 28.

59. E. Bargagli a, C. Olivieri, D. Bennett, A. Prasse,J. Muller-Quernheim, P. Rottoli. Oxidative stress in the pathogenesis of diffuse lung diseases: A review. Respiratory Medicine (2009) 103, 1245e1256.

60. Larsen GL1, White CW, Takeda K, Loader JE, Nguyen DD, Joetham A, Groner Y, Gelfand EW. Mice that overexpress Cu/Zn superoxide dismutase are resistant to allergen-induced changes in airway control. Am J Physiol Lung Cell Mol Physiol. 2000 Aug;279(2):L350-9.

61. De Raeve HR1, Thunnissen FB, Kaneko FT, Guo FH, Lewis M, Kavuru MS, Secic M, Thomassen MJ, Erzurum SC. Decreased Cu,Zn-SOD activity in asthmatic airway epithelium: correction by inhaled corticosteroid in vivo. Am J Physiol. 1997 Jan;272(1 Pt 1):148-54.

62. Lakari E1, Pääkkö P, Kinnula VL. Manganese superoxide dismutase, but not CuZn superoxide dismutase, is highly expressed in the granulomas of pulmonary sarcoidosis and extrinsic allergic alveolitis. Am J Respir Crit Care Med. 1998 Aug;158(2):589-96.

63. Lakari E, Pääkkö P, Pietarinen-Runtti P, Kinnula VL. Manganese superoxide dismutase and catalase are coordinately expressed in the alveolar region in chronic interstitial pneumonias and granulomatous diseases of the lung. Am J Respir Crit Care Med. 2000 Feb;161(2 Pt 1):615-21.

64. Chang LY, Kang BH, Slot JW, Vincent R, Crapo JD. Immunocytochemical localization of the sites of superoxide dismutase induction by hyperoxia in rat lungs. Lab Invest. 1995 Jul;73(1):29-39.

65. Harju T, Kaarteenaho-Wiik R, Sirviö R, Pääkkö P, Crapo JD, Oury TD, Soini Y, Kinnula VL. Manganese superoxide dismutase is increased in the airways of smokers' lungs. Eur Respir J. 2004 Nov;24(5):765-71.

66. Odajima N, Betsuyaku T, Nagai K, Moriyama C, Wang DH, Takigawa T, Ogino K, Nishimura M. The role of catalase in pulmonary fibrosis. Respir Res. 2010 Dec 29;11:183.

67. Comhair SA, Lewis MJ, Bhathena PR, Hammel JP, Erzurum SC. Increased glutathione and glutathione peroxidase in lungs of individuals with chronic beryllium disease. Am J Respir Crit Care Med. 1999 Jun;159(6):1824-9.

68. K.M. Beeh, J. Beier, I.C. Haas, O. Kornmann, P. Micke, R. Buhl. Glutathione deficiency of the lower respiratory tract in patients with idiopathic pulmonary fibrosis. European Respiratory Journal 2002 19: 1119-1123.

69. Park JH, Kim YS, Lee HL, Shim JY, Lee KS, Oh YJ, Shin SS, Choi YH, Park KJ, Park RW, Hwang SC. Expression of peroxiredoxin and thioredoxin in human lung cancer and paired normal lung. Respirology. 2006 May;11(3):269-75.

70. Yoshiyuki Yamadaa, Hajime Nakamurab, Tetsuya Adachia, Satoshi Sannohea, Hajime Oyamadaa, Hiroyuki Kayabaa, Junji Yodoib, Junichi Chiharaa, Elevated serum levels of thioredoxin in patients with acute exacerbation of asthma. Immunol Lett. 2003 Apr 3;86.

71. Sakuma K1, Nakamura H, Nakamura T, Hoshino Y, Ueda S, Ichikawa M, Tabata C, Fujita S, Masago K, Yodoi J, Mishima M, Mio T. Elevation of serum thioredoxin in patients with gefitinib-induced interstitial lung disease. Intern Med. 2007;46(23):1905-9.

72. Tiitto L, Kaarteenaho-Wiik R, Sormunen R, Holmgren A, Pääkkö P, Soini Y, Kinnula VL. Expression of the thioredoxin system in interstitial lung disease. J Pathol. 2003 Nov;201(3):363-70.

73. Hoshino T, Nakamura H, Okamoto M, Kato S, Araya S, Nomiyama K, Oizumi K, Young HA, Aizawa H, Yodoi J. Redox-active protein thioredoxin prevents proinflammatory cytokine- or bleomycin-induced lung injury. Am J Respir Crit Care Med. 2003 Nov 1;168(9):1075-83.

74. Peltoniemi M, Kaarteenaho-Wiik R, Säily M, Sormunen R, Pääkkö P, Holmgren A, Soini Y, Kinnula VL. Expression of glutaredoxin is highly cell specific in human lung and is decreased by transforming growth factor-beta in vitro and in interstitial lung. diseases in vivo. Hum Pathol. 2004 Aug;35(8):1000-7.

75. Niki L. Reynaert , Emiel F. M. Wouters , and Yvonne M. W. Janssen-Heininger. Modulation of Glutaredoxin-1 Expression in a Mouse Model of Allergic Airway Disease. Am J Respir Cell Mol Biol. 2007 Feb;36(2):147-51.

76. Ye Q, Dalavanga Y, Poulakis N, Sixt SU, Guzman J, Costabel U. Decreased expression of haem oxygenase-1 by alveolar macrophages in idiopathic pulmonary fibrosis. Eur Respir J. 2008 May;31(5):1030-6.

77. SW Ryter et al. Protective Functions of Heme Oxygenase-1 and Carbon Monoxide in the Respiratory System. Antioxid Redox Signal 9 (12), 2157-2173. 12 2007.

78. T. Sato, M. Takeno, K. Honma, H. Yamauchi, Y. Saito, T. Sasaki, H. Morikubo, Y. Nagashima, S. Takagi, K. Yamanaka, T. Kaneko and Y. Ishigatsubo. Heme Oxygenase-1, a Potential Biomarker of Chronic Silicosis, Attenuates Silica-induced Lung Injury. American Journal of Respiratory and Critical Care Medicine 174(8):906-14 Nov 2006.

79. Lien Ai Pham-Huy, Hua He and Chuong Pham-Huy. Free Radicals, Antioxidants in Disease and Health. Int J Biomed Sci. 2008 Jun; 4(2): 89–96.

80. I. G. Tsiligianni and T. van der Molen. A systematic review of the role of vitamin insufficiencies and supplementation in COPD. Respir Res. 2010; 11(1): 171. .

81. Parekh D, Thickett DR, Turner AM. Vitamin D deficiency and acute lung injury. Inflamm Allergy Drug Targets. 2013 Aug;12(4):253-61.

82. Agler AH, Kurth T, Gaziano JM, Buring JE, Cassano PA. Randomised vitamin E supplementation and risk of chronic lung disease in the Women's Health Study. Thorax. 2011 Apr;66(4):320-5.

83. Banerjee A, Panettieri R Jr. Vitamin D modulates airway smooth muscle function in COPD. Curr Opin Pharmacol. 2012 Jun;12(3):266-74.

84. Kolleck I, Sinha P, Rüstow B. Vitamin E as an antioxidant of the lung: mechanisms of vitamin E delivery to alveolar type II cells. Am J Respir Crit Care Med. 2002 Dec 15;166(12 Pt 2):S62-6.

85. C.-W. Chow , M. T. H. Abreu , T. Suzuki and G. P. Downey. Oxidative Stress and Acute Lung Injury. Am J Respir Cell Mol Biol. 2003 Oct;29(4):427-31.

86. Gerin F, Sener U, Erman H, Yilmaz A, Aydin B, Armutcu F, Gurel A. The Effects of Quercetin on Acute Lung Injury and Biomarkers of Inflammation and Oxidative Stress in the Rat Model of Sepsis. Inflammation. 2016 Apr;39(2):700-5. .

87. S. Ganesan, A. Comstock, S. Chattoraj, M. B. Hershenson, U. Sajjan. Quercetin Improves Lung Inflammation In Mouse Model Of COPD By Inhibiting Matrix. Am J Respir Crit Care Med 181;2010:A4434.

88. Chen WY, Huang YC, Yang ML, Lee CY, Chen CJ, Yeh CH, Pan PH, Horng CT, Kuo WH, Kuan YH. Protective effect of rutin on LPS-induced acute lung injury via down-regulation of MIP-2 expression and MMP-9 activation through inhibition of Akt phosphorylation. Int Immunopharmacol. 2014 Oct;22(2):409-13.

89. Chaumais MC, Ranchoux B, Montani D, Dorfmüller P, Tu L, Lecerf F, Raymond N, Guignabert C, Price L, Simonneau G, Cohen-Kaminsky S, Humbert M, Perros F. N-acetylcysteine improves established monocrotaline-induced pulmonary hypertension in rats. Respir Res. 2014 Jun 14;15:65.

90. Su CF, Kao SJ, Chen HI. Acute respiratory distress syndrome and lung injury: Pathogenetic mechanism and therapeutic implication. World J Crit Care Med. 2012 Apr 4;1(2):50-60.

91. J Int Med Res. 2013 Aug;41(4):1179-86. High-dose N-acetylcysteine decreases silica-induced lung fibrosis in the rat. Zhang H, Yin G, Jiang H, Zhang C.

92. Forgiarini LF, Forgiarini LA Jr, da Rosa DP, Silva MB, Mariano R, Paludo Ade O, Andrade CF. N-acetylcysteine administration confers lung protection in different phases of lung ischaemia-reperfusion injury. Interact Cardiovasc Thorac Surg. 2014 Dec;19(6):894-9.

93. Clara E. Gree and Alice M. Turner. The role of the endothelium in asthma and chronic obstructive pulmonary disease (COPD). Respir Res. 2017; 18: 20.

94. Białas AJ, Sitarek P, Miłkowska-Dymanowska J, Piotrowski WJ, Górski P. The Role of Mitochondria and Oxidative/Antioxidative Imbalance in Pathobiology of Chronic Obstructive Pulmonary Disease. Oxid Med Cell Longev. 2016.

95. Harrison W. Farber and Joseph Loscalzo. Pulmonary Arterial Hypertension. N Engl J Med 2004; 351:1655-1665.

96. Aggarwal S, Gross CM, Sharma S, Fineman JR, Black SM. Reactive oxygen species in pulmonary vascular remodeling. Compr Physiol 3: 1011-34, 2013.

97. Rawat DK, Alzoubi A, Gupte R, Chettimada S, Watanabe M, Kahn AG, Okada T, McMurtry IF, Gupte SA. Increased reactive oxygen species, metabolic maladaptation, and autophagy contribute to pulmonary arterial hypertension-induced ventricular hypertrophy and diastolic heart failure. Hypertension 64: 1266-74, 2014.

98. Natalie Hopkins and Paul McLoughlin. The structural basis of pulmonary hypertension in chronic lung disease: remodelling, rarefaction or angiogenesis? J Anat. 2002 Oct; 201(4): 335–348.

99. McLaughlin VV, Shah SJ, Souza R, Humbert M. Management of pulmonary arterial hypertension. J Am Coll Cardiol. 2015;65:1976-1997.

100. Tuder RM, Stacher E, Robinson J, Kumar R, Graham BB. Pathology of pulmonary hypertension. Clin Chest Med. 2013;34:639–650.

101. Stacher E, Graham BB, Hunt JM, Gandjeva A, Groshong SD, McLaughlin VV, et al. Modern age pathology of pulmonary arterial hypertension. Am J Respir Crit Care Med. 2012;186:261–272.

102. Tuder RM, Abman SH, Braun T, Capron F, Stevens T, Thistlethwaite PA, et al. Development and pathology of pulmonary hypertension. J Am Coll Cardiol. 2009;54:S3-9.

103. Vincent G DeMarco, Adam T Whaley-Connell, James R Sowers, Javad Habibi, and Kevin C Dellsperger. Contribution of oxidative stress to pulmonary arterial hypertension. World J Cardiol. 2010 Oct 26; 2(10): 316–324.

104. Kongara S, Karantza V. The interplay between autophagy and ROS in tumorigenesis. Front Oncol 2: 171, 2012.

105. Scherz-Shouval R, Elazar Z. Regulation of autophagy by ROS: physiology and pathology. Trends Biochem Sci 36: 30-8, 2011.

106. Filomeni G, Desideri E, Cardaci S, Rotilio G, Ciriolo MR. Under the ROS...thiol network is the principal suspect for autophagy commitment. Autophagy 6: 999-1005, 2010.

107. Scherz-Shouval R, Shvets E, Fass E, Shorer H, Gil L, Elazar Z. Reactive oxygen species are essential for autophagy and specifically regulate the activity of Atg4. EMBO J. 2007 Apr 4;26(7):1749-60.

108. Jain A, Lamark T, Sjøttem E, Larsen KB, Awuh JA, Øvervatn A, McMahon M, Hayes JD, Johansen T. p62/SQSTM1 is a target gene for transcription factor NRF2 and creates a positive feedback loop by inducing antioxidant response element-driven gene transcription. J Biol Chem. 2010 Jul 16;285(29):22576-91.

109. Elmoataz Abdel Fattah, Abhisek Bhattacharya, Alan Herron, Zeenat Safdar and N. Tony Eissa. Critical Role for IL-18 in Spontaneous Lung Inflammation Caused by Autophagy Deficiency. J Immunol June 1, 2015, 194 (11) 5407-5416

110. Krishna K. Singh et All. The essential autophagy gene ATG7 modulates organ fibrosis via regulation of endothelial-to-mesenchymal transition. J Biol Chem. 2015 Jan 30;290(5):2547-59.

111. Cabrera S, Maciel M, Herrera I, Nava T, Vergara F, Gaxiola M, López-Otín C, Selman M, Pardo A. Essential role for the ATG4B protease and autophagy in bleomycin-induced pulmonary fibrosis. Autophagy. 2015 Apr 3;11(4):670-84.

Aim

The overarching aim of my work is to understand the functional role of Peroxiredoxin-2 in a mouse model of pulmonary hypertension induced by hypoxia.

Section 1

Peroxiredoxin-2 plays a pivotal role against oxidation in the early phase of pulmonary artery hypertension

EF author contributions: EF has carried out experiments, contributed to experimental design, data analysis and paper writing.

PEROXIREDOXIN-2 PLAYS A PIVOTAL ROLE AGAINST OXIDATION IN THE EARLY PHASE OF PULMONARY HYPERTENSION

Enrica Federti[1], Alessandro Matte'[1], Alessandra Ghigo[2], Immacolata Andolfo[3], Cimino J[2,] Angela Siciliano [1], Christophe Leboeuf [4], Anne Janin [4 5, 6], Hirsch E[2], Soo Young Choi[7], Achille Iolascon[3], Dae Won Kim[7], Sonia Levi[8, 9], Lucia De Franceschi [1]

[1]Dept. of Medicine, University of Verona-AOUI Verona, Verona; Italy; [2]Molecular Biotechnology Center and Department of Molecular Biotechnology and Health Science, University of Torino, Torino; Italy; [3]CEINGE and Dept. of Biochemistry, University of Naples, Naples; Italy; [4]Inserm, U1165, Paris, F-75010, France; [5]Université Paris 7- Denis Diderot, Paris, France; [6]AP-HP, Hôpital Saint-Louis, F-75010, Paris, France; [7]Institute of Bioscience and Biotechnology, Hallym University, Gangowo-do; Korea; [8] Division of Neuroscience, San Raffaele Scientific Institute, Milano, Italy; [9]Vita-Salute San Raffaele University, Milano, Italy

words count: 3568

Corresponding Author:

Lucia De Franceschi, MD

Dept of Medicine, University of Verona- AOUI Verona

Policlinico GB Rossi- P.le L Scuro, 10; 37134 Verona, Italy

phone: +390458124401; Fx +39045 8027473; E-Mail: lucia.defranceschi@univr.it

ABSTRACT

Pulmonary-artery-hypertension (PAH) is a life-threatening and highly invalidating chronic disorder. Chronic oxidation contributes to lung damage and disease progression. Peroxiredoxin-2 (Prx2), a typical 2-cysteine (Cys) peroxiredoxin, is able to efficiently scavenge low concentration of H_2O_2, but its role on lung homestasis is yet to be fully defined. Here, we showed that $Prx2^{-/-}$ mice displayed chronic lung inflammatory disease associated with (i) abnormal pulmonary vascular dysfunction; and (ii) increased markers of extracellular-matrix remodeling. Hypoxia was used to induce PAH. We focused on the early phase PAH to dissect the role of Prx2 in generation of PAH. Hypoxic $Prx2^{-/-}$mice showed (i) amplified inflammatory response combined with cytokine storm; (ii) vascular activation and dysfunction; (iii) increased PDGF-B lung levels, used as marker of extracellular-matrix deposition and remodeling; and (iv) autophagy activation. Rescue experiments with in vivo the administration of fused-recombinant-PEP-Prx2 to hypoxic mice show a reduction in pulmonary inflammatory vasculopathy and down-regulation of autophagy. Thus, we propose Prx2 plays a pivotal role in the early stage of PAH as multimodal anti-oxidant system targeting oxidation, inflammatory vasculopathy and indirectly autophagy. Collectively, our data indicate that the potentiation of endogenous anti-oxidant systems might interrupt the oxidation related vicious circle involved in the pathogenesis of PAH.

Key words: peroxiredoxin-2, chronic hypoxia, autophagy

INTRODUCTION

Pulmonary artery hypertension (PAH) is a life threatening highly invalidating chronic disorder [1-3]. Although in the last decade progresses have been made in the identifications of factors involved in its pathogenesis, much still remains to be investigated in the mechanism involved in the early stage of PAH [3-5]. Regardless of the initial event, the combination of chronic inflammation and chronic hypoxia promote a high pro-oxidant environment, mediating disease progression [1, 2, 4, 6, 7]. Thus, endogenous antioxidant systems controlling oxidation serve also as downstream regulator of autophagic process. Studies *in vivo* in animal model of PAH have shown that the absence of endogenous anti-oxidant such as superoxide dismutase- 1 (SOD-1) or cytoprotective systems such as heme-oxygenase 1 (HO-1) accelerates the development of PAH [8-11].

In this scenario, an efficient catabolic pathway to clear intracellular damaged proteins is required. In different cell models, growing evidences link ROS to autophagy, priming cells to better tolerate oxidation [12, 13]. In addition, some autophagy related proteins (Atg) are redox-sensitive proteins and might also be functionally modulated by ROS [13, 14].

Prx2 is a typical 2-cysteine (Cys) peroxiredoxin, which is able to efficiently scavenge low concentration of H_2O_2 without inactivation due to over-oxidation. Studies in mouse genetically lacking Prx2 ($Prx2^{-/-}$) have highlighted its protective role against LPS induced lethal shock and acute distress syndrome (ARDS) [15-21]. In addition, in vitro and in vivo model of ischemic/reperfusion stress highlighted the key role of Prx2 as anti-oxidant and cytoprotective system [22, 23].

Here, we studied the role of Prx2 in development of pulmonary hypertension in mice genetically lacking Prx2 ($Prx2^{-/-}$), using hypoxic stress to explore the early stage of early phase of pulmonary hypertension. Our data collectively indicate that Prx2 plays a key role

against oxidation in the early phase of hypoxia induced pulmonary hypertension. The recombinant PEP fused Prx2 (PEP Prx2) corrects the imbalance between oxidants/anti-oxidants during hypoxic stress by (i) reducing local and systemic inflammation; (ii) preventing vascular activation and PDGF-B up-regulation and (iii) down-regulating autophagy activation in response to hypoxia. Thus, PEP Prx2 might represent an interesting new multimodal therapeutic option in the early stage PAH.

MATERIALS AND METHODS

Drugs and chemicals. Details are reported in Supplemental Materials and Methods.

Mouse strains and design of the study. C57B6/2J mice as wildtype controls (WT) and $Prx2^{-/-}$ mice aged between 4-6 months both male and female were used in the present study [16, 24]. The Institutional Animal Experimental Committee, University of Verona (CIRSAL) and by the Italian Ministry of Health approved the experimental protocols. Where indicated WT and $Prx2^{-/-}$ mice were treated with 1) N-Acetyl-Cysteine (NAC) at the dosage of 100 mg/Kg/d (in NaCl 0.9%, NaOH 36 mM, pH 9.4; ip) or vehicle only for 3 weeks [16, 18]; 2) PEP Prx2 (in PBS) or vehicle at the dosage of 3 mg/Kg/d ip or vehicle for 4 weeks before and during hypoxia [16]. Whenever indicated, mice were exposed to hypoxia (8% oxygen for 10 hours, 3 days, 7 days) (Hy) as previously described [25-27]. To collect organs, animals were first anesthetized with isofluorane, bronchoalveolar lavage (BAL) was collected and then mice were euthanized. Organs were immediately removed and divided into two and either immediately frozen in liquid nitrogen or fixed in 10% formalin and embedded in paraffin for histology.

Bronchoalveolar lavage (BAL) measurements. BAL fluids were collected and cellular contents were recovered by centrifugation and counted by microcytometry as previously reported [25]. Percentage of neutrophils was determined on cytospin centrifugation. Remaining BAL samples were centrifuged at 1,500 x g for 10 min at 4°C. The supernatant fluids were used for determination of total protein content [25].

Lung molecular analysis

Lung histology. Multiple (at least five) three micron whole mount sections were obtained for each paraffin-embedded lung and stained with hematoxylin eosin, Masson's trichome, and May-Grünwald-Giemsa. α-smooth muscle actin immunohistochemistry (IHC) on lungs

was carried out as previously reported [25, 28]. Lung pathological analysis was carried out by blinded pathologists as previously described [25, 28]. Based on previous reports (18, 38), the pathological criteria for lung histopatholgy were as follows: i) Bronchus: Mucus: 0: no mucus; +: mucus filling less than 50% of the area of the bronchus section; ++: mucus filling more than 50% of the area of the bronchus section. (ii) Inflammatory infiltrate density: 0: less than 5 inflammatory cells per field; +: 5-30 inflammatory cells per field; ++ more than 30 inflammatory cells per field. (iii) Thrombi: 0: no thrombus; + presence of a thrombus in one field, at magnification 250.

Immunoblot analysis. Frozen lung and heart from each studied group were homogenized and lysed with iced lyses buffer (LB containing: 150 mM NaCl, 25 mM bicine, 0.1% SDS, Triton 2%, EDTA 1 mM, protease inhibitor cocktail tablets (Roche), 1 mM Na_3VO_4 final concentration) then centrifuged 10 min at 4°C at 12,000 *g*. Proteins were quantified and analysed by mono-dimensional SDS polyacrylamide gel electrophoresis. Gels were transferred to nitrocellulose membranes for immuno-blot analysis with specific antibody. Details are reported in Supplemental materials and Methods [25, 29].

RNA isolation, cDNA preparation and quantitative RT-PCR. Total RNA was extracted from tissues using Trizol reagent (Life Technologies, Monza, Italy). Synthesis of cDNA from total RNA (1µg) was performed using Super Script II First Strand kits (Life Technologies). Quantitative RT-PCR (qRT- PCR) was performed using the SYBR-green method, following standard protocols with an Applied Biosystems ABI PRISM 7900HT Sequence Detection system. Relative gene expression was calculated using the $2^{(-\Delta Ct)}$ method, where ΔCt indicates the differences in the mean Ct between selected genes and the internal control (GAPDH). qRT-PCR primers for each gene were designed with Primer Express 2.0 (Life Technologies) (primer sequences are reported in Table 1S) [25, 28].

MDA assay. MDA was determined as previously reported [30].

Evaluation of right ventricular hypertrophy and echocardiography measurements.

Hearts were fixed with 10% formaldehyde for 24 hours. The right ventricular (RV) free wall was separated from the left ventricular with septum (LV+S) under dissection microscope. RV and LV+S were separately weighed and used to calculate the ratios RV/(LV+S)/body weight [31]. Transthoracic echocardiography was performed with a Vevo 2100 echocardiograph (Visual Sonics, Toronto, Canada) equipped with a 22-55 MHz transducer (MicroScan Transducers, MS500D) as previously reported [25].

Statistical analysis. Data were analyzed using either *t*-test or the 2-way analysis of variance (ANOVA) for repeated measures between the mice of various genotypes. A difference with a *P* value less than 0.05 was considered significant.

RESULTS

Mice genetically lacking Prx2 show lung inflammation, increased pulmonary vascular activation and extracellular-matrix remodeling

Under normoxia Prx2$^{-/-}$ mice show increased peribronchial oedema without changes in the number of mucus cells (Fig. 1A, upper panel). The systematic study for α-smooth cells expression showed a staining in broken line only on bronchial sections of Prx2$^{-/-}$ mice, suggesting an initial pulmonary vessel muscularization in the absence of Prx2 (Fig. 1A, lower panel). The analysis of bronchoalveolar lavage (BAL) revealed increased levels of proteins and of total leukocytes in Prx2$^{-/-}$ mice compared to wildtype, indicating an abnormal pulmonary vascular leakage (Fig. 1B).

In Prx2$^{-/-}$ mice, we found increased active form of NF-kB and Nrf2, two redox related transcriptional factors, compared to wild-type animal (Fig. 1C; Fig. 1SA). This was associated with increased lung MDA levels (Fig. 1SB) and up-regulation at mRNA levels of cytokines such as IL-6, IL-1b and IL10, known targets of NF-kB (Fig. 1D). We confirmed the increased expression of IL-6 in lung from Prx2$^{-/-}$ mice compared to wildtype animals (Fig. 1E, Fig. 1SC). In addition, in Prx2$^{-/-}$ mice, we observed increased expression of two cytoprotective systems related to Nrf2 activity: HO-1, a vascular and lung cytoprotector, and SOD-1, a potent anti-oxidant enzyme [32]. This was associated with higher levels of (i) endothelin-1 (ET-1), the most potent vasoconstrictive and bronchoconstrictive cytokine [28]; (ii) VCAM-1, a marker of vascular endothelial activation [25]; and (iii) PDGF-B, a known factor involved in lung extra-cellular matrix remodeling [33] (Fig. 1E; Fig. 1SC). These data link the absence of Prx2 with persistent lung inflammation, endothelial vascular activation, and extracellular matrix remodeling.

Prolonged hypoxia promotes the development of early stage pulmonary hypertension in Prx2$^{-/-}$ mice

Based on our previous report, showing the development of early stage PAH in a mouse model for sickle cell disease but not in wildtype mice [31], we exposed both mouse strains to hypoxia (Hy) 8% oxygen for 7 days. As shown in Fig. 2A, hypoxia induced sparse inflammatory cell infiltrate with some peribronchial oedema in Prx2$^{-/-}$ mice. On the bronchial epithelium there was no significant change in the number of mucus cells in both mouse strains. On vascular sections, no thrombus was found in any of the mouse groups. The systematic study for α-actin deposition revealed the presence of almost linear staining around bronchial and vascular sections in Prx2$^{-/-}$ mice (Fig. 2A, lower panel). While, α-actin depositions were sparse in hypoxic wildtype mice.

We evaluated the presence of RV hyperthrophy in both mouse strains exposed to 7days hypoxia. In Prx2$^{-/-}$ mice, we observed a slight but significant increase in RV/(LV+S) ratio (normoxia: 0.21±0.03 vs hypoxia 0.34±0.05; n=6, P<0.05), whereas no changes were observed in wildtype mice in agreement with our previous report [31]. This was associated with a significant increase in mitral valve deceleration time and a reduction in pulmonary acceleration time/ ejection time ratio (Fig. 2B), indicating early diastolic dysfunction and increased right ventricular systolic pressure in Prx2$^{-/-}$ mice. In addition, we found hypoxia induced increased expression of SOD-1 in heart from both mouse strains, but to a higher extent in Prx2$^{-/-}$ mice (Fig. 1SD). Hypoxia induced up-regulation of (i) VCAM-1 and ICAM-1; and (ii) atrial natriuretic peptide (ANP) was also observed in both mouse strains (Fig. 1SD).

Our findings are consistent with the development of early stage of PAH promoted by severe oxidation and amplified inflammatory response in Prx2$^{-/-}$ mice exposed to 7 days hypoxia.

Prx2 plays an important role as cytoprotective system against hypoxia induced PAH

In order to follow-up the generation of PAH in Prx2$^{-/-}$ mice, we studied both mouse strains at different time intervals between 0 to 7 days hypoxia to identify the optimal window-time to analyze mechanism(s) involved in development of PAH. BAL protein and leukocyte count were significantly increased in Prx2$^{-/-}$ mice during hypoxia at 10 hours, 3 days and 7 days compared to wildtype animals (data not shown).

Hypoxia markedly increased Prx2 expression in lung from wildtype mice at 10 hours, 3 days and 7 days of exposure (Fig. 2C; Fig. 2SA). This was associated with time dependent increased expression of the Prx2 repairing systems: sestrin-2 and thioredoxin-reductase (Trdx; Fig. 2C; Fig. 2SA). The modulation of Trdx expression during hypoxia even in the absence of Prx2, one of its main functional targets, may be possible related to the fact that Trdx is part of different NADPH-dependent pathways [16, 34].

In Prx2$^{-/-}$ mice exposed to hypoxia, we observed a rapid and sustained activation of Nrf2 in response to hypoxia, while there was a reduction in activation of NF-kB (Fig. 2D, 2SB). Otherwise, wildtype mice showed an early response of Nrf2 at 10 and 3 hours hypoxia, partially overlapping the activation of NF-kB observed at 3 and 7 days hypoxia (Fig. 2D, 2SB). These data suggest that Nrf2 might be a precocious back-up mechanism in response to hypoxia, which is early activated in both mouse strains, but to higher extent in mice genetically lacking Prx2.

Since pro-inflammatory cytokines are modulated by oxidation and participates to the development of PAH [3, 35, 36], we evaluated IL1b and IL6 expression in lung from both mouse strains during hypoxia. In Prx2$^{-/-}$ mice, IL-1b mRNA levels were significantly increased at 3 days of hypoxia compared to wildtype animals, which displayed increased IL-1b expression only at 7 days hypoxia (Fig. 3A). In Prx2$^{-/-}$ mice, lung IL-6 mRNA expression was significantly upregulated at 3 days of hypoxia followed by a decreased at 7 days of hypoxia to levels still higher than those observed in wildtype mice (Fig. 3B). These

data support an earlier and amplified inflammatory response in Prx2$^{-/-}$ mice in response to hypoxia compared to wildtype animals.

We then evaluated markers of pulmonary vascular remodeling (ET-1, PDGF-B, ANP) and vascular endothelial activation (VCAM-1 and ICAM-1). As shown in Fig. 3C, ET-1 expression was increased in both mouse strains but to a higher extent in Prx2$^{-/-}$ mice compared to wildtype; while PDGF-B levels increased earlier, reaching higher and constant levels in Prx2$^{-/-}$ mice compared to wildtype during hypoxia. VCAM-1 and ICAM1 expression was similarly increased in both mouse strains at 7 days hypoxia (Fig. 3D). Whereas, ANP expression was higher in Prx2$^{-/-}$ mice than in wildtype exposed to prolonged hypoxia (Fig. 3D).

Collectively, these data indicate that the absence of Prx2 accelerates vascular activation and extra-matrix remodeling, amplifying inflammatory response during hypoxia.

PEP Prx2 treatment rescues prolonged hypoxia induced heart and lung inflammatory vasculopathy

To address the question whether Prx2 plays a role in lung chronic inflammatory disease, we firstly evaluated the impact of recombinant fusion protein PEP Prx2 (1.5mg/Kg/day ip, 3weeks) to both mouse strains under room air condition. In normoxic Prx2$^{-/-}$ mice, PEP Prx2 treatment (i) prevented Nrf2 and NF-kB activation (Fig. 3SA); (ii) reduced HO-1 protein expression (Fig. 3SB); and (iii) decreased the levels of ET-1, VCAM-1 and PDGF-B (Fig. 3SB). No major changes were observed in wildtype animals (Fig. 3SA, 3SB).

In Prx2$^{-/-}$ mice exposed to 7 days hypoxia, PEP Prx2 treatment significantly reduced the hypoxia mediated diastolic dysfunction and ameliorated RVSP, as suggested by the increased in PAT/ET ratio (Fig. 4A, 4SA). In agreement, in heart from PEP Prx2 treated Prx2$^{-/-}$ mice exposed to 7 days hypoxia, we found a reduction of ANP expression as well as of markers of vascular endothelial activation (Fig.4B, 4SB). This was associated with a

decrease in levels of SOD-1 and in the oxidation state of proteins from heart of hypoxic $Prx2^{-/-}$ mice treated with PEP Prx2 (Fig. 4SC). We found similar evidences of the beneficial effects of PEP Prx2 on lung from $Prx2^{-/-}$ mice exposed to prolonged hypoxia. As shown in Fig. 4C, PEP Prx2 promoted a significant reduction in hypoxia induced increase of ANP, VCAM-1, ICAM-1 and PDGF-B levels compared to vehicle treated $Prx2^{-/-}$ animals.

In order to evaluate whether the effects of PEP Prx2 treatment were specific of Prx2 or related to a general anti-oxidant effect, we treated both mouse strains with NAC (100 mg/kg/day for 3 weeks), a known anti-oxidant agent previously used in other *in vitro* and *in vivo* models of PAH [6, 37]. No changes were present in the levels of Nfr2 and NF-kB activation in $Prx2^{-/-}$ mice treated with NAC, suggesting that the effects of PEP Prx2 are peculiar of Prx2 and not only related to its general antioxidant effects (data not shown).

To test the role of Prx2 in development of PAH, we chose to further study $Prx2^{-/-}$ mice at day 3 of hypoxia, when we expect to be the turning point in the imbalance between oxidation/ anti-oxidant activities based on the increased of Prx2 in wild-type mice (Fig. 2C) and the activation of redox-related transcriptional factors (Fig. 2D).

In $Prx2^{-/-}$ mice, PEP Prx2 prevents the hypoxia induced oxidative stress and reduces inflammatory vascular activation and extracellular matrix remodeling

As shown in Fig. 5A, PEP Prx2 treatment prevented the hypoxia induced increased in BAL protein and leukocyte content in both mouse strains. This was associated with a marked reduction in protein oxidation state in both mouse strains exposed to 3 days hypoxia and treated with PEP Prx2, supporting the local anti-oxidant effect of exogenous PEP Prx2 treatment during hypoxia stress (Fig. 5B). In agreement, we found that PEP Prx2 administration prevented the hypoxia induced Nrf2 and NF-kB activation in both mouse strains (Fig. 5C, 5SA). This was paralleled by the reduction in HO-1, IL-6, ET-1, VCAM-1 and PDGF-B (Fig. 6A, 5SB-C).

These data suggest that PEP Prx2 treatment during hypoxia is able to (i) decrease local pulmonary inflammation and oxidation, (ii) reduce systemic inflammatory response; (iii) beneficially affect hypoxia abnormalities in pulmonary vascular leakage; and (iv) prevent hypoxia activation of redox-sensitive transcriptional factors Nrf2 and NF-kB.

PEP Prx2 down-regulates autophagy in Prx2$^{-/-}$ mice exposed to hypoxia

Autophagy has been recently linked to cellular oxidation and transition of smooth muscle cells in response to PDGF-B [12, 38]. In mice exposed to 3 days hypoxia, we evaluated key elements of autophagy machinery and the effects of PEP Prx2 treatment. Based on revision of the literature, we chose to analyze the expression of (i) autophagy related proteins ULk1 that is required for initiation of autophagy; (ii) LC3 I/II, a coordinator of phagosomal membranes and (iii) p62, a key cargo protein and component of inclusion bodies; and (iv) pro-caspase 3/caspase 3, involved in digestion of damaged proteins [13, 39-41].

As shown in Fig. 6B, normoxic Prx2$^{-/-}$ mice showed increased LC3-II formation associated with increased expression of Ulk1 and p62 compared to wildtype mice (see also Fig. 5SA). This was associated with higher expression of pro-caspase 3/caspase 3, indicating an activation of autophagy to clear intracellular oxidative damaged proteins in Prx2$^{-/-}$ mice.

In both mouse strains, hypoxia markedly activated autophagy as supported by increased LC3I/II expression, consumption of Ulk1 and reduction of p62, suggesting a clearance of p62 positive inclusion bodies containing damaged proteins (Fig. 6B, 6S). It is of note that the pro-caspase/caspase 3 ratio was also increased in both mouse models exposed to hypoxia, but to higher extent in Prx2$^{-/-}$ mice compared to wildtype (Fig.6B, 6S).

As a proof of concept that Prx2 is important in the crossroad between hypoxia induced oxidation and autophagy, we evaluated the effects of PEP Prx2 treatment on autophagy in mice exposed to 3 days hypoxia. As shown in Fig. 6B, PEP Prx2 administration rescued

the hypoxia induced activation of autophagy, indicating that Prx2 acts as multimodal anti-oxidant system (see also Fig. 6S).

DISCUSSION

Here, we firstly show the novel role of Prx2 as lung cytoprotector against hypoxia induced PAH. Our data also indicate that Prx2 is required in management of the physiologic oxidation in lung. In fact, under room air condition In $Prx2^{-/-}$ mice show we lung chronic inflammatory vasculopathy and vascular dysfunction, associated with activation of extra-matrix remodeling (Fig.1). This is in agreement with previous studies in mouse models genetically lacking other anti-oxidant systems such as SOD-1, which show increased susceptibility to both acute and chronic lung injury [8, 42, 43].

$Prx2^{-/-}$ mice exposed to prolonged hypoxia developed signs of PAH, combined with inflammatory vasculopathy and increased in PDGF-B as marker of extra-matrix remodeling on both lung and heart site. We found a significant increase in ANP lung and heart levels in both mouse strains exposed to hypoxia, but again to a higher extent in $Prx2^{-/-}$ mice. This indicates an attempt of endogenous system to induce pulmonary vaso-relaxation and to modulate lung and heart remodeling in response to hypoxia [44, 45].

Since hypoxia promotes oxidative stress, we evaluated the behavior of two key redox-related transcriptional factors, Nrf2 and NF-kB in both mouse srtains during hypoxia. Nrf2 was early activated in both mouse strains, but to a higher extent in $Prx2^{-/-}$ mice compared to wildtype animals (Fig. 2). Whereas, NF-kB seems to be more important in prolonged hypoxia for wildtype mice compared to $Prx2^{-/-}$ animals. These data support the early activation of Nrf2 as back-up mechanism against severe oxidation in mice genetically lacking Prx2 [16].

The rescue experiments with PEP Prx2 in $Prx2^{-/-}$ mice exposed to prolonged hypoxia corroborate the importance of Prx2 in the functional cascade activated in response to hypoxia. The evidences in $Prx2^{-/-}$ mice undergoing to 3 days hypoxia further support the pivotal role of Prx2 in lung homeostasis.

In this scenario, autophagy becames an important mechanism in the cross-road between hypoxia and oxidation. In fact, autophagy is a cytoprotective process against oxidation and hypoxia induced cellular damage, but it also protects hypoxia induced hyperproliferating cells (i.e.: vascular cells and fibroblasts), which are involved in vascular and extracellular matrix remodeling [13, 46-48]. Our data on autophagy highlight the janus bifront behavior of defensive autophagy in lung of $Prx2^{-/-}$ mice exposed to hypoxia. In $Prx2^{-/-}$ mice, we found activation of autophagy already under normoxia, possibly related to the impairment of endogenous anti-oxidant system due the absence of Prx2. Hypoxia induced a further activation of autophagy in $Prx2^{-/-}$ mice, which also displayed high levels of PDGF-B, promoting extra-matrix remodeling and alpha actin-deposition. The redox-related trascriptional factor Nrf2 has been recently linked to autophagy through p62 to ensure cell survival against severe oxidation [13, 46]. Indeed, the treatment with PEP Prx2 reduced Nrf2 activation and switched-off autophagy as supported by the reduction in LC3II and accumulation of p62 (fig. 6). Previous studies have shown the partial effect of NAC, an exogenous anti-oxidant, in modulating autophagy in chronic lung disease [14]. Here, we found that PEP Prx2 potentiates the endogenous anti-oxidant system during hypoxia, with a multimodal action targeting: inflammatory response, cytokine storm, vascular and extracellular matrix remodeling (Fig. 6C). The correction of the imbalance between oxidation and anti-oxidant systems might interrupt the vicious circle, established between oxidation-chronic inflammation and chronic activation of autophagy towards the generation of PAH (Fig. 6C).

In conclusion, we have firstly highlighted the novel pivotal role of Prx2 in preventing PAH induced by hypoxia. The high bio-complexity of PAH requires multimodal therapeutic approaches, which simultaneously act on different targets involved in its pathogenesis. Our data collectively support a rationale for considering the potentiation of endogenous anti-oxidant systems, such as Prx2, as novel therapeutic option in treatment of the early phase of PAH.

ABBREVIATIONS

PAH: pulmonary arthery hypertension; PBS: phosphate buffer; (qRT)-PCR: quantitative real time; ARDS: acute respiratory distress syndrome; ARE: anti-oxidant responsive element; Atg4: autophagy related 4; BAL: bronchoalveolar lavage; ET-1: endothelin 1; GAPDH: glyceraldehyde 3-phosphate dehydrogenase; HO-1: heme oxygenase 1; HY stress: hypoxia/reoxigenation stress; IL-1b: interleukin 1b; IL-6: interleukin 6; IL-10: interleukin 10; LPS: lipopolysaccharides; NAC: N-acetyl-cysteine; NF-kB: nuclear factor kappa-light-chain-enhancer of activated B cells; Nrf2: nuclear factor-erythroid 2; PAH: pulmonary artery hypertension; PDGF-B Platelet-derived growth factor subunit B; PEP Prx2: Prx2 fused to cell penetrating carrier PEP1 peptide; Prx2: peroxiredoxin-2; ROS: reactive oxygen species; SMCs: smooth muscle cells; SOD-1: superoxide dismutase 1; Trdx: Thioredoxin reductase; VCAM-1: vascular cell adhesion molecule 1; MDA: malondialdehyde; RV: right ventricular; RVSP: right ventricular systolic pressure; PAT: pulmonary acceleration time; ET: ejection time; ICAM-1: intercellular adhesion molecule 1; ANP: atrial natriuretic peptide; Ulk 1: Serine/threonine-protein kinase Ulk1; LC3 I/II: microtubule-associated protein 1A/1B-light chain 3

ACKNOWLEDGMENTS

This work was supported by PRIN (LDF and AI: 201228PNX83) and FUR_UNIVR (LDF).

AUTHORSHIP AND CONTRIBUTIONS

EF, AM, LDF, IA designed the experiments, analyzed data and wrote the paper; AJ, CL carried out the histologic analysis; AM, AS, LDF carried out the experiments; IA performed the molecular experiments and analyzed the data; CSY and KDW generated the PEP Prx2; SL carried out MDA measurements and analyzed data.

CONFLICT OF INTEREST AND DISCLOSURE

The authors have nothing to disclose.

REFERENCES

[1] Rawat, D. K.; Alzoubi, A.; Gupte, R.; Chettimada, S.; Watanabe, M.; Kahn, A. G.; Okada, T.; McMurtry, I. F.; Gupte, S. A. Increased reactive oxygen species, metabolic maladaptation, and autophagy contribute to pulmonary arterial hypertension-induced ventricular hypertrophy and diastolic heart failure. *Hypertension* **64:**1266-1274; 2014.

[2] Zelko, I. N.; Folz, R. J. Regulation of Oxidative Stress in Pulmonary Artery Endothelium. Modulation of Extracellular Superoxide Dismutase and NOX4 Expression Using Histone Deacetylase Class I Inhibitors. *Am J Respir Cell Mol Biol* **53:**513-524; 2015.

[3] Aggarwal, S.; Gross, C. M.; Sharma, S.; Fineman, J. R.; Black, S. M. Reactive oxygen species in pulmonary vascular remodeling. *Compr Physiol* **3:**1011-1034; 2013.

[4] Morales-Cano, D.; Menendez, C.; Moreno, E.; Moral-Sanz, J.; Barreira, B.; Galindo, P.; Pandolfi, R.; Jimenez, R.; Moreno, L.; Cogolludo, A.; Duarte, J.; Perez-Vizcaino, F. The flavonoid quercetin reverses pulmonary hypertension in rats. *PLoS One* **9:**e114492; 2014.

[5] Van Houten, B. Pulmonary Arterial Hypertension Is Associated with Oxidative Stress-induced Genome Instability. *Am J Respir Crit Care Med* **192:**129-130; 2015.

[6] Chaumais, M. C.; Ranchoux, B.; Montani, D.; Dorfmuller, P.; Tu, L.; Lecerf, F.; Raymond, N.; Guignabert, C.; Price, L.; Simonneau, G.; Cohen-Kaminsky, S.; Humbert, M.; Perros, F. N-acetylcysteine improves established monocrotaline-induced pulmonary hypertension in rats. *Respir Res* **15:**65; 2014.

[7] Schmidt, H. H.; Stocker, R.; Vollbracht, C.; Paulsen, G.; Riley, D.; Daiber, A.; Cuadrado, A. Antioxidants in Translational Medicine. *Antioxid Redox Signal* **23:**1130-1143; 2015.

[8] Delaney, C.; Wright, R. H.; Tang, J. R.; Woods, C.; Villegas, L.; Sherlock, L.; Savani, R. C.; Abman, S. H.; Nozik-Grayck, E. Lack of EC-SOD worsens alveolar and vascular development in a neonatal mouse model of bleomycin-induced bronchopulmonary dysplasia and pulmonary hypertension. *Pediatr Res* **78:**634-640; 2015.

[9] Ahmed, M. N.; Suliman, H. B.; Folz, R. J.; Nozik-Grayck, E.; Golson, M. L.; Mason, S. N.; Auten, R. L. Extracellular superoxide dismutase protects lung development in hyperoxia-exposed newborn mice. *Am J Respir Crit Care Med* **167:**400-405; 2003.

[10] Auten, R. L.; O'Reilly, M. A.; Oury, T. D.; Nozik-Grayck, E.; Whorton, M. H. Transgenic extracellular superoxide dismutase protects postnatal alveolar epithelial proliferation and development during hyperoxia. *Am J Physiol Lung Cell Mol Physiol* **290:**L32-40; 2006.

[11] Yet, S. F.; Perrella, M. A.; Layne, M. D.; Hsieh, C. M.; Maemura, K.; Kobzik, L.; Wiesel, P.; Christou, H.; Kourembanas, S.; Lee, M. E. Hypoxia induces severe right ventricular dilatation and infarction in heme oxygenase-1 null mice. *J Clin Invest* **103:**R23-29; 1999.

[12] Scherz-Shouval, R.; Elazar, Z. Regulation of autophagy by ROS: physiology and pathology. *Trends Biochem Sci* **36:**30-38; 2011.

[13] Kongara, S.; Karantza, V. The interplay between autophagy and ROS in tumorigenesis. *Front Oncol* **2:**171; 2012.

[14] Filomeni, G.; Desideri, E.; Cardaci, S.; Rotilio, G.; Ciriolo, M. R. Under the ROS...thiol network is the principal suspect for autophagy commitment. *Autophagy* **6:**999-1005; 2010.
[15] Low, F. M.; Hampton, M. B.; Winterbourn, C. C. Peroxiredoxin 2 and peroxide metabolism in the erythrocyte. *Antioxid Redox Signal* **10:**1621-1630; 2008.
[16] Matte, A.; De Falco, L.; Iolascon, A.; Mohandas, N.; An, X.; Siciliano, A.; Leboeuf, C.; Janin, A.; Bruno, M.; Choi, S. Y.; Kim, D. W.; De Franceschi, L. The Interplay Between Peroxiredoxin-2 and Nuclear Factor-Erythroid 2 Is Important in Limiting Oxidative Mediated Dysfunction in beta-Thalassemic Erythropoiesis. *Antioxid Redox Signal* **23:**1284-1297; 2015.
[17] Matte, A.; Pantaleo, A.; Ferru, E.; Turrini, F.; Bertoldi, M.; Lupo, F.; Siciliano, A.; Ho Zoon, C.; De Franceschi, L. The novel role of peroxiredoxin-2 in red cell membrane protein homeostasis and senescence. *Free Radic Biol Med* **76C:**80-88; 2014.
[18] Franco, S. S.; De Falco, L.; Ghaffari, S.; Brugnara, C.; Sinclair, D. A.; Matte, A.; Iolascon, A.; Mohandas, N.; Bertoldi, M.; An, X.; Siciliano, A.; Rimmele, P.; Cappellini, M. D.; Michan, S.; Zoratti, E.; Anne, J.; De Franceschi, L. Resveratrol accelerates erythroid maturation by activation of FoxO3 and ameliorates anemia in beta-thalassemic mice. *Haematologica* **99:**267-275; 2014.
[19] Matte, A.; Low, P. S.; Turrini, F.; Bertoldi, M.; Campanella, M. E.; Spano, D.; Pantaleo, A.; Siciliano, A.; De Franceschi, L. Peroxiredoxin-2 expression is increased in beta-thalassemic mouse red cells but is displaced from the membrane as a marker of oxidative stress. *Free Radic Biol Med* **49:**457-466; 2010.
[20] Yang, D.; Song, Y.; Wang, X.; Sun, J.; Ben, Y.; An, X.; Tong, L.; Bi, J.; Wang, X.; Bai, C. Deletion of peroxiredoxin 6 potentiates lipopolysaccharide-induced acute lung injury in mice. *Crit Care Med* **39:**756-764; 2011.
[21] Yang, C. S.; Lee, D. S.; Song, C. H.; An, S. J.; Li, S.; Kim, J. M.; Kim, C. S.; Yoo, D. G.; Jeon, B. H.; Yang, H. Y.; Lee, T. H.; Lee, Z. W.; El-Benna, J.; Yu, D. Y.; Jo, E. K. Roles of peroxiredoxin II in the regulation of proinflammatory responses to LPS and protection against endotoxin-induced lethal shock. *J Exp Med* **204:**583-594; 2007.
[22] Gan, Y.; Ji, X.; Hu, X.; Luo, Y.; Zhang, L.; Li, P.; Liu, X.; Yan, F.; Vosler, P.; Gao, Y.; Stetler, R. A.; Chen, J. Transgenic overexpression of peroxiredoxin-2 attenuates ischemic neuronal injury via suppression of a redox-sensitive pro-death signaling pathway. *Antioxid Redox Signal* **17:**719-732; 2012.
[23] Boulos, S.; Meloni, B. P.; Arthur, P. G.; Bojarski, C.; Knuckey, N. W. Peroxiredoxin 2 overexpression protects cortical neuronal cultures from ischemic and oxidative injury but not glutamate excitotoxicity, whereas Cu/Zn superoxide dismutase 1 overexpression protects only against oxidative injury. *J Neurosci Res* **85:**3089-3097; 2007.
[24] de Franceschi, L.; Turrini, F.; Honczarenko, M.; Ayi, K.; Rivera, A.; Fleming, M. D.; Law, T.; Mannu, F.; Kuypers, F. A.; Bast, A.; van der Vijgh, W. J.; Brugnara, C. In vivo reduction of erythrocyte oxidant stress in a murine model of beta-thalassemia. *Haematologica* **89:**1287-1298; 2004.
[25] Kalish, B. T.; Matte, A.; Andolfo, I.; Iolascon, A.; Weinberg, O.; Ghigo, A.; Cimino, J.; Siciliano, A.; Hirsch, E.; Federti, E.; Puder, M.; Brugnara, C.; De Franceschi, L. Dietary omega-3 fatty acids protect against vasculopathy in a transgenic mouse model of sickle cell disease. *Haematologica* **100:**870-880; 2015.
[26] De Franceschi, L.; Brugnara, C.; Rouyer-Fessard, P.; Jouault, H.; Beuzard, Y. Formation of dense erythrocytes in SAD mice exposed to chronic hypoxia: evaluation of different therapeutic regimens and of a combination of oral clotrimazole and magnesium therapies. *Blood* **94:**4307-4313; 1999.
[27] Dalle Carbonare, L.; Matte, A.; Valenti, M. T.; Siciliano, A.; Mori, A.; Schweiger, V.; Zampieri, G.; Perbellini, L.; De Franceschi, L. Hypoxia-reperfusion affects osteogenic lineage and promotes sickle cell bone disease. *Blood* **126:**2320-2328; 2015.

[28] Sabaa, N.; de Franceschi, L.; Bonnin, P.; Castier, Y.; Malpeli, G.; Debbabi, H.; Galaup, A.; Maier-Redelsperger, M.; Vandermeersch, S.; Scarpa, A.; Janin, A.; Levy, B.; Girot, R.; Beuzard, Y.; Leboeuf, C.; Henri, A.; Germain, S.; Dussaule, J. C.; Tharaux, P. L. Endothelin receptor antagonism prevents hypoxia-induced mortality and morbidity in a mouse model of sickle-cell disease. *J Clin Invest* **118:**1924-1933; 2008.
[29] Matte, A.; Bertoldi, M.; Mohandas, N.; An, X.; Bugatti, A.; Brunati, A. M.; Rusnati, M.; Tibaldi, E.; Siciliano, A.; Turrini, F.; Perrotta, S.; De Franceschi, L. Membrane association of peroxiredoxin-2 in red cells is mediated by the N-terminal cytoplasmic domain of band 3. *Free Radic Biol Med* **55:**27-35; 2013.
[30] Cozzi, A.; Corsi, B.; Levi, S.; Santambrogio, P.; Albertini, A.; Arosio, P. Overexpression of wild type and mutated human ferritin H-chain in HeLa cells: in vivo role of ferritin ferroxidase activity. *J Biol Chem* **275:**25122-25129; 2000.
[31] De Franceschi, L.; Platt, O. S.; Malpeli, G.; Janin, A.; Scarpa, A.; Leboeuf, C.; Beuzard, Y.; Payen, E.; Brugnara, C. Protective effects of phosphodiesterase-4 (PDE-4) inhibition in the early phase of pulmonary arterial hypertension in transgenic sickle cell mice. *FASEB J* **22:**1849-1860; 2008.
[32] Niture, S. K.; Khatri, R.; Jaiswal, A. K. Regulation of Nrf2-an update. *Free Radic Biol Med* **66:**36-44; 2014.
[33] Schermuly, R. T.; Dony, E.; Ghofrani, H. A.; Pullamsetti, S.; Savai, R.; Roth, M.; Sydykov, A.; Lai, Y. J.; Weissmann, N.; Seeger, W.; Grimminger, F. Reversal of experimental pulmonary hypertension by PDGF inhibition. *J Clin Invest* **115:**2811-2821; 2005.
[34] Thamsen, M.; Kumsta, C.; Li, F.; Jakob, U. Is overoxidation of peroxiredoxin physiologically significant? *Antioxid Redox Signal* **14:**725-730; 2011.
[35] Adegunsoye, A.; Balachandran, J. Inflammatory response mechanisms exacerbating hypoxemia in coexistent pulmonary fibrosis and sleep apnea. *Mediators Inflamm* **2015:**510105; 2015.
[36] Fartoukh, M.; Emilie, D.; Le Gall, C.; Monti, G.; Simonneau, G.; Humbert, M. Chemokine macrophage inflammatory protein-1alpha mRNA expression in lung biopsy specimens of primary pulmonary hypertension. *Chest* **114:**50S-51S; 1998.
[37] Li, Q.; Qiu, Y.; Mao, M.; Lv, J.; Zhang, L.; Li, S.; Li, X.; Zheng, X. Antioxidant mechanism of Rutin on hypoxia-induced pulmonary arterial cell proliferation. *Molecules* **19:**19036-19049; 2014.
[38] Salabei, J. K.; Cummins, T. D.; Singh, M.; Jones, S. P.; Bhatnagar, A.; Hill, B. G. PDGF-mediated autophagy regulates vascular smooth muscle cell phenotype and resistance to oxidative stress. *Biochem J* **451:**375-388; 2013.
[39] Marino, G.; Niso-Santano, M.; Baehrecke, E. H.; Kroemer, G. Self-consumption: the interplay of autophagy and apoptosis. *Nat Rev Mol Cell Biol* **15:**81-94; 2014.
[40] Xiong, J. Atg7 in development and disease: panacea or Pandora's Box? *Protein Cell* **6:**722-734; 2015.
[41] Lupo, F.; Tibaldi, E.; Matte, A.; Sharma, A. K.; Brunati, A. M.; Alper, S. L.; Zancanaro, C.; Benati, D.; Siciliano, A.; Bertoldi, M.; Zonta, F.; Storch, A.; Walker, R. H.; Danek, A.; Bader, B.; Hermann, A.; De Franceschi, L. A new molecular link between defective autophagy and erythroid abnormalities in chorea-acanthocytosis. *Blood* **128:**2976-2987; 2016.
[42] Zhuang, T.; Zhang, M.; Zhang, H.; Dennery, P. A.; Lin, Q. S. Disrupted postnatal lung development in heme oxygenase-1 deficient mice. *Respir Res* **11:**142; 2010.
[43] Liang, O. D.; Mitsialis, S. A.; Chang, M. S.; Vergadi, E.; Lee, C.; Aslam, M.; Fernandez-Gonzalez, A.; Liu, X.; Baveja, R.; Kourembanas, S. Mesenchymal stromal cells expressing heme oxygenase-1 reverse pulmonary hypertension. *Stem Cells* **29:**99-107; 2011.

[44] Wang, D.; Gladysheva, I. P.; Fan, T. H.; Sullivan, R.; Houng, A. K.; Reed, G. L. Atrial natriuretic peptide affects cardiac remodeling, function, heart failure, and survival in a mouse model of dilated cardiomyopathy. *Hypertension* **63:**514-519; 2014.
[45] Werner, F.; Kojonazarov, B.; Gassner, B.; Abesser, M.; Schuh, K.; Volker, K.; Baba, H. A.; Dahal, B. K.; Schermuly, R. T.; Kuhn, M. Endothelial actions of atrial natriuretic peptide prevent pulmonary hypertension in mice. *Basic Res Cardiol* **111:**22; 2016.
[46] Nakahira, K.; Cloonan, S. M.; Mizumura, K.; Choi, A. M.; Ryter, S. W. Autophagy: a crucial moderator of redox balance, inflammation, and apoptosis in lung disease. *Antioxid Redox Signal* **20:**474-494; 2014.
[47] Ryter, S. W.; Choi, A. M. Autophagy in lung disease pathogenesis and therapeutics. *Redox Biol* **4:**215-225; 2015.
[48] Lee, S. J.; Smith, A.; Guo, L.; Alastalo, T. P.; Li, M.; Sawada, H.; Liu, X.; Chen, Z. H.; Ifedigbo, E.; Jin, Y.; Feghali-Bostwick, C.; Ryter, S. W.; Kim, H. P.; Rabinovitch, M.; Choi, A. M. Autophagic protein LC3B confers resistance against hypoxia-induced pulmonary hypertension. *Am J Respir Crit Care Med* **183:**649-658; 2011.

FIGURE LEGENDS

Fig. 1. The absence of Prx2 promotes lung inflammation, increased pulmonary vascular activation and extra-matrix remodeling markers. A. Comparison of $Prx2^{-/-}$ with WT mice shows an increased peribronchial edema in $Prx2^{-/-}$ mice (upper panel Hematoxylin Eosin x250) and deposits of alpha actin in vascular walls in $Prx2^{-/-}$ mice (lower panel Immunohistochemistry using anti alpha actin antibody x 600)**. B. Upper panel.** BAL protein content from wildtype (WT) and $Prx2^{-/-}$ mice under normoxic condition. Data are presented as means± SD (n=6; *p<0.05 compared to WT mice). **Lower panel.** BAL leukocyte content from wildtype (WT) and $Prx2^{-/-}$ mice under normoxic condition. Data are presented as means± SD (n=6; *p<0.05 compared to WT mice). **C.** Immunoblot analysis with specific antibodies against phospho-NF-kB (P-NF-kB), NF-kB, phospho-Nrf2 (P-Nrf2) and Nrf2 of lung from wildtype (WT) and $Prx2^{-/-}$ mice under normoxic condition. One representative gel from six with similar results is presented. Densitometric analysis of immunoblots is shown in Fig. 1SA. **D.** IL-6, IL-1B , IL-10 mRNA levels in lung tissues (normalized to GADPH) from WT and $Prx2^{-/-}$ mice. * p <0.05 (WT vs $Prx2^{-/-}$). Each sample (WT; $Prx2^{-/-}$) is a pool from 5 mice. Representative of three independent experiments. **E.** Immunoblot analysis with specific antibodies against IL-6, heme-oxygenase 1 (HO-1), endothelin-1 (ET-1), superoxide dismutase (SOD-1), vascular cell adhesion molecule-1 (VCAM-1), platelet derived growth factor-B (PDGF-B) and peroxiredoxin-2 (Prx2) of lung from wildtype (WT) and $Prx2^{-/-}$ mice under normoxic condition. One representative gel

from six with similar results is presented. Densitometric analysis of immunoblots is shown in Fig. 1SC.

Fig. 2. In Prx2$^{-/-}$ mice, hypoxia induces early stage pulmonary hypertension and is associated with activation of redox-related transcriptional factors. A. Comparison of Prx2$^{-/-}$ with WT mice shows a sparse inflammatory infiltrate and an increased peribronchial edema in Prx2$^{-/-}$ mice (upper panel Hematoxylin Eosin x250) and deposits of alpha actin in vascular walls in Prx2$^{-/-}$ mice (lower panel Immunohistochemistry using anti alpha actin antibody x 600). **B.** Representative images of mitral inflow pattern recorded by Doppler echo imaging in wildtype (WT) and Prx2$^{-/-}$ mice under hypoxia as in Fig. 1A. **Lower panels.** Average mitral valve deceleration time (left panel) and pulmonary acceleration time (PAT) to ejection time (ET) ratio (right panel). *p<0.05 and **p<0.01 WT *vs* Prx2$^{-/-}$ mice; #p<0.05 and ##p<0.01 hypoxia *vs* basal by one-way ANOVA followed by Newman-Keuls Multiple Comparison test. **C.** Immunoblot analysis with specific antibodies against peroxiredoxin-2 (Prx2), sestrin-2 and thioredoxin-reductase 1 (Trdx) of lung wildtype (WT) and Prx2$^{-/-}$ mice under normoxia (N) exposed to hypoxia) for 10 hours (10 h), 3 days (3D), 7 days (7D). One representative gel from six with similar results is presented. Densitometric analysis of immunoblots is shown in Fig. 2SA. **D.** Immunoblot analysis with specific antibodies against phospho-NF-kB (P-NF-kB), NF-kB, phospho-Nrf2 (P-Nrf2) and Nrf2 of lung wildtype (WT) and Prx2$^{-/-}$ mice under normoxia (N) and exposed to hypoxia (Hy) for 10 hours (10 h), 3 days (3D), 7 days (7D). One representative gel from six with similar results is presented. Densitometric analysis of immunoblots is shown in Fig. 2SB.

Fig. 3. In Prx2$^{-/-}$ mice, hypoxia is associated with amplified inflammatory response, vascular activation and increased expression of PDGF-B, a marker of extracellular matrix remodeling. A-B. IL-1b **(A)** and IL-6 **(B)** mRNA levels in lung tissues (normalized to GADPH) wildtype (WT) and Prx2$^{-/-}$ mice under normoxia (N) and exposed to hypoxia for 10 hours (10 h), 3 days (3D), 7 days (7D). *p<0.05 compared to wildtype; ^ p value <0.05

compared to normoxic mice. Each sample is a pool from 5 mice. Representative of three independent experiments. **C. Upper panel.** Immunoblot analysis with specific antibodies against endothelin-1 (ET-1) and platelet derived growth factor-B (PDGF-B) of lung from wildtype (WT) and $Prx2^{-/-}$ mice under normoxia (N) and exposed to hypoxia for 10 hours (10 h), 3 days (3D), 7 days (7D). One representative gel from six with similar results is presented. **Lower panel.** Relative quantification of immunoreactivity of ET-1 and PDGF-B in lung from wildtype (WT) and $Prx2^{-/-}$ mice under normoxia (N) and exposed to hypoxiafor 10 hours (10 h), 3 days (3D), 7 days (7D). Data are shown as means ±SD (*n*=6). *p<0.05 compared to wildtype; ^ p<0.05 compared to normoxic mice. The grey area highlights the changes in the ET-1 and PDGF-B expression in the mouse strains at 3 days hypoxia. **D. Upper panel.** Immunoblot analysis with specific antibodies against atrial natriuretic peptide (ANP), vascular adhesion molecule -1 (VCAM-1) and intracellular adhesion-molecule- 1 (ICAM-1) of lung from wildtype (WT) and $Prx2^{-/-}$ mice under normoxia (lane 1 and 2) and exposed to 7 days (7D) hypoxia. One representative gel from six with similar results is presented. **Lower panel.** Relative quantification of immunoreactivity of ANP, VCAM-1, ICAM-1 in lung from wildtype (WT) and $Prx2^{-/-}$ mice under normoxia and exposed to 7 days (7D) hypoxia. Data are shown as means ±SD (*n*=6). *p<0.05 compared to wildtype; ^ p<0.05 compared to normoxic mice.

Fig. 4. The administration of PEP Prx2 prevented the hypoxia induced diastolic dysfunction and increased right ventricular pressure with associated reduction in heart/lung oxidation and vascular endothelial activation. A. Average mitral valve deceleration time (left panel) and pulmonary acceleration time (PAT) to ejection time (ET) ratio (right panel); *p<0.05 vehicle treated $Prx2^{-/-}$ mice *vs* PEP Prx2 treated $Prx2^{-/-}$ mice; by one-way ANOVA followed by Newman-Keuls Multiple Comparison test. Representative images of mitral inflow pattern recorded by Doppler echo imaging in $Prx2^{-/-}$ mice treated with PEP Prx2 are shown in Fig. 4SA. **B.** Immunoblot analysis with specific antibodies

against atrial natriuretic peptide (ANP), vascular adhesion molecule -1 (VCAM-1), intracellular adhesion-molecule- 1 (ICAM-1) and superoxide dismutase-1 (SOD-1) of heart from $Prx2^{-/-}$ mice under normoxia (lane 1) and exposed to 7 days (7D) hypoxia treated with either vehicle or PEP Prx2. One representative gel from six with similar results is presented; GAPDH was used as protein loading control. The related densitomeytric analysis is shown in Fig. 4SB. **C.** Immunoblot analysis with specific antibodies against atrial natriuretic peptide (ANP), vascular adhesion molecule -1 (VCAM-1), intracellular adhesion-molecule- 1 (ICAM-1) and PDGF-B of lung from $Prx2^{-/-}$ mice under normoxia (lane 1) and exposed to 7 days (7D) hypoxia treated with either vehicle or PEP Prx2. One representative gel from six with similar results is presented; GAPDH was used as protein loading control. **Right panel.** Relative quantification of immunoreactivity of ANP, VCAM-1, ICAM-1 and PDGF-B in lung from $Prx2^{-/-}$ mice under normoxia (lane 1) and exposed to 7 days (7D) hypoxia treated with either vehicle or PEP Prx2. Data are shown as means ±SD (*n*=6); ^ $p<0.05$ compared to $Prx2^{-/-}$ normoxic mice; ° $p<0.05$ compared to $Prx2^{-/-}$ treated with vehicle.

Fig. 5. PEP Prx2 administration reduces the hypoxia related abnormal pulmonary vascular leakage and prevents the hypoxia induced lung oxidative damage.

A. BAL protein content and BAL Leukocyte count from under either normoxic condition (N) or exposed to 3 days hypoxia treated with either vehicle or penetrating peptide fusion protein peroxiredoxin-2 (PEP Prx2). Data are presented as means± SD (n=6; *$p<0.05$ compared to WT mice; ^ $p<0.05$ compared to normoxic mice; °$p<0.05$ compare to vehicle treated mice). **B.** The carbonylated proteins (1ug) were detected by treating with DNPH and blotted with anti-DNP antibody. **Lower panel.** Quantification of band area was performed by densitometry and expressed as % of WT. The data are presented as means ± SD of at least three independent experiments *$p<0.05$ compared to WT; ° $p<0.05$ compared to vehicle treated mice (*n*=3). **(C)** mmunoblot analysis with specific antibodies

against phospho-NF-kB (P-NF-kB), NF-kB, phospho-Nrf2 (P-Nrf2) and Nrf2 of lung from wildtype (WT) and Prx2$^{-/-}$ mice under normoxic condition treated with either vehicle or penetrating peptide fusion protein peroxiredoxin-2 (PEP Prx2). One representative gel from six with similar results is presented. Densitometric analysis of immunoblots is shown in Fig.5SA.

Fig. 6. In Prx2$^{-/-}$ mice, PEP Prx2 administration reduces hypoxia related inflammatory vasculopathy and down-regulates hypoxia induced autophagy. A. Immunoblot analysis with specific antibodies against IL-6, endothelin-1 (ET-1), vascular cell adhesion molecule-1 (VCAM-1), platelet derived growth factor-B (PDGF-B) of lung from wildtype (WT) and Prx2$^{-/-}$ mice under normoxic condition treated (lane 1-2) or exposed to hypoxia (3D) and treated with either vehicle or penetrating peptide fusion protein peroxiredoxin-2 (PEP Prx2). One representative gel from six with similar results is presented. Densitometric analysis of immunoblots is shown in Fig. 5SB. **B.** Immunoblot analysis with specific antibodies against LC3I/II, Ulk1, p62, pro-caspase-caspase 3 of lung from wildtype (WT) and Prx2$^{-/-}$ mice under normoxic condition or exposed to 3 days (3D) hypoxia/reoxygenation stress (H/R) treated with either vehicle or penetrating peptide fusion protein peroxiredoxin-2 (PEP Prx2). One representative gel from six with similar results is presented. Densitometric analysis for LC3I/II, Ulk1, p62, pro-caspase-caspase 3 is shown in Fig. 6S. **(C)** Diagram of the novel role of Prx2 in pathogenesis of PAH induced by hypoxia/reoxygenation stress and the interplay between ROS and autophagy. Hypoxia promotes oxidation and increased levels of ROS. Oxidation induced activation of Nrf2, NF-kB and autophagy to limit oxidation related damage of cellular organelles and proteins. In turn p62 is affectd by Nrf2 activation. Up-regulation of Prx2 in response to hypoxia controls oxidation induced by hypoxia. The acute phase response factors modulated by Nrf2 and/or NF-kB are (i) HO-1 and SOD-1 as cytoprotector; (ii) VCAM-1, ET-1, ANP affecting vascular tone and vascular activation; (iii) and PDGF-B, involved in extra-matrix

remodeling and deposition. The hypoxia induced results in (i) conversion of LC3I to LC3II; (ii) clearance of p62 positive lysosomes combined with the activation of caspase 3 pathway. PEP Prx2 treatment prevents the redox related activation of Nrf2, NF-kB and autophagy in wild-type and $Prx2^{-/-}$ mice exposed to hypoxia, resulting in reduction in markers of vascular remodelling, of matrix deposition and abnormalities in pulmonary vascular leakage. ARE: anti-oxidant responsive element; ET-1: endothelin-1; HO-1: heme-oxygenase-1; NF-kB: nuclear factor kappa-light-chain-enhancer of activated B cells; Nrf2: nuclear erythroid factor 2; P: phosphorylate form of indicated transcriptional factor; PAH: pulmonary artery hypertension; PDGF-B: platelet derived growth factor-B; PEP Prx2: recombinant fusion penetrating protein Prx2; Prx2: peroxiredoxin 2; ROS: radical oxygen species; VCAM-1: vascular cell adhesion molecule 1.

Fig. 1

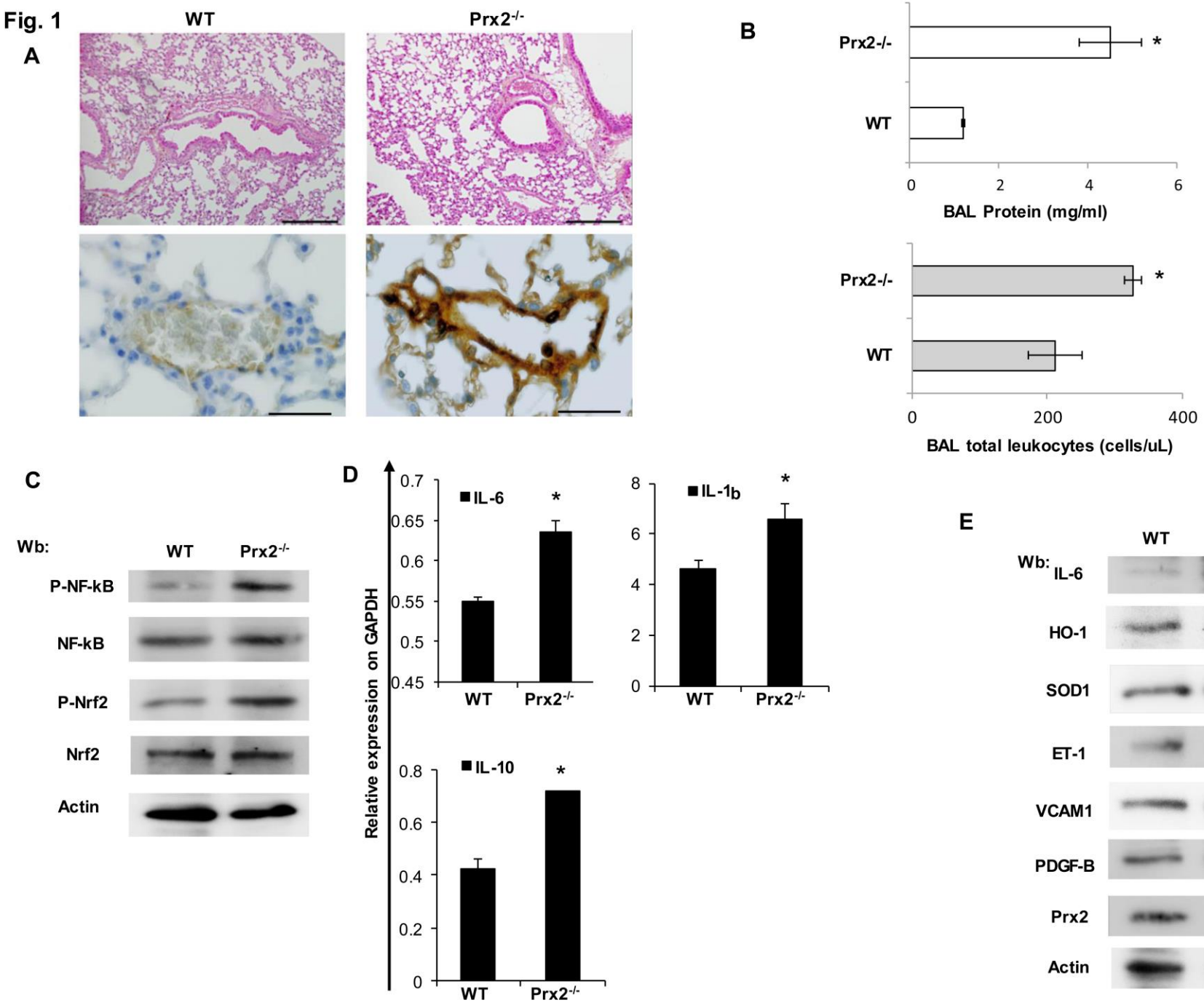
A
WT
Prx2-/-
B
Prx2-/-
WT
*
0
2
4
6
BAL Protein (mg/ml)
Prx2-/-
WT
*
0
200
400
BAL total leukocytes (cells/uL)
C
Wb:
WT
Prx2-/-
P-NF-kB
NF-kB
P-Nrf2
Nrf2
Actin
D
Relative expression on GAPDH
IL-6
*
0.7
0.65
0.6
0.55
0.5
0.45
WT
Prx2-/-
IL-1b
*
8
6
4
2
0
WT
Prx2-/-
IL-10
*
0.8
0.6
0.4
0.2
0
WT
Prx2-/-
E
WT
Prx2-/-
Wb:
IL-6
HO-1
SOD1
ET-1
VCAM1
PDGF-B
Prx2
Actin

Fig. 2

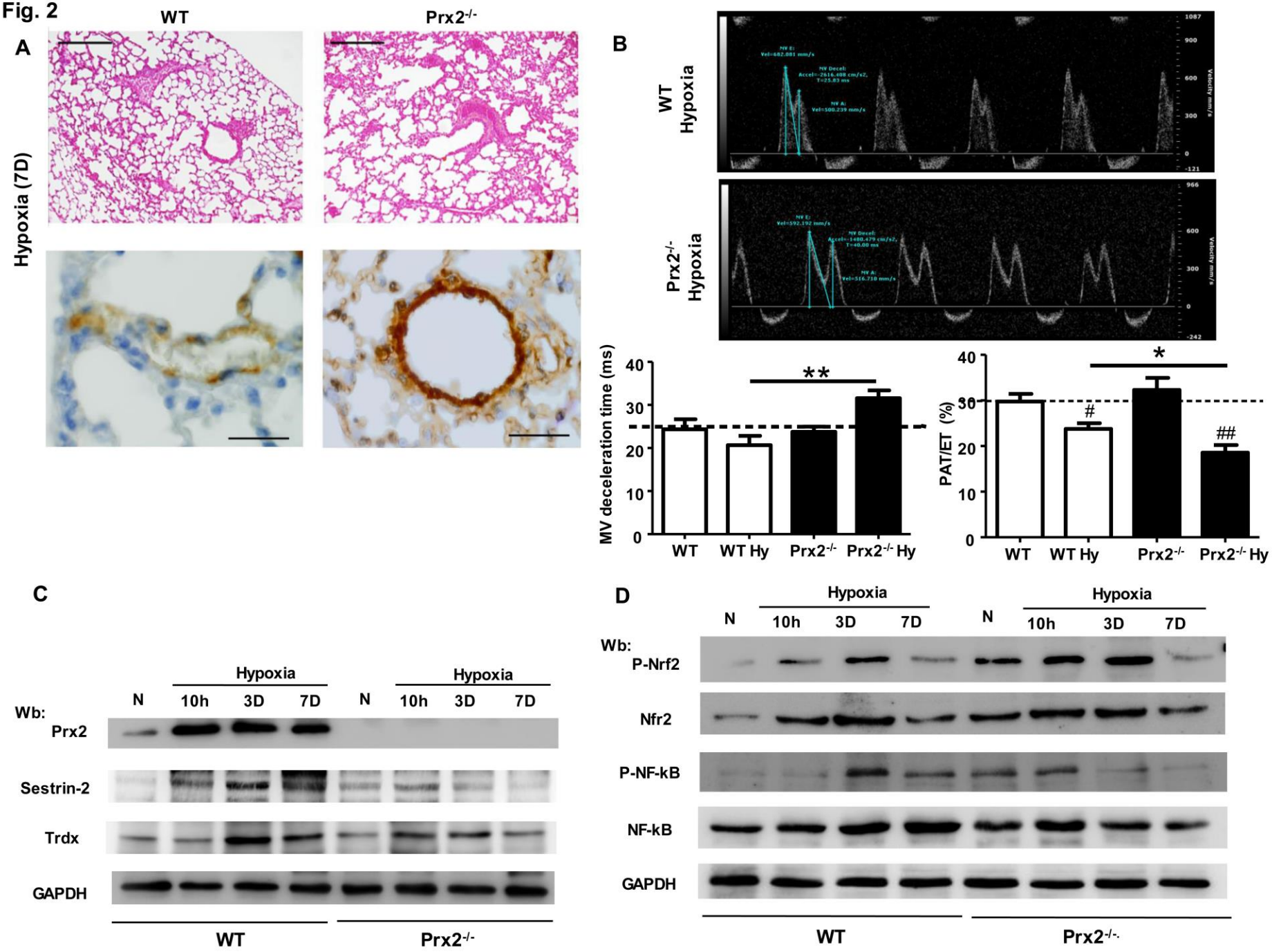
A
WT
Prx2-/-
Hypoxia (7D)
B
WT Hypoxia
Prx2-/- Hypoxia
MV deceleration time (ms)
PAT/ET (%)
WT
WT Hy
Prx2-/-
Prx2-/- Hy
C
Hypoxia
N
10h
3D
7D
Wb:
Prx2
Sestrin-2
Trdx
GAPDH
WT
Prx2-/-
D
Wb:
P-Nrf2
Nfr2
P-NF-kB
NF-kB
GAPDH

Fig. 3

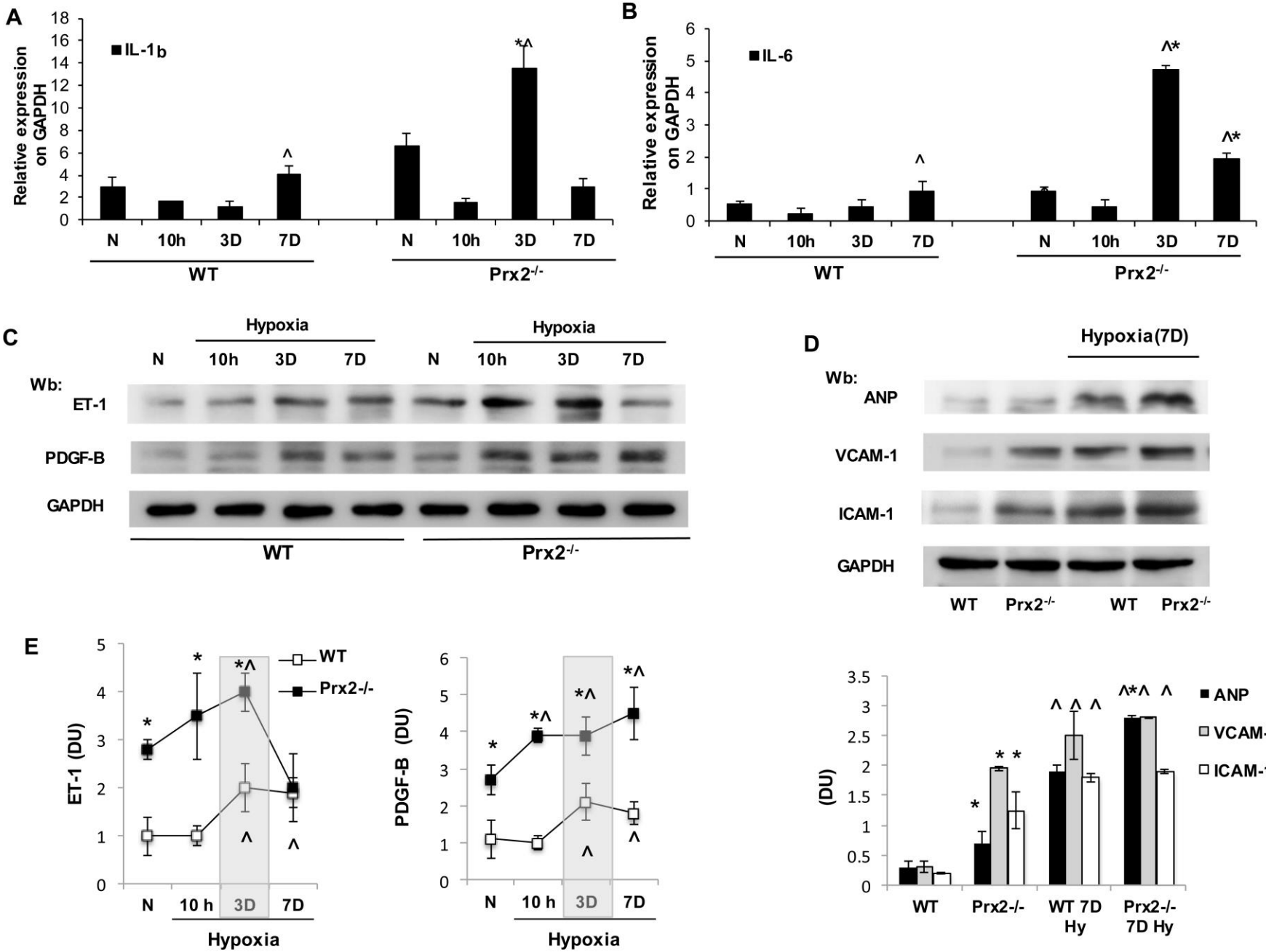
A
IL-1b
Relative expression on GAPDH
N
10h
3D
7D
WT
Prx2-/-
B
IL-6
C
Hypoxia
Wb:
ET-1
PDGF-B
GAPDH
D
Hypoxia(7D)
ANP
VCAM-1
ICAM-1
E
WT
Prx2-/-
ET-1 (DU)
PDGF-B (DU)
Hypoxia
(DU)
WT 7D Hy
Prx2-/- 7D Hy

Fig. 4

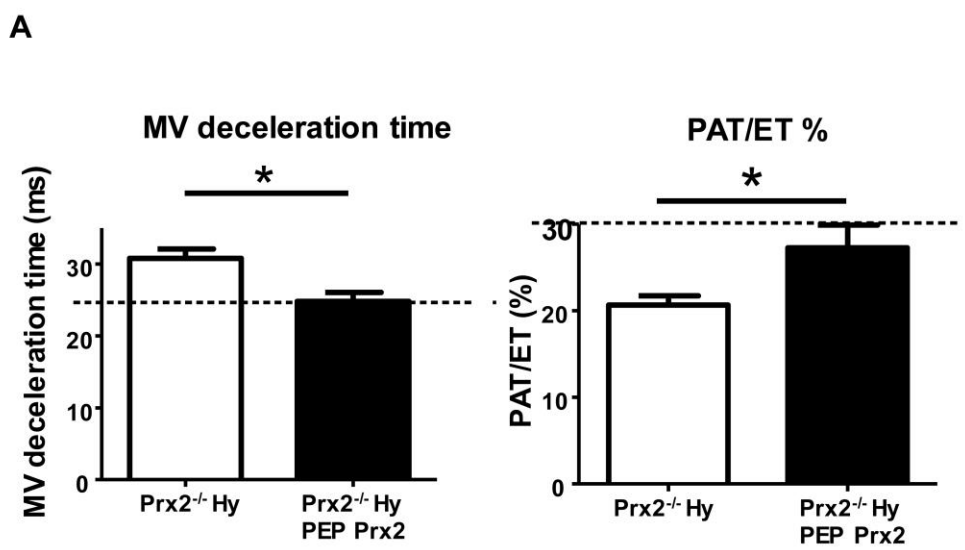
A
MV deceleration time
MV deceleration time (ms)
*
30
20
10
0
Prx2-/- Hy
Prx2-/- Hy PEP Prx2
PAT/ET %
PAT/ET (%)
*
30
20
10
0
Prx2-/- Hy
Prx2-/- Hy PEP Prx2

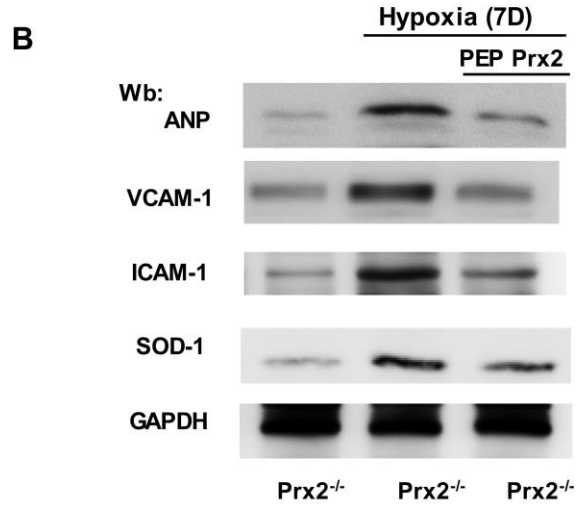
B
Hypoxia (7D)
PEP Prx2
Wb:
ANP
VCAM-1
ICAM-1
SOD-1
GAPDH
Prx2-/-
Prx2-/-
Prx2-/-

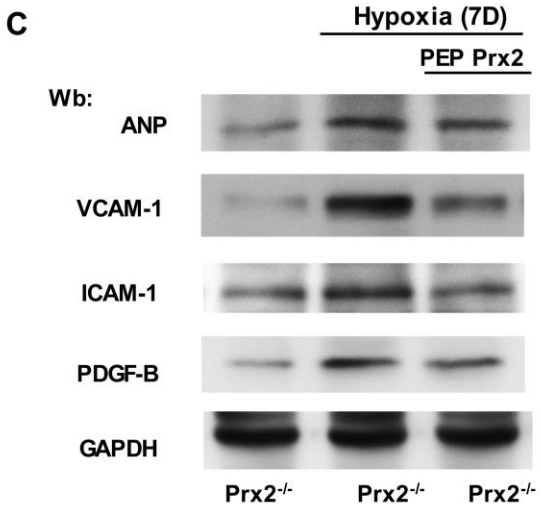
C
Hypoxia (7D)
PEP Prx2
Wb:
ANP
VCAM-1
ICAM-1
PDGF-B
GAPDH
Prx2-/-
Prx2-/-
Prx2-/-

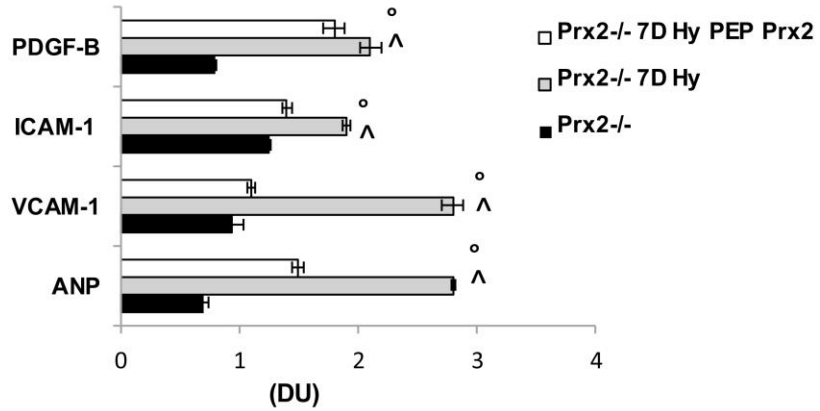
PDGF-B
ICAM-1
VCAM-1
ANP
°
^
0
1
2
3
4
(DU)
Prx2-/- 7D Hy PEP Prx2
Prx2-/- 7D Hy
Prx2-/-

Fig. 5

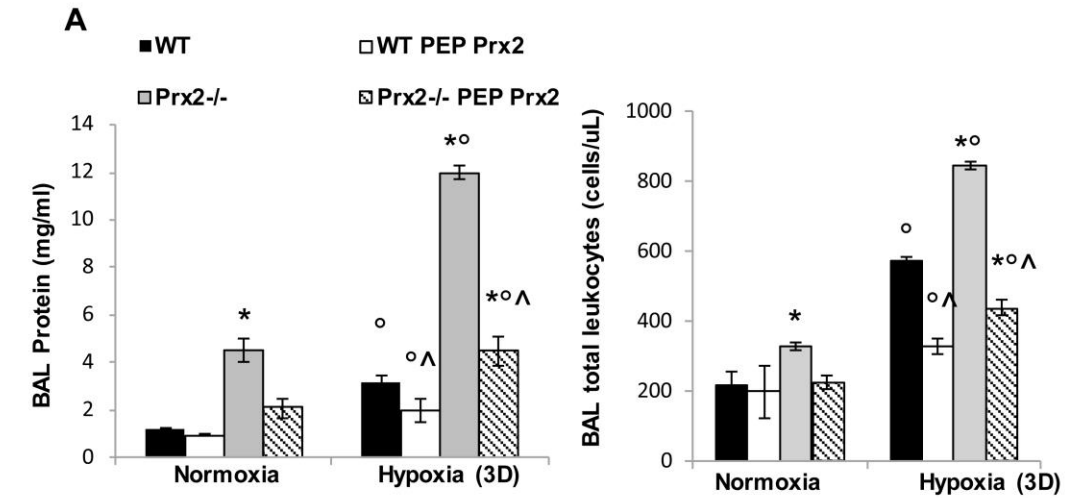
A
WT
WT PEP Prx2
Prx2-/-
Prx2-/- PEP Prx2
BAL Protein (mg/ml)
BAL total leukocytes (cells/uL)
Normoxia
Hypoxia (3D)

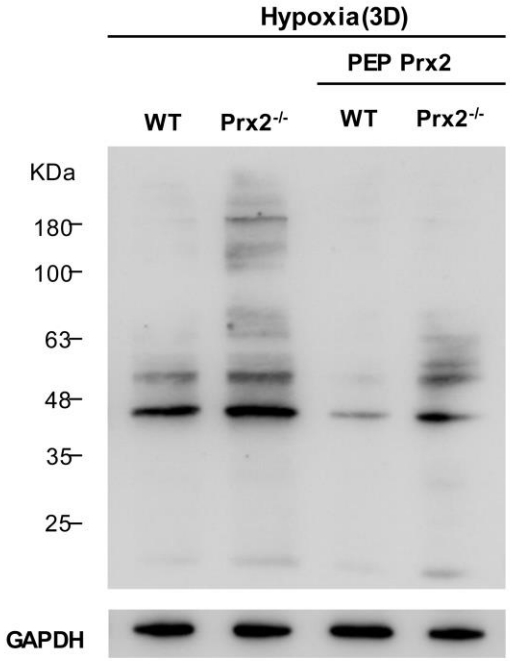
B
Hypoxia(3D)
PEP Prx2
WT
Prx2-/-
KDa
GAPDH

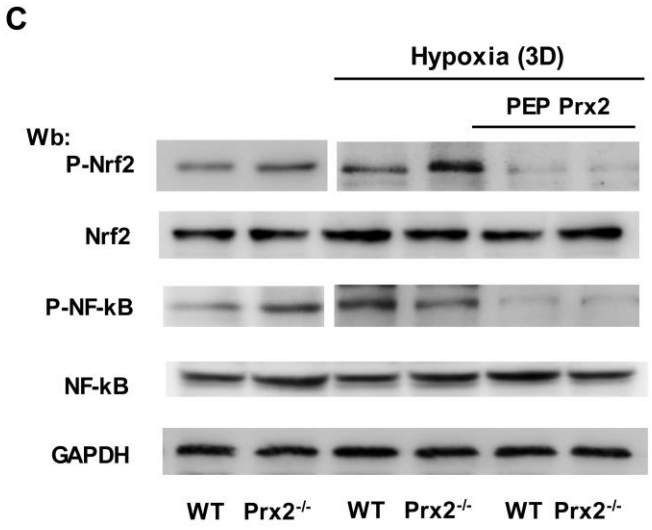
C
Hypoxia (3D)
PEP Prx2
Wb:
P-Nrf2
Nrf2
P-NF-kB
NF-kB
GAPDH
WT Prx2-/- WT Prx2-/- WT Prx2-/-

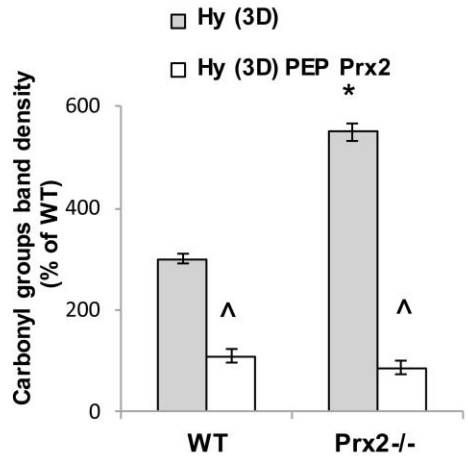
Hy (3D)
Hy (3D) PEP Prx2
Carbonyl groups band density (% of WT)
WT
Prx2-/-

Fig. 6

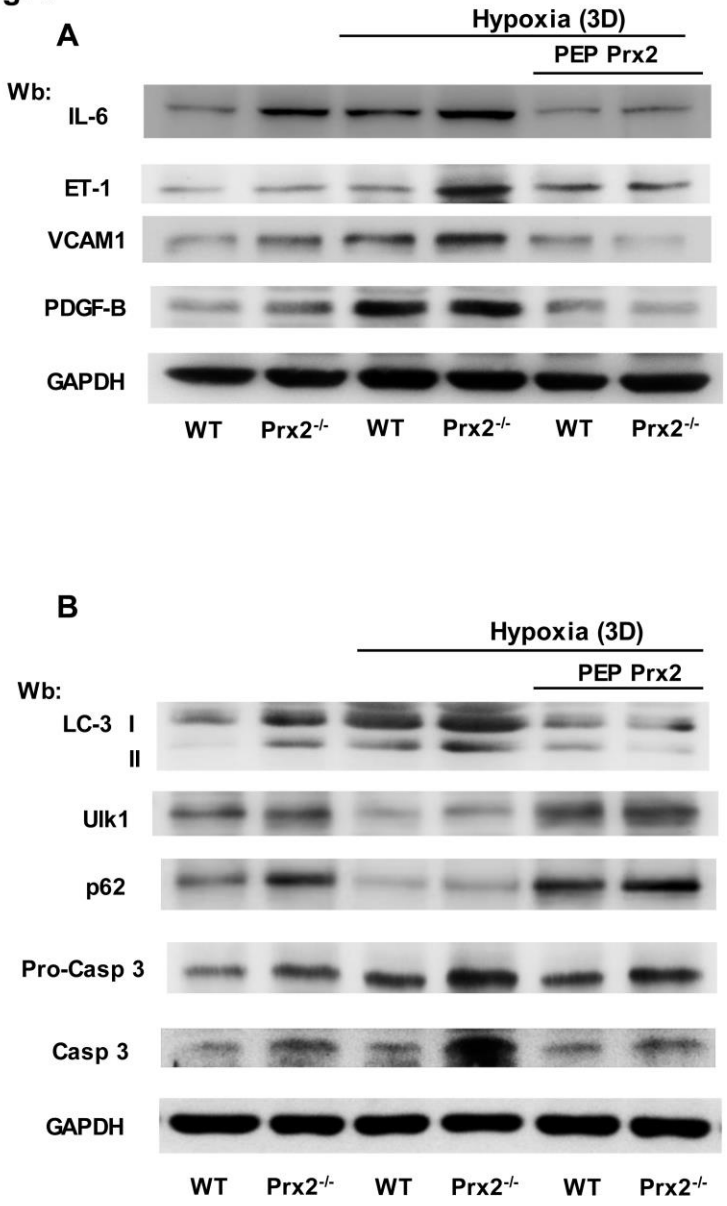
A
Hypoxia (3D)
PEP Prx2
Wb:
IL-6
ET-1
VCAM1
PDGF-B
GAPDH
WT
Prx2-/-
WT
Prx2-/-
WT
Prx2-/-
B
Hypoxia (3D)
PEP Prx2
Wb:
LC-3 I
II
Ulk1
p62
Pro-Casp 3
Casp 3
GAPDH
WT
Prx2-/-
WT
Prx2-/-
WT
Prx2-/-

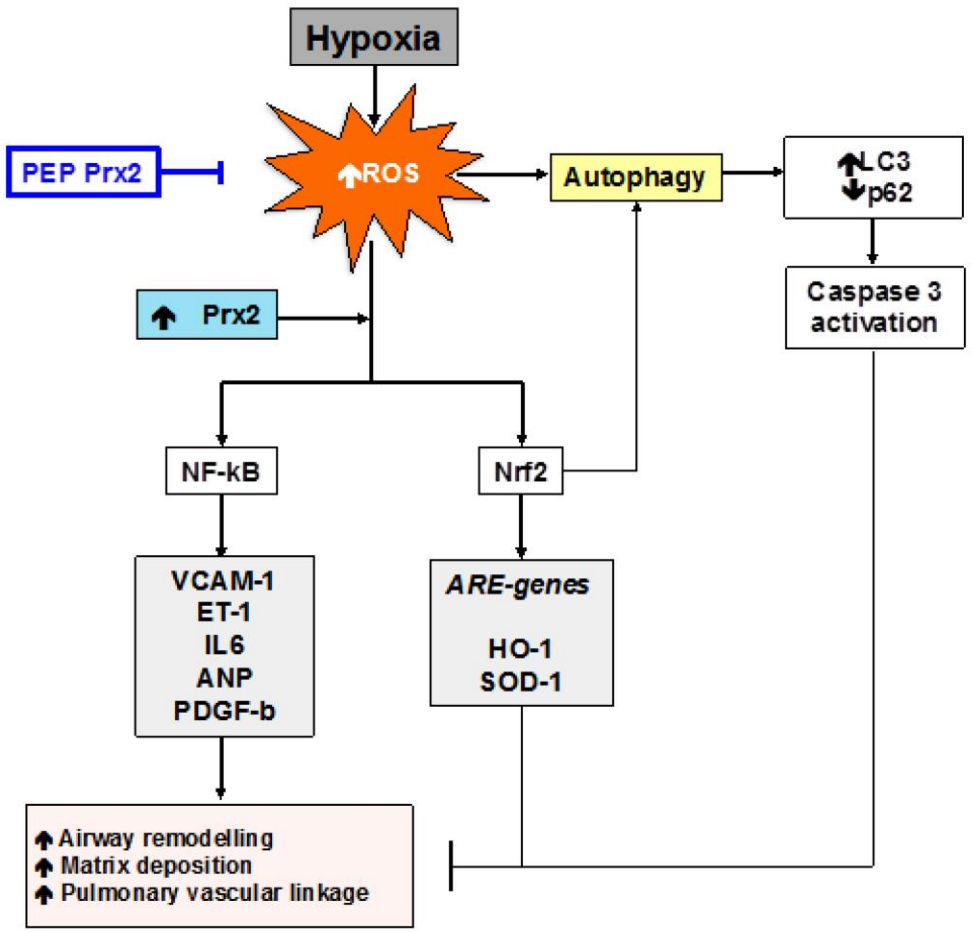
C
Hypoxia
PEP Prx2
ROS
Autophagy
LC3
p62
Caspase 3 activation
Prx2
NF-kB
Nrf2
VCAM-1
ET-1
IL6
ANP
PDGF-b
ARE-genes
HO-1
SOD-1
Airway remodelling
Matrix deposition
Pulmonary vascular linkage

SUPPLEMENTARY MATERIALS AND METHODS

Drugs and chemicals. NaCl, Na_3VO_4, PBS phosphate buffer, bicine, β-mercaptoethanol, sodium dodecyl sulphate (SDS), albumin from bovine serum (BSA) was obtained from Sigma/Aldrich (St Louis, MO, USA), protease inhibitor cocktail tablets were from Roche (Basel, Switzerland) 40% Acrylamide/Bis Solution, 37.5:1 was from BIO-RAD (Hercules, CA, USA), Dulbecco's Phosphate Buffered Saline (DPBS) was from Lonza (Verviers, Belgium), Luminata Forte and Luminata Classico Hrp solutions were from Merck Millipore (Armstadt, Germany).

Immunoblot analysis. Gels were transferred to nitrocellulose membranes for immuno-blot analysis with specific antibody: anti NFkB-phospho-S536 (93H1) (Cell Signaling Technology, Leiden, NL); anti NFkB p65 (C22B4) (Cell Signaling Technology, Leiden, NL); anti Nrf2-phospho-S40 (Clone EP1809Y, AbCam, Cambridge, UK); anti Nrf2 (AbCam, Cambridge, UK); anti Interleukin-6 (IL-6) (Santa Cruz Biotechnology, Heidelberg, Germany); anti Heme Oxygenase-1 (HO-1) (Santa Cruz Biotechnology, Heidelberg, Germany), anti Superoxide Dismutase 1 (SOD-1) (Santa Cruz Biotechnology, Heidelberg, Germany); anti Endothelin-1 (ET-1) (Santa Cruz Biotechnology, Heidelberg, Germany); anti VCAM-1 (R and D Systems, Minneapolis, MN, USA); anti PDGF-B (AbCam, Cambridge, UK); anti Peroxiredoxin 2 (Prx 2, Clone 1E8, AbCam, Cambridge, UK); anti Sestrin-2 (Sigma Aldrich, Saint Louis, MO, USA); anti Thioredoxin Reductase (Trdx) (Santa Cruz Biotechnology, Heidelberg, Germany); anti ANP (Gene Tex, Irvine, CA, USA); anti ICAM-1(AbCam, Cambridge, UK); anti LC3A/B (AbCam, Cambridge, UK); anti ULK-1 (H-240) (Santa Cruz Biotechnology, Heidelberg, Germany); anti APG7 (Atg7) (ProSci, Poway, CA, USA); anti SQSTM1/P62 (AbCam, Cambridge, UK); anti pro Caspase 3 (E83-103) (AbCam, Cambridge, UK). Anti Actin (Sigma Aldrich, Saint Louis, MO, USA) and anti-GAPDH (Sigma Aldrich, Saint Louis, MO, USA) were used as loading control. Secondary donkey anti-rabbit

and anti-mouse IgG HRP conjugated were from GE Healthcare Life Sciences and secondary donkey anti-goat IgG HRP conjugated was from SCBT. Blots were developed using the Immobilon Western Chemiluminescent HRP Substrate from Millipore (Billerica, MA, USA) and images were acquired using Image Quant Las Mini 4000 Digital Imaging System (GE Healthcare Life Sciences). Densitometric analyses were performed using the ImageQuant TL software (GE Healthcare Life Sciences) [26, 30]. Oxidized proteins were revealed by the Oxyblot Protein Oxidation Detection Kit (EMD Millipore). In brief, the soluble protein extracts were derivatized to 2,4-dinitrophenylhydrazone (DNP) and 1 µg was loaded on 12% SDS-PAGE, blotted and incubated with an anti-DNP antibody, followed by an HRP conjugated secondary antibody. The bound activity was revealed by ECL (GE Healthcare). Oxidized proteins were revealed by the Oxyblot Protein Oxidation Detection Kit (EMD Millipore). In brief, the soluble protein extracts were derivatized to 2,4-dinitrophenylhydrazone (DNP) and 1 □g was loaded on 12% SDS-PAGE, blotted and incubated with an anti-DNP antibody, followed by an HRP conjugated secondary antibody. The bound activity was revealed by ECL (GE Healthcare).

Echocardiographic measurements. Transthoracic echocardiography was performed with a Vevo 2100 echocardiograph (Visual Sonics, Toronto, Canada) equipped with a 22-55 MHz transducer (MicroScan Transducers, MS500D). Mice were anesthetized by isoflurane inhalation (2%), maintained by mask ventilation (isoflurane 1%) and placed in a shallow left lateral decubitus position, with strict thermoregulation (37+-1°C) to optimize physiological conditions and reduce hemodynamic variability. LV diastolic function was measured by analyzing the characteristic flow profile of the mitral valve Doppler and tissue Doppler flow, which was visualized in apical four-chamber view. The E deceleration time (DT) was taken from the maximum of the E wave to its baseline. Two-dimensional images of the

pulmonary infundibulum were obtained from the parasternal short-axis view at the level of the aortic valve and pulsed-wave Doppler recording of the pulmonary blood flow was obtained. The pulsed-wave Doppler sample was positioned at the tip of the pulmonary valve leaflets and aligned to maximize laminar flow according to published methods (PMID 20044514). Measurements were performed offline by an operator blinded to the condition or genotype of the mice. The following variables were measured: systolic time-velocity integral of pulmonary flow (TVI, the area under the flow curve), Pulmonary acceleration time (PAT), and right ventricle ejection time (ET). All measurements were averaged on 3 consecutive cardiac cycles per experiment and cardiac function was assessed when heart rate was 400-450 bpm.

Table 1S. Oligonucleotide primer sequences used for qRT-PCR of analyzed mouse genes

Gene symbol	Forward primer (5'- 3')	Reverse primer (5'- 3')
IL-6	5'-GCCAGAGTCCTTCAGAGAGA-3'	5'-**TGGAAATTGGGGTAGGAAGGA**-3'

For Il-1b and IL.10 oligonucleotide primer sequences see *Kalish BT, Matte A, Andolfo I, Iolascon A, Weinberg O, Ghigo A, Cimino J, Siciliano A, Hirsch E, Federti E, Puder M, Brugnara C, De Franceschi L. Dietary ω-3 fatty acids protect against vasculopathy in a transgenic mouse model of sickle cell disease. Haematologica. 2015 Jul;100(7):870-80.*

SUPPLEMENTAL FIGURE LEGENDS

Fig. 1S. A. Relative quantification of immunoreactivity of phospho-NF-kB (P-NF-kB), NF-k, phospho-Nrf2 (P-Nrf2) and Nrf2 of lung from wildtype (WT) and $Prx2^{-/-}$ mice under normoxic condition. Data are shown as means ±SD (*n*=6). *p<0.05 compared to wildtype. **B.** 10 μg of soluble proteins of lung homogenate were tested for MDA-protein adducts. Quantification of band area was performed by densitometry and expressed as % of WT. The data are presented as means ± SD of at least three independent experiments; statistically significant differences were determined by Student's t-test. *p<0.05. **C.** Relative quantification of immunoreactivity of interleukin 6 (IL-6), heme-oxygenase 1 (HO-1), superoxide dismutase 1 (SOD-1); IL-6, heme-oxygenase 1 (HO-1), endothelin-1 (ET-1), vascular cell adhesion molecule-1 (VCAM-1), platelet derived growth factor-B (PDGF-B) and peroxiredoxin-1 (Prx2) of lung from wildtype (WT) and $Prx2^{-/-}$ mice under normoxic condition. Data are shown as means ±SD (*n*=6). *p<0.05 compared to wildtype. **D.** Immunoblot analysis with specific antibodies against superoxide dismutase-1 (SOD-1)m atrial natriuretic peptide (ANP), vascular cell adhesion molecule-1 and intracellular adhesion molecule-1 (ICAM-1) of heart from wildtype (WT) and $Prx2^{-/-}$ mice under normoxia (lane 1-2) and exposed to hypoxia for 7 days (7D) and treated with either vehicle or PEP Prx2. One representative gel from six with similar results is presented. **Right panel.** Relative quantification of immunoreactivity of SOD-1, ANP, VCAM-1 and ICAM-1. Data are shown as means ±SD (*n*=6). *p<0.05 compared to wildtype; ^ p<0.05 compared to normoxic mice.

Fig. 2S. A. Peroxiredoxin-2 (Prx2), Sestrin-2, Thioredoxin- reductase (Trdx) expression in lung tissues (normalized to GADPH) from WT and $Prx2^{-/-}$ mice under normoxia (N) and exposed to hypoxia/reoxygenation (H/R) stress (H/R) for 10 hours (10 h), 3 days (3D), 7 days (7D). *p<0.05 compared to wildtype; ^p<0.05 compared to normoxic condition. Each sample (WT; $Prx2^{-/-}$) is a pool

from 5 mice. Representative of three independent experiments. **B.** Relative quantification of immunoreactivity of phospho-NF-kB (P-NF-kB), NF-kB, phospho-Nrf2 (P-Nrf2) and Nrf2 of lung from wildtype (WT) and $Prx2^{-/-}$ mice under normoxia (N) and exposed to hypoxia/reoxygenation stress (H/R) for 10 hours (10 h), 3 days (3D), 7 days (7D). Data are shown as means ±SD (*n*=6). *p<0.05 compared to wildtype; ^ p<0.05 compared to normoxic mice. The grey area highlights the changes in theP-Nrf2/Nrf2 and P-NF-kB/NF-kB ratio in the mouse strains at 3 days H/R stress.

Fig. 3S. A. Immunoblot analysis with specific antibodies against phospho-Nrf2 (P-Nrf2), Nrf2 phospho-NF-kB (P-NF-kB) and NF-kB of lung from wildtype (WT) and $Prx2^{-/-}$ mice under normoxic condition. One representative gel from six with similar results is presented. **Right panel.** Relative quantification of immunoreactivity of phospho-NF-kB (P-NF-kB), NF-k, phospho-Nrf2 (P-Nrf2) and Nrf2 of lung from wildtype (WT) and $Prx2^{-/-}$ mice under normoxic condition treated with either vehicle or penetrating peptide fusion protein peroxiredoxin-2 (PEP Prx2). Data are shown as means ±SD (*n*=6). *p<0.05 compared to wildtype; °p<005 compared to vehicle treated mice. **B.** Immunoblot analysis with specific antibodies against heme-oxygenase 1 (HO-1), endothelin-1 (ET-1), vascular cell adhesion molecule-1 (VCAM-1), under normoxic condition or exposed to 3 days (3D) hypoxiatreated with either vehicle or penetrating peptide fusion protein peroxiredoxin-2 (PEP Prx2). One representative gel from six with similar results is presented. Right panel. Relative quantification of immunoreactivity of heme-oxygenase 1 (HO-1), endothelin-1 (ET-1), vascular cell adhesion molecule-1 (VCAM-1), platelet derived growth factor-B (PDGF-B) of lung from wildtype (WT) and $Prx2^{-/-}$ mice under normoxic condition treated with either vehicle or penetrating peptide fusion protein peroxiredoxin-2 (PEP Prx2). Data are shown as means ±SD (*n*=6). *p<0.05 compared to wildtype; ° p<005 compared to vehicle treated mice

Fig. 4S. A. Representative images of mitral inflow pattern recorded by Doppler echo imaging in wildtype (WT) and Prx2$^{-/-}$ mice under hypoxia as in Fig. 2B and treated with PEP-Prx2. **B.** Relative quantification of immunoreactivity of atrial natriuretic peptide (ANP), vascular adhesion molecule -1 (VCAM-1), intracellular adhesion-molecule- 1 (ICAM-1) and superoxide dismutase-1 (SOD-1) of heart from Prx2$^{-/-}$ mice under normoxia and exposed to 7 days (7D) hypoxia treated with either vehicle or PEP Prx2. Data are presented as means± SD (n=6); ^p<0.05 compared to Prx2$^{-/-}$ normoxic mice; ° p<005 compared to vehicle treated mice. **C.** The carbonylated proteins (1ug) were detected by treating with DNPH and blotted with anti-DNP antibody. **Lower panel.** Quantification of band area was performed by densitometry and expressed as % of Prx2 under normoxia. The data are presented as means ± SD of at least three independent experiments; ^p<0.05 compared to Prx2$^{-/-}$ normoxic mice; ° p<005 compared to vehicle treated mice. (*n*=3).

Fig. 5S. A. Relative quantification of immunoreactivity of phospho-NF-kB (P-NF-kB), NF-k, phospho-Nrf2 (P-Nrf2) and Nrf2 of lung from wildtype (WT) and Prx2$^{-/-}$ mice under normoxia or exposed to 3 days hypoxia and treated with either vehicle or penetrating peptide fusion protein peroxiredoxin-2 (PEP Prx2). Data are shown as means ±SD (*n*=6). *p<0.05 compared to wildtype; ^ P<0.05 compared to normoxia; °p<005 compared to vehicle treated mice. **B.** Relative quantification of immunoreactivity interleukin 6 (IL-6), endothelin-1 (ET-1), vascular cell adhesion molecule-1 (VCAM-1), platelet derived growth factor (PDGF-B) under normoxic condition or exposed to 3 days (3D) hypoxia/reoxygenation stress (H/R) treated with either vehicle or penetrating peptide fusion protein peroxiredoxin-2 (PEP Prx2). Data are shown as means ±SD (*n*=6). *p<0.05 compared to wildtype; ^p<0.05 compared to normoxic mice; °p<005 compared to vehicle treated mice**. C.** Immunoblot analysis with specific antibodies against heme-oxygenase-1 (HO-1) of lung from wildtype

(WT) and Prx2$^{-/-}$ mice under normoxic condition or exposed to 3 days (3D) hypoxia/reoxygenation stress (H/R) treated with either vehicle or penetrating peptide fusion protein peroxiredoxin-2 (PEP Prx2). One representative gel from five with similar results is presented.

Fig. 6S. Relative quantification of immunoreactivity of LC3I/II, Ulk1, p62, pro-caspase-caspase 3 under normoxic condition or exposed to 3 days (3D) hypoxia/reoxygenation stress (H/R) treated with either vehicle or penetrating peptide fusion protein peroxiredoxin-2 (PEP Prx2). Data are shown as means ±SD (*n*=6). *p<0.05 compared to wildtype; ° p<0.05 compared to vehicle treated mice; ^ p<0.05 compared to normoxic mice.Data are shown as means ±SD (*n*=6). *p<0.05 compared to wildtype; ^ p<0.05 compared to normoxic mice; °p<005 compared to vehicle treated mice.

Fig. 1S

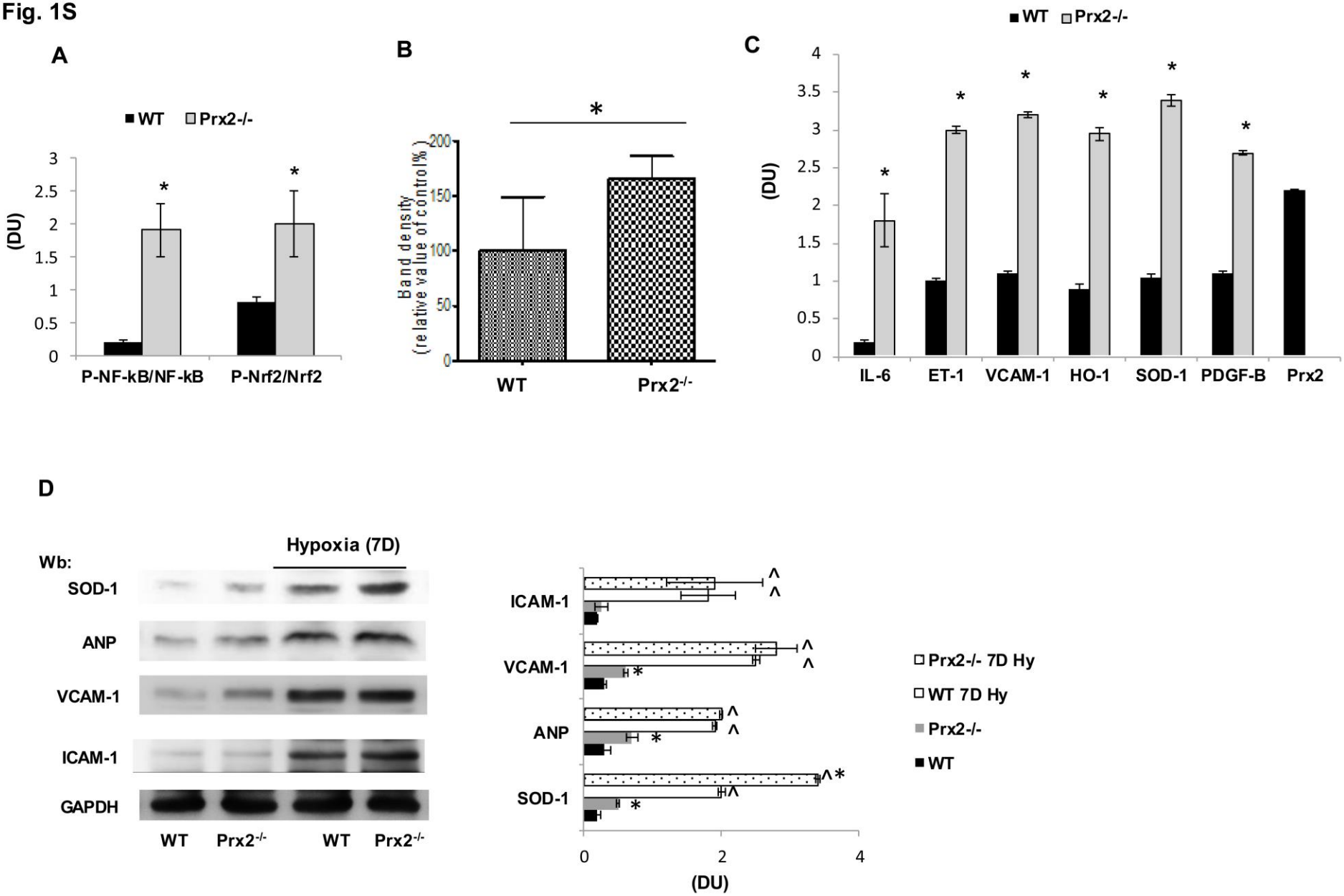
A
WT
Prx2-/-
(DU)
P-NF-kB/NF-kB
P-Nrf2/Nrf2
B
Band density (relative value of control%)
WT
Prx2-/-
C
WT
Prx2-/-
(DU)
IL-6
ET-1
VCAM-1
HO-1
SOD-1
PDGF-B
Prx2
D
Wb:
Hypoxia (7D)
SOD-1
ANP
VCAM-1
ICAM-1
GAPDH
WT
Prx2-/-
WT
Prx2-/-
ICAM-1
VCAM-1
ANP
SOD-1
(DU)
Prx2-/- 7D Hy
WT 7D Hy
Prx2-/-
WT

Fig. 2S

A

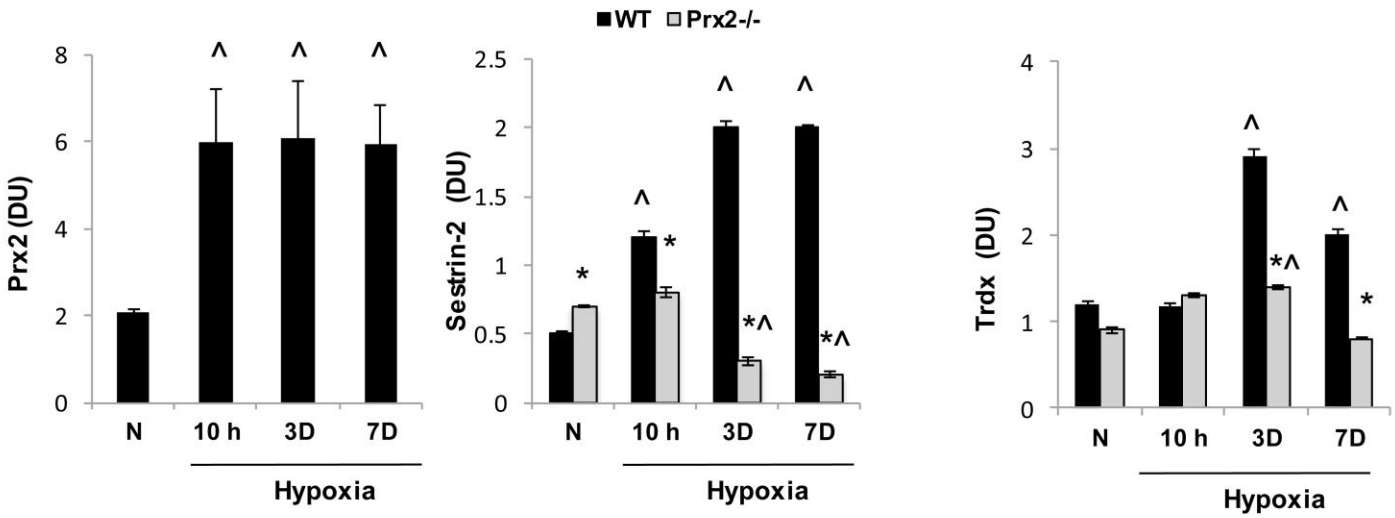
WT
Prx2-/-
Prx2 (DU)
Sestrin-2 (DU)
Trdx (DU)
N
10 h
3D
7D
Hypoxia

B

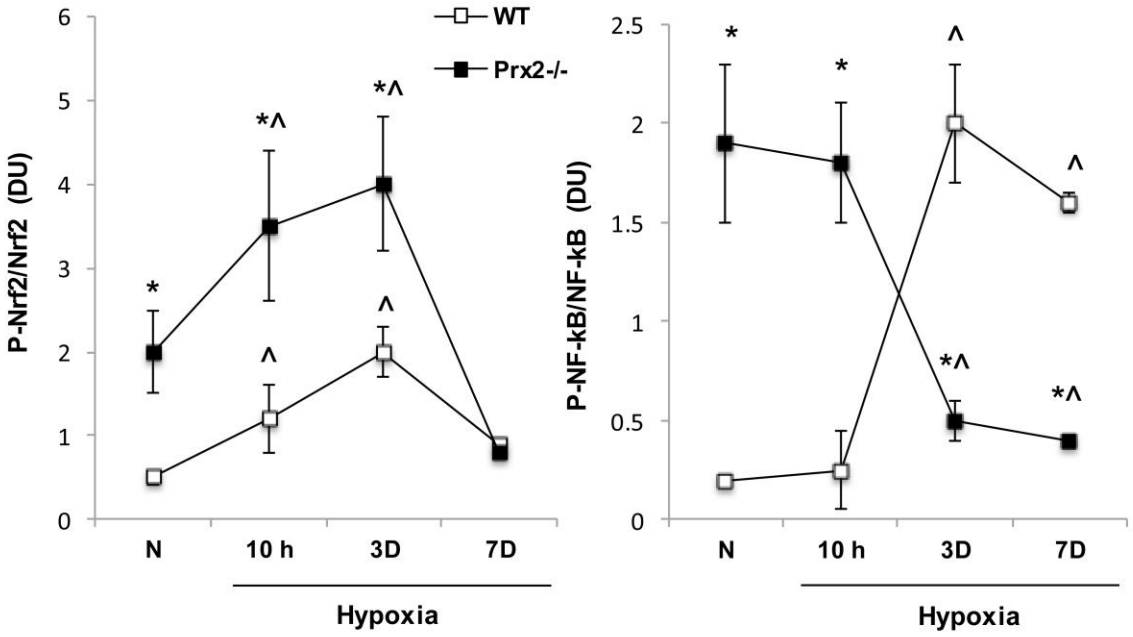
WT
Prx2-/-
P-Nrf2/Nrf2 (DU)
P-NF-kB/NF-kB (DU)
N
10 h
3D
7D
Hypoxia

Fig. 3S

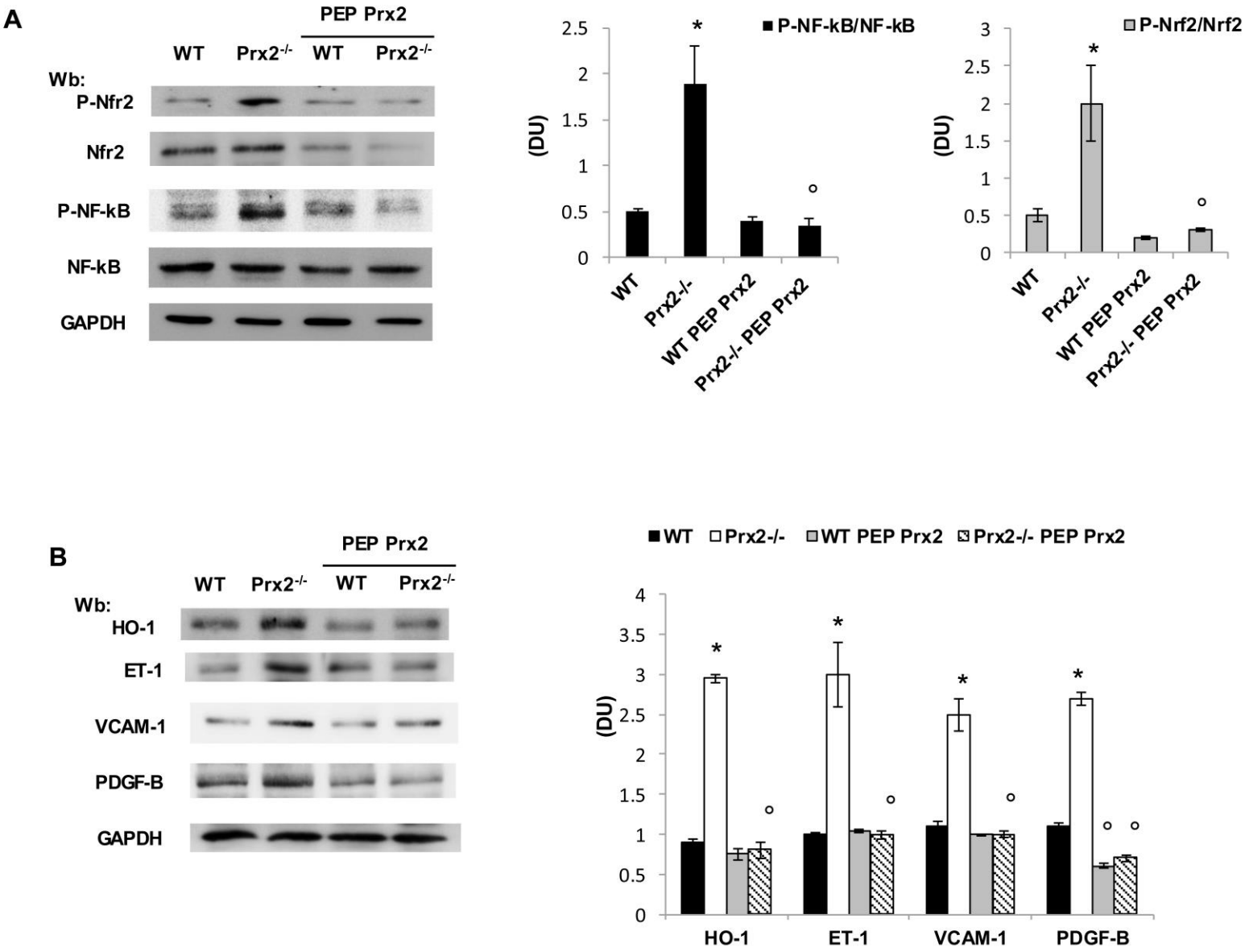
A
PEP Prx2
WT
Prx2-/-
WT
Prx2-/-
Wb:
P-Nfr2
Nfr2
P-NF-kB
NF-kB
GAPDH
P-NF-kB/NF-kB
(DU)
2.5
2
1.5
1
0.5
0
*
°
WT
Prx2-/-
WT PEP Prx2
Prx2-/- PEP Prx2
P-Nrf2/Nrf2
(DU)
3
2.5
2
1.5
1
0.5
0
*
°
WT
Prx2-/-
WT PEP Prx2
Prx2-/- PEP Prx2
B
PEP Prx2
WT
Prx2-/-
WT
Prx2-/-
Wb:
HO-1
ET-1
VCAM-1
PDGF-B
GAPDH
WT
Prx2-/-
WT PEP Prx2
Prx2-/- PEP Prx2
(DU)
4
3.5
3
2.5
2
1.5
1
0.5
0
*
°
HO-1
ET-1
VCAM-1
PDGF-B

Fig. 4S

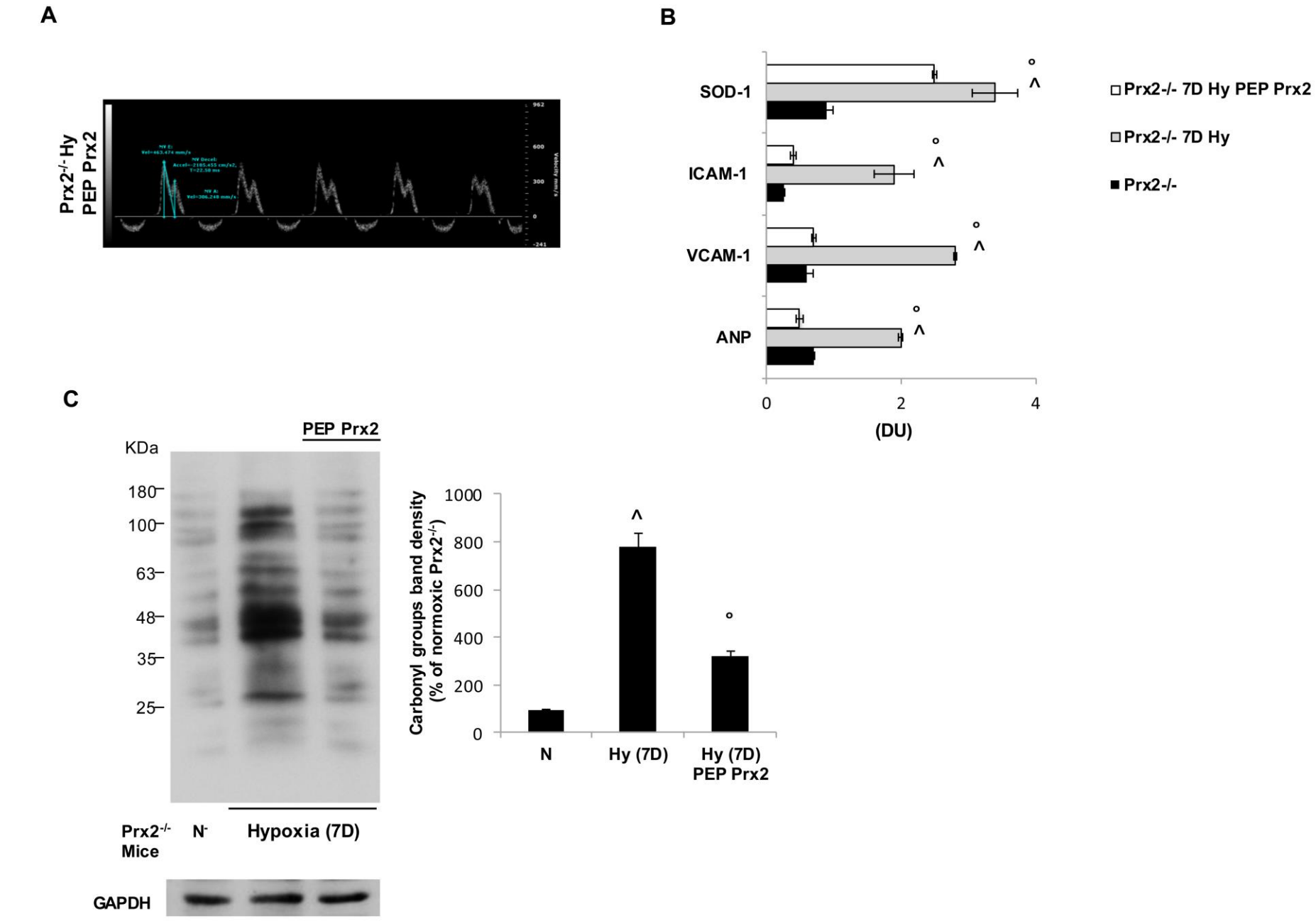
A
Prx2-/- Hy PEP Prx2
B
SOD-1
ICAM-1
VCAM-1
ANP
0
2
4
(DU)
Prx2-/- 7D Hy PEP Prx2
Prx2-/- 7D Hy
Prx2-/-
C
PEP Prx2
KDa
180
100
63
48
35
25
Prx2-/- Mice
N-
Hypoxia (7D)
GAPDH
Carbonyl groups band density (% of normoxic Prx2-/-)
1000
800
600
400
200
0
N
Hy (7D)
Hy (7D) PEP Prx2

Fig. 5S

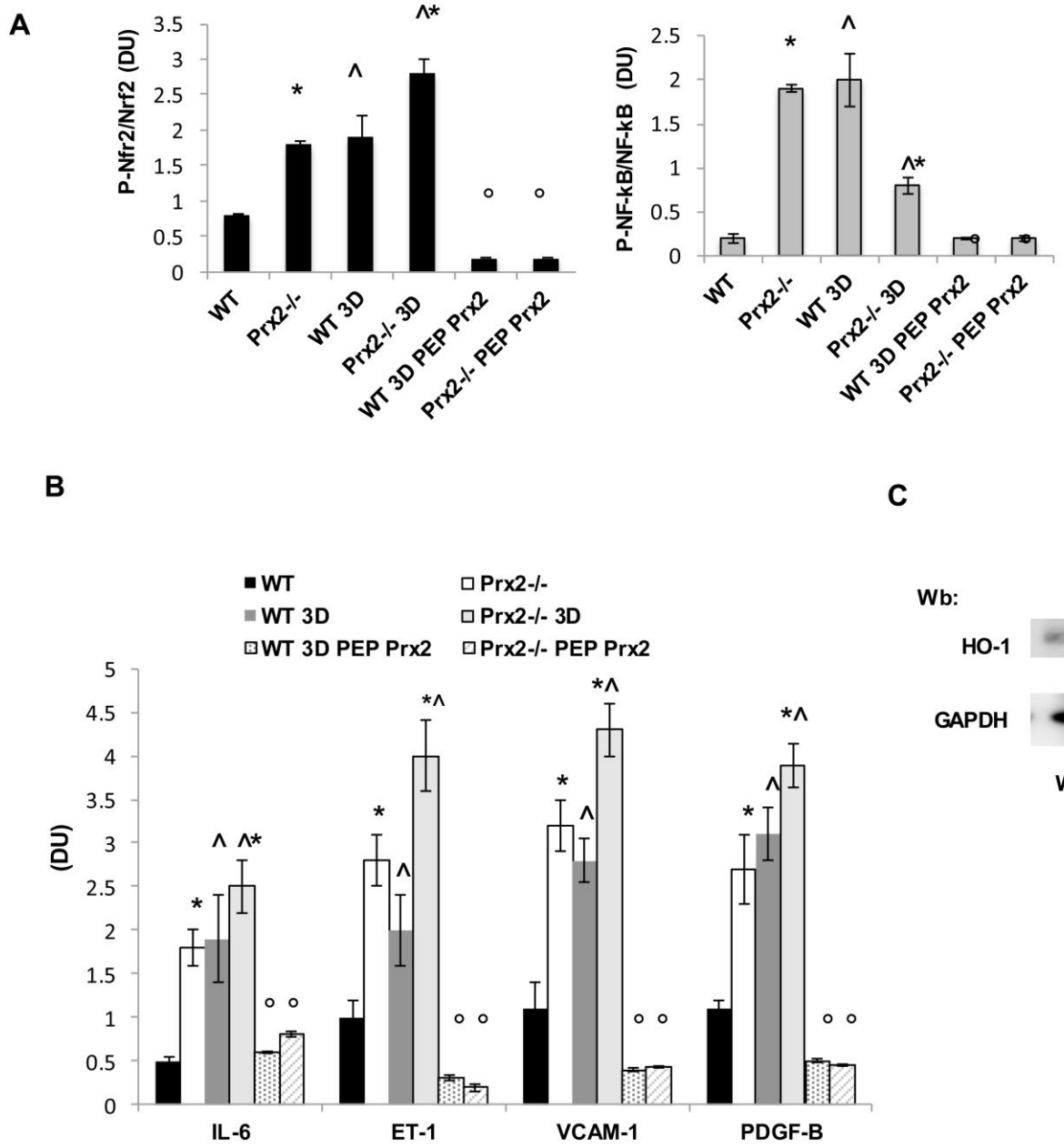
A
P-Nfr2/Nrf2 (DU)
P-NF-kB/NF-kB (DU)
WT
Prx2-/-
WT 3D
Prx2-/- 3D
WT 3D PEP Prx2
Prx2-/- PEP Prx2
B
WT
Prx2-/-
WT 3D
Prx2-/- 3D
WT 3D PEP Prx2
Prx2-/- PEP Prx2
(DU)
IL-6
ET-1
VCAM-1
PDGF-B
C
Hypoxia (3D)
PEP Prx2
Wb:
HO-1
GAPDH
WT
Prx2-/-
WT
Prx2-/-
WT
Prx2-/-

Fig. 6S

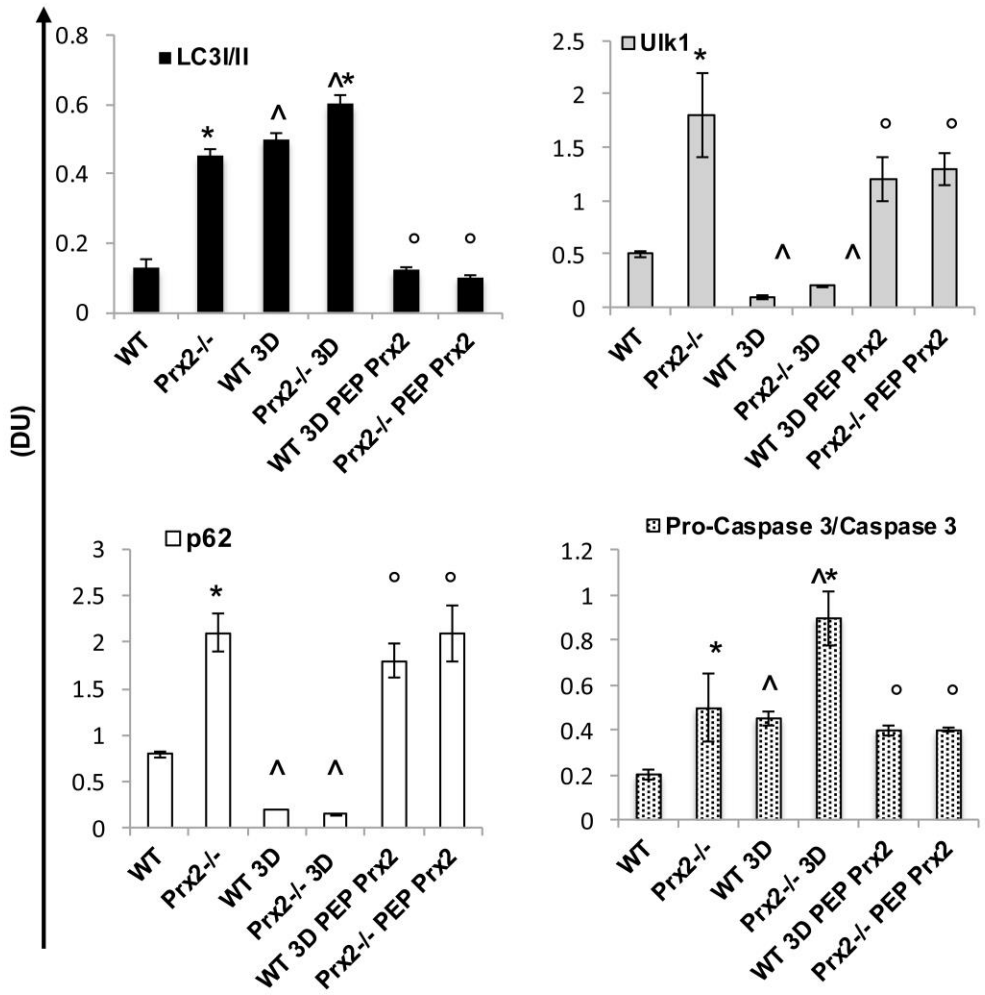
(DU)
LC3I/II
Ulk1
p62
Pro-Caspase 3/Caspase 3
WT
Prx2-/-
WT 3D
Prx2-/- 3D
WT 3D PEP Prx2
Prx2-/- PEP Prx2

Section 2

Peroxiredoxin-2: a novel regulator of iron homeostasis in ineffective erythropoiesis

EF author contributions: EF has carried out experiments, contributed to experimental design, and data analysis.

Haematologica
HAEMATOL/2017/166488
Version 1

PEROXIREDOXIN-2: A NOVEL REGULATOR OF IRON HOMEOSTASIS IN INEFFECTIVE ERYTHROPOIESIS

Alessandro Matte, Luigia de Falco, Enrica Federti, Anna Cozzi, Achille Iolascon, Sonia Levi, Mohandas Narla, Alberto Zamò, Mariasole Bruno, Christophe Lebeouf, Anne Janin, Angela Siciliano, Tom Ganz, Giorgia Federico, Francesca Carlomangno, Carmine Carbone, Davide Melisi, Dae Won Kim, Soo Young Choi, and Lucia De Franceschi

Disclosures: The authors have nothing to disclose.

Contributions: AM, LDF, NM, IA designed the experiments, analyzed data and wrote the paper; TG designed the experiments, wrote the paper and carried out Erfe soluble measurements, FC and SL analyzed the data and wrote the paper; AJ, CL carried out the histologic analysis; AM, AS, EF LDF carried out the experiments; LdF and MB performed the molecular experiments and analyzed the data; GF carried out the analysis on LIC, CSY and KDW generated the PEPPrx2; SL and AC carried out the analysis of liver oxidative stress and high ferritin levels determination; DM and CC carried out EMSA experiments and analyzed data.

PEROXIREDOXIN-2: A NOVEL REGULATOR OF IRON HOMEOSTASIS IN INEFFECTIVE ERYTHROPOIESIS

Alessandro Matte'[1], De Falco Luigia[2], Enrica Federti[1], Anna Cozzi[3], Achille Iolascon[2], Sonia Levi[3, 4], Narla Mohandas[5], Alberto Zamo[6], Mariasole Bruno[2], Christophe Lebouef[7], Anne Janin[7,8,9], Angela Siciliano[1], Tom Ganz, [11] Giorgia Federico[10], Francesca Carlomagno[10], Carmine Carbone,[1] Davide Melisi,[1] Dae Won Kim,[12] Soo Young Choi,[12] Lucia De Franceschi[1]

[1]Dept. of Medicine, University of Verona-AOUI Verona, Verona; Italy; [2] CEINGE and Dept. of Biochemistry, Federico II University, Naples; Italy; [3]Division of Neuroscience, San Raffaele Scientific Institute, Milano, Italy; [4]Vita-Salute San Raffaele University, Milano, Italy; [5] New York Blood Center, NY, USA; [6]Dept. of Pathology and Diagnostic University of Verona-AOUI Verona, Verona; Italy; [7]Inserm, U1165, Paris, F-75010, France; [8]Université Paris 7- Denis Diderot, Paris, France; [9]AP-HP, Hôpital Saint-Louis, Paris, France; [10] Dept of Molecular Medicine and Medical Biotechnologies Federico II University, Naples, Italy; [11] Department of Pathology and Lab of Medicine, UCLA School of Medicine, Los Angels, CA; USA; [12]Department of Biomedical Sciences and Institute of Bioscience and Biotechnology, Hallym University, Chunchon, Korea

Running title: Prx2 limits iron overload cytotoxycity
Words count: 3296

Corresponding Author:
Lucia De Franceschi, MD
Dept of Medicine, University of Verona and AOUI Verona; Policlinico GB Rossi; P.Le L. Scuro, 10; 37134 Verona, Verona; Italy; E-mail: lucia.defranceschi@univr.it; phone+390458124401; Fax +39045802747

ABSTRACT

Peroxiredoxin-2 (Prx2), a typical 2-cysteine-(Cys)-peroxiredoxin, is part of cyto-protective systems, controlling cellular oxidation. Here, we studied the effects of iron-overload (IO) diet on Prx2 knockout mice ($Prx2^{-/-}$). The absence of Prx2 enhanced toxicity due to IO on erythropoiesis. We found that $Prx2^{-/-}$ mice were unable to induce the typical hepcidin (*Hamp*) overexpression in IO due to failure to activate STAT3. In $Prx2^{-/-}$ mice, the loss of *Hamp* response was also observed after single dose oral iron administration. In IO $Prx2^{-/-}$ mice, PEP-fusion-recombinant-Prx2 (PEP-Prx2) treatment significantly (i) decreases ineffective erythropoiesis and ameliorates anemia; (ii) increases STAT3-activation in liver; (iii) up-regulates *Hamp* expression; (iv) reduces liver iron-content. We also confirmed the beneficial effects of PEP-Prx2 on *Hamp* expression through STAT3 activation in β-thalassemic mice. In conclusion, Prx2 limits IO cytotoxicity on erythropoiesis and affects STAT3 transcription activity, regulating *Hamp* expression. Our data collectively support a novel role of Prx2 in iron homeostasis.

INTRODUCTION

Prx2 is a typical 2-cysteine (Cys) peroxiredoxin is part of the cyto-protective systems involved in the tight control of the levels of reactive oxygen species (ROS) generated during cell's life span or related to cellular stress such as in iron-overload (1-4). Since ROS might also function as a second messenger through transient oxidation of cysteine residues on signaling targets, it has been proposed that the redox state of cysteine residues of Prxs might control the redox state of partner proteins possibly with on-off switching mechanism of proteins sensitive to redox conditions (5, 6).

Recently, we reported that Prx2 is a key anti-oxidant system in both stress and pathologic erythropoiesis characterized by oxidative damage, such as β-thalassemia (4, 7-10). The ablation of Prx2 on β-thalassemic mouse genotype ($Prx2^{-/-}Hbb^{3th/+}$) worsens the ineffective erythropoiesis with increased ROS accumulation, amplified cell apoptosis and severe extra-medullary erythropoiesis compared to β-thalassemic ($Hbb^{3th/+}$) mice (9). In addition, $Prx2^{-/-}Hbb^{3th/+}$ mice display higher iron accumulation in the liver compared to either $Prx2^{-/-}$ or $Hbb^{3th/+}$ mice (9). Administration of Prx2 fused to cell-penetrating carrier PEP (cell penetrating peptide; PEP Prx2) significantly ameliorated anemia in $Hbb^{3th/+}$ mice, while decreasing the extent of liver and spleen iron overload (9).

Iron homeostasis is tightly regulated by a complex system converging on the iron-regulatory hormone hepcidin (*Hamp*), which interacts with the cellular iron exporter ferroportin to control iron acquisition, storage and plasma iron concentrations (11-17). Since the liver is the main site for iron accumulation, redox-sensitive transcription factor such as STAT3 might be activated in response to iron accumulation and oxidative stress (5, 18-21). Recent studies have noted that physiological levels of ROS promote STAT3 activation and up-regulate *Hamp* expression, independently of the well-documented role of IL-6 signaling (18). Importantly, high ROS levels down-regulate *Hamp* expression. (20). It is of note that STAT3 transcription activity has been recently linked to Prx2 in presence of low levels of H_2O_2 (5).

In the present study, we explored the effects of iron overload (IO) in a mice genetically lacking Prx2. The absence of Prx2 results in severe anemia and is associated with the lack of *Hamp* induction in response to either IO or following the administration of a single dose of oral iron through the loss of STAT3 activation in response to IO. Treatment with fused recombinant PEP Prx2 restored both STAT3 activation and Hamp expression in response to IO. These findings were also confirmed in $Hbb^{3th/+}$ mice, used as a mouse

and immune-blot protocols used for the analysis of sorted erythroblasts are described in supplementary materials and methods (29, 30).

Generation of recombinant-PEP-1 Prx2 fusion protein (PEP Prx2). The fusion protein PEP Prx2 was generated as previously reported (9, 31).

Histological analysis of spleen and liver. Immediately following dissection, spleen and liver were formalin-fixed and paraffin-embedded (32). Details are presented in supplementary materials and methods.

Molecular analysis of liver. Protocols used for RNA isolation, cDNA preparation and quantitative qRT-PCR have been previously described. (9, 32) Detailed primer sequences are available on request and shown in Table 1S. Liver immuno-blot analysis was performed as previously described (33, 34).

EMSA. Liver nuclear extract was used for non-radioactive electrophoretic mobility shift assay. Detailed protocol is described in supplementary material and methods (35).

Ferroportin-1 quantification. Ferroportin (Fpn1) quantitation was carried out as previously reported (25). Detailed protocol is described in supplementary material and methods (25).

Ferritin quantification. Ferritin content was determined by ELISA as previously described (36).

Dectection of oxidized proteins and peroxidation of lipids. Oxidized proteins were monitored using Oxyblot Protein Oxidation Detection Kit (EMD Millipore) as previously reported (36, 37). The extent of lipid peroxidation was determined by measuring of MDA levels.

Statistical analysis. Data were analyzed using the 2-way analysis of variance (ANOVA) for repeated measures between the mice of various mouse groups. A difference with a $P < 0.05$ was considered significant.

RESULTS

Prx2 is an important cyto-protective factor in modulating erythropoiesis under condition of excess iron

In iron-overloaded mice, the ablation of Prx2 is associated with early development of a more severe anemia compared to wildtype (Fig. 1A). As shown in Fig. 1A, $Prx2^{-/-}$ mice showed a rapid drop in hemoglobin (Hb) levels with associated increase in mean cell volume (MCV), red cell distribution width (RDW; Fig. 1SA) and mean cell hemoglobin content (MCH wildtype day 0: 14.5±1.2 *vs* day 60: 17.9±1.1 pg; $p<0.05$; MCH $Prx2^{-/-}$ day 0: 13.9±0.4 *vs* day 60: 18.4±1.9 $p<0.05$) and a reduction in reticulocyte count compared to wildtype mice (Fig. 1A, right panel). These findings are compatible with the appearance of a severe anemia in $Prx2^{-/-}$ in conjunction with significant reduction in $CD44+TER119+FSC^{high}$ erythroid cells in both bone marrow and spleen in IO $Prx2^{-/-}$ mice compared to standard diet $Prx2^{-/-}$ mice (Fig. 1B, upper panel; Fig. 1SB; 1SC). IO cytotoxic effect on $Prx2^{-/-}$ erythroid precursors was also supported by the reduction in the ratio between immature/ mature erythroblasts compared to wildtype (Fig. 1B, lower panel). This finding in combination with marked reduction in reticulocyte count in the context of severe anemia in IO $Prx2^{-/-}$ mice implies marked ineffective erythropoiesis. Indeed, in both mouse strains at 60 days of IO diet, we found a marked increase in the amount of apoptotic orthochromatic erythroblasts compared to standard diet groups (Fig. 1SD). However, the extent of apoptosis was more pronounced in IO $Prx2^{-/-}$ mice compared to IO wildtype mice. It is notable that wildtype mice showed increased Prx2 expression in erythroblasts in response to IO (Fig. 1SE). Erythropoietin expression was significantly increased in both mouse strains in response to anemia induced by IO, but we found higher levels in IO $Prx2^{-/-}$ mice than in IO WT animals (Fig. 1SF). The lack of reticulocyte response in the context of very high levels of EPO in IO $Prx2^{-/-}$ mice implies inability of erythroblasts to complete terminal erythroid differentiation.

Since erythroferrone (Erfe; *Fam132b*) has been linked to iron homeostasis and erythropoiesis, (11, 12) we evaluated *Erfe* expression in sorted erythroblasts from both mouse strains. We used the CD44-TER119 strategy to isolate and purify erythroid cells (9, 25, 28). Under standard diet in wildtype mice, we found up-regulation of *Erfe* gene expression in orthochromatic erythroblasts (pop IV) compared to polychromatic erythroblasts (pop III) (Fig. 1C). Conversely, we observed up-regulation of *Erfe* expression in $Prx2^{-/-}$ polychromatic erythroblasts (Pop III) and down-regulation of *Erfe* in $Prx2^{-/-}$ orthochromatic erythroblasts (Pop IV) compared to wildtype (Fig. 1C). This altered

expression of *Erfe* might be related to ineffective erythropoiesis in Prx2$^{-/-}$, which is similar to that described in β-thalassemic mice (Hbb$^{3th/+}$) (9). Our data are in agreement with up-regulation of *Erfe* previously reported in polychromatic erythroblasts from Hbb$^{3th/+}$ mice (11). IO promoted down-regulation of *Erfe* to similar extent in both mouse strains (Fig. 1C) and this is associated with almost undetectable soluble levels of Erfe in both IO mouse strains (data not shown). Collectively these data suggest that the absence of Prx2 is associated with amplified iron cytotoxicity.

Iron overloaded Prx2$^{-/-}$ mice show down-regulation of hepcidin expression and reduced STAT3 activation

We then evaluated liver iron concentration (LIC), which was similarly increased in both mouse strains exposed to IO (data not shown). However, Perl's staining analysis revealed different patterns of iron distribution in cellular components of the liver. In Prx2$^{-/-}$ mice, iron accumulated in hepatocytes and Kupffer cells, while, iron-deposits were present only in hepatocytes of wildtype liver (Fig. 1D). This may be related to hyper- activation response of macrophages lacking Prxs as previously shown in other models (38, 39). Iron distribution pattern in the spleen of Prx2$^{-/-}$ mice was similar to that of the liver (Fig. 2SA). Oxyblot analysis and quantification of MDA levels were used to evaluate the degree of protein oxidation and lipid peroxidation respectively in the liver. Both oxidative processes were significantly increased in IO Prx2$^{-/-}$ compared to wildtype mice (Fig. 2A). The levels of ferritin H chain, the expression of which increases in response to IO and oxidative stress (36, 37), were higher in Prx2$^{-/-}$ mice than in wildtype mice (Fig. 2SB).

Expression of Prx2 in liver was significantly increased in IO wildtype compared to animals under standard diet, indicating that Prx2 is part of the adaptive liver cellular response to IO (Fig. 2B). Indeed, we found increase in other known cyto-protective systems, including Nqo1 and HO-1 (Fig. 2B). It is interesting to note that up-regulation of Nqo1 and HO-1 in response to IO was higher in Prx2$^{-/-}$ mice than in wildtype, while basal levels were similar in the two strains (Fig. 2B). These findings suggest that in the absence of Prx2 there is a severe oxidative stress in liver of IO Prx2$^{-/-}$ compared to IO wildtype mice.

Since Prx2 has been recently linked to STAT3 function and oxidative stress, we then evaluated the activity of STAT3, which contributes to the regulation of *Hamp* expression (18, 20). In IO wildtype mice, we found increased activation of STAT3 compared to mice on standard diet. However, this activation was absent in IO Prx2$^{-/-}$ mice (Fig. 2C, upper panel; Fig. 2SC). This finding was further confirmed by DNA-binding activity of STAT3, which was increased in liver from WT IO and markedly reduced in IO Prx2$^{-/-}$ mice (Fig. 2C,

lower panel). No major change in liver IL-6 expression was detectable in either IO mouse strains (data not shown, see also Fig. 7SB). As expected we found up-regulation of *Hamp* in IO wildtype mice, while no change in *Hamp* expression was observed in IO Prx2$^{-/-}$ compared to standard diet Prx2$^{-/-}$ mice (Fig. 2D). To better understand the role of Prx2 in the signaling pathway involved in *Hamp* regulation, we evaluated Smad 1/5 activation and *Id1* expression in IO mice (14). Smad activation and up-regulation of *Id1* in response to IO was similar in both mouse strains (Fig. 2SD, 3SA). We found reduced staining for Fpn1 in C-duodenal from IO WT mice compared to standard diet, while no changes were observed in Prx2$^{-/-}$ mice with and without IO (Fig. 3SB).

Prx2 is required to ensure adequate hepcidin expression in response to acute iron stimuli

In order to better understand the interplay between Prx2 and *Hamp* in response to iron, we administered single dose of oral iron (acute iron, AI). Prx2 liver expression significantly increased in WT mice at 24 hours after AI (Fig. 2E, 3SC left panel). STAT3 was activated in WT but not in Prx2$^{-/-}$ mice treated with AI (Fig. 2E, 3SC right panel). No change in IL-6 levels was observed in both mouse strains exposed to AI (data not shown). As expected, we found significantly increased *Hamp* expression in liver from WT mice but not in Prx2$^{-/-}$ mice (Fig. 2F). No changes were observed in soluble levels of Erfe in repose to acute iron administration in both mouse strains (data not shown). *Id1* expression was similar in both mouse strains after AI (see Fig. 3SD).

We then evaluated the effects of low iron (LI) diet on hematologic phenotype and *Hamp* expression in both mouse strains. Mice were studied at 3 and 7 weeks of LI. *Hamp* expression was significantly reduced in both mouse strains at 3 and 7 weeks of LI (Fig. 4SA for Perls staining; Fig. 4SB). Soluble Erfe levels were significantly increased following 7 weeks of LI diet in both mouse strains (data not shown). EPO expression was significantly increased at 7 weeks of LI in both mouse strains (Fig. 4SC).

Collectively these data indicate that in Prx2$^{-/-}$ mice *Hamp* response to iron overload is absent and is associated with loss of STAT3 transcription activity.

Recombinant fused PEP Prx2 ameliorates the IO induced anemia and is associated with increased *Erfe* expression

Recently, we showed that PEP Prx2 is able to reduce ineffective erythropoiesis, ameliorate anemia and decrease liver iron-overload in a mouse model for β-thalassemia (9). To determine whether PEP Prx2 also protects erythroid cells against the toxicity of IO, we administrated PEP Prx2 to wildtype and Prx2$^{-/-}$ mice under IO diet. PEP Prx2

administration was started at the same time as the IO diet. In both IO wildtype and IO $Prx2^{-/-}$ mice, PEP Prx2 to a large extent rescued the IO induced hematologic phenotype with (i) amelioration of red cell morphology and reduction in hemichromes (Fig. 5SA, 5SB); (ii) increased Hb levels and reduced RDW (Fig. 3A upper panel, 5SC); (iii) increased reticulocyte count (Fig. 3A, lower panel). In agreement, we found a significant increase in total erythroblasts (CD44+TER119+ FSC^{high}) in both mouse strains exposed to IO and treated with PEP Prx2 (Fig. 3B). We also noted a significant reduction in the amount of IO-induced apoptotic orthochromatic erythroblasts in both mouse strains treated with PEP Prx2 (Fig. 5SD). The decrease in IO induced ineffective erythropoiesis by PEP Prx2 was associated with up-regulation of *Erfe* in both polychromatic and orthochromatic erythroblasts from wildtype and polychromatic erythroblasts from $Prx2^{-/-}$ mice compared to erythroid precursors from IO treated mice (Fig. 3C).

PEP Prx2 treatment supports STAT3 activation with up-regulation of *Hamp* expression in response to IO

PEP Prx2 treated IO mice showed a marked reduction of iron overload in liver (Fig. 3D, 6SA) and reduced protein oxidant damage (Fig. 6SB). In both PEP Prx2 treated IO mouse strains, we found a marked activation of STAT3 compared to vehicle treated mice (Fig. 3D, 6SC). *Hamp* expression was significantly increased in both PEP Prx2 treated IO mouse strains (Fig. 3E). Smad activation was reduced by PEP Prx2 treatment in both IO mouse strains compared to vehicle treated IO mice (Fig. 6SD). No changes in IL-6 expression were observed in liver from PEP Prx2 treated IO mice (Fig. 7S). These findings imply PEP Prx2 blunts IO-related Smad activation, but promotes STAT3 activation with up-regulation of *Hamp* expression in both mouse strains.

In β-thalassemic mice, PEP Prx2 treatment up-regulates *Hamp* expression in liver and is associated with STAT3 activation

We previously reported that PEP Prx2 administration significantly ameliorates β-thalassemic anemia in conjunction with decreased ineffective erythropoiesis and reduced liver iron overload (9). In both PEP Prx2 treated $Hbb^{3th/+}$ and wildtype mice, we found increased *Hamp* mRNA levels compared to vehicle treated mice (Fig. 4A). STAT3 was significantly activated in both PEP Prx2 treated mouse strains compared to vehicle treated groups (Fig. 4B). These data collectively suggest that Prx2 modulates STAT3-regulated hepatic *Hamp* expression in both $Hbb^{3th/+}$ and wildtype mice.

DISCUSSION

Our study documented for the first time that Prx2 plays a critical role as cyto-protector against toxic effects of iron overload on erythropoiesis. Absence of Prx2 and associated loss of the expected iron-induced increase in *Hamp* expression in $Prx2^{-/-}$ mouse liver in part account for deleterious effects of iron overload.

In response to IO, $Prx2^{-/-}$ mice displayed reduced STAT3 activation compared to wildtype animals. Previous studies have shown that ROS levels significantly influence the activation status of STAT3 affecting *Hamp* expression in response to IO or IL-6 mediated inflammatory system (18, 20). Thus, the failure in STAT3 activation in IO $Prx2^{-/-}$ mice represents the key event responsible for the lack of *Hamp* up-regulation in response to IO. This conclusion is bolstered by our finding that in contrast to STAT3, Smad activation was similar in both IO mouse strains. In addition, the reduced expression of *Erfe* in erythroid precursors as well as of circulating Erfe levels in both mouse strains exposed to IO is in agreement with previous reports and indicates that Erfe is not involved in the loss of *Hamp* expression observed in IO $Prx2^{-/-}$ mice. By exploring the effects of acute iron administration of *Hamp* expression in $Prx2^{-/-}$ mice, we documented that the absence of Prx2 affects *Hamp* expression in $Prx2^{-/-}$ mice and is associated with reduced STAT3 activation. Taken together these findings imply a robust interplay between iron and Prx2 *Hamp* pathway. The loss of the functional connection between *Erfe* and *Hamp* in the absence of Prx2 is another novel element in the scenario of iron homeostasis and ineffective erythropoiesis in presence of adequate EPO levels. Indeed, the administration of PEP Prx2, which we previously reported to ameliorate ineffective erythropoiesis in both $Prx2^{-/-}$ and $Hbb^{3th/+}$ mice (9), significantly ameliorated the IO induced cytotoxic effect on erythropoiesis and was associated with up-regulation of *Erfe* in both mouse strains. This effect was more pronounced in wildtype than in $Prx2^{-/-}$ mice, most likely related to the fact that the exogenous PEP Prx2 does not fully compensate the absence of Prx2 in $Prx2^{-/-}$ mice. Data from the mouse model of β-thalassemia ($Hbb^{3th/+}$) further support a functional connection between Prx2 and STAT3 towards *Hamp* expression. We took the advantage of our previous observation that PEP-Prx2 administration ameliorates the ineffective erythropoiesis and iron overload in β-thalassemic mice (9) and showed marked activation of STAT3 and up-regulation of liver *Hamp* expression in PEP Prx2 treated $Hbb^{3th/+}$ mice, supporting a key role of Prx2 in iron homestasis.

In summary, we propose that Prx2 controls oxidative stress and modulates targets sensitive to redox conditions such as STAT3 (Fig. 4C). Thus, Prx2 levels might act as a

on-off switch of STAT3 transcription activity, profoundly affecting *Hamp* expression in response to IO (Fig. 4C). The effects of PEP Prx2 on STAT3 activation and *Hamp* expression in either IO mice or β-thalassemic mice further support this working model. The amelioration of IO induced ineffective erythopoiesis in PEP Prx2 treated mice supports the role of Prx2 as “big brother” in controlling IO induced cytotoxicity and optimizing the functional pathway involved in iron homeostasis. These findings suggest a novel therapeutic strategy to control clinical consequences of iron overload through modulation of Prx2 activity.

AUTORS CONTRIBUTIONS

AM, LDF, NM, IA designed the experiments, analyzed data and wrote the paper; TG designed the experiments, wrote the paper and carried out Erfe soluble measurements, FC and SL analyzed the data and wrote the paper; AJ, CL carried out the histologic analysis; AM, AS, EF LDF carried out the experiments; LdF and MB performed the molecular experiments and analyzed the data; GF carried out the analysis on LIC, CSY and KDW generated the PEPPrx2; SL and AC carried out the analysis of liver oxidative stress and high ferritin levels determination; DM and CC carried out EMSA experiments and analyzed data.

ACKNOWLEDGMENTS

We are grateful to E. Nementh for support and fruitful discussion.
This work was supported by PRIN (LDF and AI: 201228PNX83) and FUR_UNIVR (LDF).

CONFLICT OF INTEREST STATEMENT

The Authors have no conflict of interest to disclose.

REFERENCES

1. Johnson RM, Ho YS, Yu DY, Kuypers FA, Ravindranath Y, Goyette GW. The effects of disruption of genes for peroxiredoxin-2, glutathione peroxidase-1, and catalase on erythrocyte oxidative metabolism. Free radical biology & medicine. 2010;48(4):519-25.
2. Low FM, Hampton MB, Winterbourn CC. Peroxiredoxin 2 and peroxide metabolism in the erythrocyte. Antioxidants & redox signaling. 2008;10(9):1621-30.
3. Matte A, Low PS, Turrini F, Bertoldi M, Campanella ME, Spano D, et al. Peroxiredoxin-2 expression is increased in beta-thalassemic mouse red cells but is displaced from the membrane as a marker of oxidative stress. Free radical biology & medicine. 2010;49(3):457-66.
4. De Franceschi L, Bertoldi M, Matte A, Santos Franco S, Pantaleo A, Ferru E, et al. Oxidative stress and beta-thalassemic erythroid cells behind the molecular defect. Oxidative medicine and cellular longevity. 2013;2013:985210.
5. Sobotta MC, Liou W, Stocker S, Talwar D, Oehler M, Ruppert T, et al. Peroxiredoxin-2 and STAT3 form a redox relay for H2O2 signaling. Nature chemical biology. 2015;11(1):64-70.
6. Bertoldi M. Human Peroxiredoxins 1 and 2 and Their Interacting Protein Partners; Through Structure Toward Functions of Biological Complexes. Protein Pept Lett. 2016;23(1):69-77.
7. Franco SS, De Falco L, Ghaffari S, Brugnara C, Sinclair DA, Matte A, et al. Resveratrol accelerates erythroid maturation by activation of FoxO3 and ameliorates anemia in beta-thalassemic mice. Haematologica. 2014;99(2):267-75.
8. De Franceschi L, Bertoldi M, De Falco L, Santos Franco S, Ronzoni L, Turrini F, et al. Oxidative stress modulates heme synthesis and induces peroxiredoxin-2 as a novel cytoprotective response in beta-thalassemic erythropoiesis. Haematologica. 2011;96(11):1595-604.
9. Matte A, De Falco L, Iolascon A, Mohandas N, An X, Siciliano A, et al. The Interplay Between Peroxiredoxin-2 and Nuclear Factor-Erythroid 2 Is Important in Limiting Oxidative Mediated Dysfunction in beta-Thalassemic Erythropoiesis. Antioxidants & redox signaling. 2015;23(16):1284-97.
10. de Franceschi L, Turrini F, Honczarenko M, Ayi K, Rivera A, Fleming MD, et al. In vivo reduction of erythrocyte oxidant stress in a murine model of beta-thalassemia. Haematologica. 2004;89(11):1287-98.
11. Kautz L, Jung G, Du X, Gabayan V, Chapman J, Nasoff M, et al. Erythroferrone contributes to hepcidin suppression and iron overload in a mouse model of beta-thalassemia. Blood. 2015;126(17):2031-7.
12. Kautz L, Jung G, Valore EV, Rivella S, Nemeth E, Ganz T. Identification of erythroferrone as an erythroid regulator of iron metabolism. Nat Genet. 2014;46(7):678-84.
13. Kautz L, Nemeth E. Molecular liaisons between erythropoiesis and iron metabolism. Blood. 2014;124(4):479-82.
14. Kautz L, Meynard D, Monnier A, Darnaud V, Bouvet R, Wang RH, et al. Iron regulates phosphorylation of Smad1/5/8 and gene expression of Bmp6, Smad7, Id1, and Atoh8 in the mouse liver. Blood. 2008;112(4):1503-9.
15. Nemeth E, Tuttle MS, Powelson J, Vaughn MB, Donovan A, Ward DM, et al. Hepcidin regulates cellular iron efflux by binding to ferroportin and inducing its internalization. Science. 2004;306(5704):2090-3.
16. Gardenghi S, Ramos P, Marongiu MF, Melchiori L, Breda L, Guy E, et al. Hepcidin as a therapeutic tool to limit iron overload and improve anemia in beta-thalassemic mice. The Journal of clinical investigation. 2010;120(12):4466-77.
17. Camaschella C, Nai A. Ineffective erythropoiesis and regulation of iron status in iron loading anaemias. Br J Haematol. 2016;172(4):512-23.

18. Millonig G, Ganzleben I, Peccerella T, Casanovas G, Brodziak-Jarosz L, Breitkopf-Heinlein K, et al. Sustained submicromolar H2O2 levels induce hepcidin via signal transducer and activator of transcription 3 (STAT3). J Biol Chem. 2012;287(44):37472-82.
19. Harrison-Findik DD, Schafer D, Klein E, Timchenko NA, Kulaksiz H, Clemens D, et al. Alcohol metabolism-mediated oxidative stress down-regulates hepcidin transcription and leads to increased duodenal iron transporter expression. J Biol Chem. 2006;281(32):22974-82.
20. Miura K, Taura K, Kodama Y, Schnabl B, Brenner DA. Hepatitis C virus-induced oxidative stress suppresses hepcidin expression through increased histone deacetylase activity. Hepatology. 2008;48(5):1420-9.
21. Morgan MJ, Liu ZG. Crosstalk of reactive oxygen species and NF-kappaB signaling. Cell Res. 2011;21(1):103-15.
22. De Franceschi L, Turrini F, del Giudice EM, Perrotta S, Olivieri O, Corrocher R, et al. Decreased band 3 anion transport activity and band 3 clusterization in congenital dyserythropoietic anemia type II. Experimental hematology. 1998;26(9):869-73.
23. De Franceschi L, Olivieri O, Miraglia del Giudice E, Perrotta S, Sabato V, Corrocher R, et al. Membrane cation and anion transport activities in erythrocytes of hereditary spherocytosis: effects of different membrane protein defects. Am J Hematol. 1997;55(3):121-8.
24. De Franceschi L, Brugnara C, Rouyer-Fessard P, Jouault H, Beuzard Y. Formation of dense erythrocytes in SAD mice exposed to chronic hypoxia: evaluation of different therapeutic regimens and of a combination of oral clotrimazole and magnesium therapies. Blood. 1999;94(12):4307-13.
25. Bellelli R, Federico G, Matte A, Colecchia D, Iolascon A, Chiariello M, et al. NCOA4 Deficiency Impairs Systemic Iron Homeostasis. Cell Rep. 2016;14(3):411-21.
26. De Franceschi L, Brugnara C, Beuzard Y. Dietary magnesium supplementation ameliorates anemia in a mouse model of beta-thalassemia. Blood. 1997;90(3):1283-90.
27. Matte A, Pantaleo A, Ferru E, Turrini F, Bertoldi M, Lupo F, et al. The novel role of peroxiredoxin-2 in red cell membrane protein homeostasis and senescence. Free radical biology & medicine. 2014;76C:80-8.
28. Liu J, Zhang J, Ginzburg Y, Li H, Xue F, De Franceschi L, et al. Quantitative analysis of murine terminal erythroid differentiation in vivo: novel method to study normal and disordered erythropoiesis. Blood. 2013;121(8):e43-9.
29. Matte A, Bertoldi M, Mohandas N, An X, Bugatti A, Brunati AM, et al. Membrane association of peroxiredoxin-2 in red cells is mediated by the N-terminal cytoplasmic domain of band 3. Free radical biology & medicine. 2013;55:27-35.
30. Lupo F, Russo R, Iolascon A, Ieluzzi D, Siciliano A, Toniutto P, et al. Protease inhibitors-based therapy induces acquired spherocytic-like anaemia and ineffective erythropoiesis in chronic hepatitis C virus patients. Liver Int. 2016;36(1):49-58.
31. Choi JH, Kim DW, Yoo DY, Jeong HJ, Kim W, Jung HY, et al. Repeated administration of PEP-1-Cu,Zn-superoxide dismutase and PEP-1-peroxiredoxin-2 to senescent mice induced by D-galactose improves the hippocampal functions. Neurochemical research. 2013;38(10):2046-55.
32. De Franceschi L, Daraio F, Filippini A, Carturan S, Muchitsch EM, Roetto A, et al. Liver expression of hepcidin and other iron genes in two mouse models of beta-thalassemia. Haematologica. 2006;91(10):1336-42.
33. Kalish BT, Matte A, Andolfo I, Iolascon A, Weinberg O, Ghigo A, et al. Dietary omega-3 fatty acids protect against vasculopathy in a transgenic mouse model of sickle cell disease. Haematologica. 2015;100(7):870-80.

34. Siciliano A, Malpeli G, Platt OS, Lebouef C, Janin A, Scarpa A, et al. Abnormal modulation of cell protective systems in response to ischemic/reperfusion injury is important in the development of mouse sickle cell hepatopathy. Haematologica. 2011;96(1):24-32.
35. Melisi D, Xia Q, Paradiso G, Ling J, Moccia T, Carbone C, et al. Modulation of pancreatic cancer chemoresistance by inhibition of TAK1. J Natl Cancer Inst. 2011;103(15):1190-204.
36. Santambrogio P, Cozzi A, Levi S, Rovida E, Magni F, Albertini A, et al. Functional and immunological analysis of recombinant mouse H- and L-ferritins from Escherichia coli. Protein Expr Purif. 2000;19(1):212-8.
37. Cozzi A, Corsi B, Levi S, Santambrogio P, Albertini A, Arosio P. Overexpression of wild type and mutated human ferritin H-chain in HeLa cells: in vivo role of ferritin ferroxidase activity. J Biol Chem. 2000;275(33):25122-9.
38. Park JG, Yoo JY, Jeong SJ, Choi JH, Lee MR, Lee MN, et al. Peroxiredoxin 2 deficiency exacerbates atherosclerosis in apolipoprotein E-deficient mice. Circ Res. 2011;109(7):739-49.
39. Han YH, Kwon T, Kim SU, Ha HL, Lee TH, Kim JM, et al. Peroxiredoxin I deficiency attenuates phagocytic capacity of macrophage in clearance of the red blood cells damaged by oxidative stress. BMB Rep. 2012;45(10):560-4.

FIGURES

Fig. 1. Iron overload (IO) bone marrow and liver cytoxicity is amplified in the absence of Prx2. (A) Hemoglobin (Hb), mean cell volume (MCV) and reticulocyte count in wildtype (WT; *n*=12) and Prx2$^{-/-}$ (*n*=12) mice exposed to iron-overload (IO) diet. No data were available on red cell indices and reticulocyte count for Prx2$^{-/-}$ exposed to 90 days IO due to the severe anemia (Hb g/dL). Data are presented as means ±SD; *p< 0.05 compared to WT mice; °p<0.05 compared to baseline values. **(B) Upper panel.** CD44+/TER119+/FSC^{high} bone marrow erythroid cells in wildtype (WT; *n*=6) and Prx2$^{-/-}$ (*n*=6) mice after 90 days of either standard diet or iron-overload (IO) diet. Data are presented as means ±SD; *p< 0.05 compared to WT mice; °p<0.05 compared to standard diet. **Lower Panel.** Bar graph showing the ratio between early erythroid precursors (pro-basophilic- polychromatic- erythroblasts) and late erythroid precursors (orthochromatic erythroblasts) in bone marrow analyzed by flow cytometry from wildtype (WT; *n*=6) and Prx2-/- (*n*=6) after 90 days of either standard diet or iron-overload (IO) diet. Data are presented as means ±SD; *p< 0.05 compared to standard diet. **(C)** RT-PCR expression of erythroferrone (*Erfe*; *Fam132b*) on sorted mouse polychromatic (Pop III) and orthochromatic (Pop IV) erythroblasts from bone marrow of wildtype and Prx2$^{-/-}$ mice after under either standard diet or iron-overload (IO) diet. Experiments were performed in triplicate. Error bars represent the standard deviations (mean ± SD); *p<0.05, **p ≤0.001. The graphs were created using the Software GraphPad Prism 6. **(D) Left panel.** Macroscopic appearance of liver from wildtype (WT) and Prx2$^{-/-}$ mice exposed to iron-overload diet (IO). One representative image from the other 6 with similar results is presented. Iron staining (Pearl's Prussian blue) in liver from wildtype (WT) and Prx2$^{-/-}$ mice exposed to iron-overload diet (IO). One representative image from the other 6 with similar results is presented. In the inset, the arrow indicates macrophages with iron accumulation. **Right panel.** Quantification of iron staining on Pearl's Prussian blue liver from wildtype (WT) and Prx2$^{-/-}$ mice (see Methods). Data are shown as means ±SD (*n*=10); *P<0.05 compared to WT (*n*=6).

Fig.2. Lacking in STAT3 activation and *Hamp* up-regulation in response to iron-overload and acute iron administration characterized Prx2$^{-/-}$ mice. (A) Upper panel. Soluble fractions of liver of WT IO and Prx2$^{-/-}$IO were analyzed on 12% SDS-PAGE and subjected to immunoblotting. The carbonylated proteins were detected by treating with DNPH and blotted with anti-DNP antibody. **Lower panel.** 10 μg of soluble proteins of liver

homogenate were tested for MDA-protein adducts. Quantification of band area was performed by densitometry and expressed as % of WT. The data are presented as means ± SD of at least three independent experiments; statistically significant differences were determined by Student's t-test. *p<0.05, **p<0.001. **(B)** Western-blot (Wb) analysis with specific antibodies against Peroxiredoxin-2 (Prx2), NAD(P)H dehydrogenase quinone (Nqo1) and heme-oxygenase (HO-1) of liver from wildtype (WT) and Prx2$^{-/-}$ mice exposed to either standard diet or iron-overload diet (IO). One representative gel from 6 with similar results is presented. Densitometric analysis of immunoblots is shown in bar graph (lower panel); Data are presented as means ±SD; *p<0.05 compared to WT, °p<0.05 standard diet. **(C) Upper panel.** Western-blot (Wb) analysis with specific antibodies against phospho-STAT3 (P-STAT3) and STAT3 of liver from wildtype (WT) and Prx2$^{-/-}$ mice exposed to either standard diet or iron-overload diet (IO). One representative gel from 6 with similar results is presented (see Fig. 2SC for densitometric analysis). **Lower panel.** Non-radioactive EMSA analysis of nuclear protein extracted from pooled liver of four to six mice under standard (St) diet or iron overload (IO). Arrows indicates STA3 homodimer. **(D)** RT-PCR expression of hepcidin (*Hamp*) on liver from wildtype and Prx2$^{-/-}$ mice exposed to either standard diet or iron-overload diet (IO). Experiments were performed in triplicate. Error bars represent the standard deviations (mean ± SD); *p<0.05 compared to WT, °p<0.05 standard diet. The graphs were created using the Software GraphPad Prism 6. **(E)** Western-blot (Wb) analysis with specific antibodies against peroxiredoxin-2 (Prx2), phospho-Nrf2 (P-Nrf2), Nrf2, phospho-STAT3 (P-STAT3) and STAT3 of liver from wildtype (WT) and Prx2$^{-/-}$ mice exposed to either vehicle or acute single iron dose (AI). One representative gel from 6 with similar results is presented (see Fig. 3SC for densitometric analysis). **(F)** RT-PCR expression of hepcidin (*Hamp*) on liver from wildtype and Prx2$^{-/-}$ mice exposed to either vehicle or acute single iron dose (AI). Experiments were performed in triplicate. Error bars represent the standard deviations (mean ± SD); °p<0.05 vehicle mouse groups. The graphs were created using the Software GraphPad Prism 6.

Fig.3. Recombinant fusion PEP Prx2 protein ameliorates IO induced anemia and ineffective erythropoiesis with activation of STAT3 and up-regulation of hepcidin. **(A)** Hemoglobin (Hb), mean cell volume (MCV) and reticulocyte count in wildtype (WT; *n*=8) and Prx2$^{-/-}$ (*n*=8) mice exposed to either iron-overload (IO) diet or IO plus PEP Prx2 treatment. No data were available on red cell indices and reticulocyte count for Prx2$^{-/-}$ exposed to IO due to the severe anemia (Hb g/dL). Data are presented as means ±SD;

*p< 0.05 compared to WT mice; §p<0.05 compared to IO vehicle treated mice. **(B)** Bar graph showing CD44+/TER119+/FSC^{high} bone marrow cells in wildtype (WT; *n*=8) and Prx2$^{-/-}$ (*n*=8) mice exposed to either iron-overload (IO) diet or IO plus PEP Prx2 treatment. Data are presented as means ±SD; *p< 0.05 compared to WT mice; §p<0.05 compared to IO vehicle treated mice. **(C)** RT-PCR expression of erythroferrone (*Erfe*; *Fam132b*) on sorted mouse polychromatic (Pop III) and orthochromatic (Pop IV) erythroblasts from bone marrow of wildtype and Prx2$^{-/-}$ mice under either iron-overload (IO) diet without or with PEP Prx2 treatment. Experiments were performed in triplicate. Error bars represent the standard deviations (mean ± SD); *p< 0.05 compared to WT mice, §p<0.05 compared to IO vehicle treated mice; ^p<0.05 Pop III *vs* Pop IV (*n*=6 from each mouse strains). The graphs were created using the Software GraphPad Prism 6. **(D)** Iron staining (Pearl's Prussian blue) in liver from wildtype (WT) and Prx2$^{-/-}$ mice exposed to iron-overload diet (IO) and treated with either vehicle or PEP Prx2**.** One representative image from the other 6 with similar results is presented (related iron score is shown in Fig. 6SA) **(E)** Western-blot (Wb) analysis with specific antibodies against phospho-STAT3 (P-STAT3) and STAT3 of liver from wildtype (WT) and Prx2$^{-/-}$ mice exposed to iron-overload diet (IO) with or without PEP Prx2 treatment. One representative gel from eight with similar results is presented. Densitometric analysis of immunoblots are shown in bar graph in Fig. 6SC. **(F)** RT-PCR expression of hepcidin (*Hamp*) on liver from wildtype and Prx2$^{-/-}$ mice exposed to either standard diet or iron-overload diet (IO) with or without PEP Prx2. Experiments were performed in triplicate. Error bars represent the standard deviations (mean ± SD; *n*=6); p<0.05 compared to WT, °p<0.05 standard diet, § p<0.05 IO vehicle treated mice. The graphs were created using the Software GraphPad Prism 6.

Fig.4 Recombinant fusion PEP Prx2 protein is associated with STAT3 activation and up-regulation of hepcidin in a mouse model for β-thalassemia (Hbb$^{3th/+}$). (A) RT-PCR expression of hepcidin (*Hamp*) on liver from wildtype and Hbb$^{3th/+}$ mice exposed to either vehicle or PEP-Prx2 treatment. Experiments were performed in triplicate. Error bars represent the standard deviations (mean ± SD; *n*=6); *p<0.05 compared to WT, § p<0.05 vehicle treated mice. The graphs were created using the Software GraphPad Prism 6. **(B)** Western-blot (Wb) analysis with specific antibodies against phospho-STAT3 (P-STAT3) and STAT3 of liver from wildtype (WT) and Hbb$^{3th/+}$ mice with or without PEP Prx2 treatment. One representative gel from 6 with similar results is presented. Densitometric analysis of immunoblots is shown in bar graph (right panel); Data are presented as means

±SD (*n*=6 from each strains); *p<0.05 compared to WT, § p<0.05 IO vehicle treated mice. **(C)** Schematic diagram of the novel role of Prx2 in iron homeostasis facing iron overload induced ineffective erythropoiesis. Prx2 controls oxidative stress, modulating targets sensitive to redox conditions STAT3. Prx2 levels might act as a switch of on-off STAT3 transcription activity, profoundly affecting *Hamp* expression in response to IO. ROS: radical oxygen species; Prx2: peroxiredoxin 2; Hamp: hepcidin; P: phosphorylate form of indicated transcriptional factor; STAT3: signal transducer and activator of transcription 3.

Fig. 1

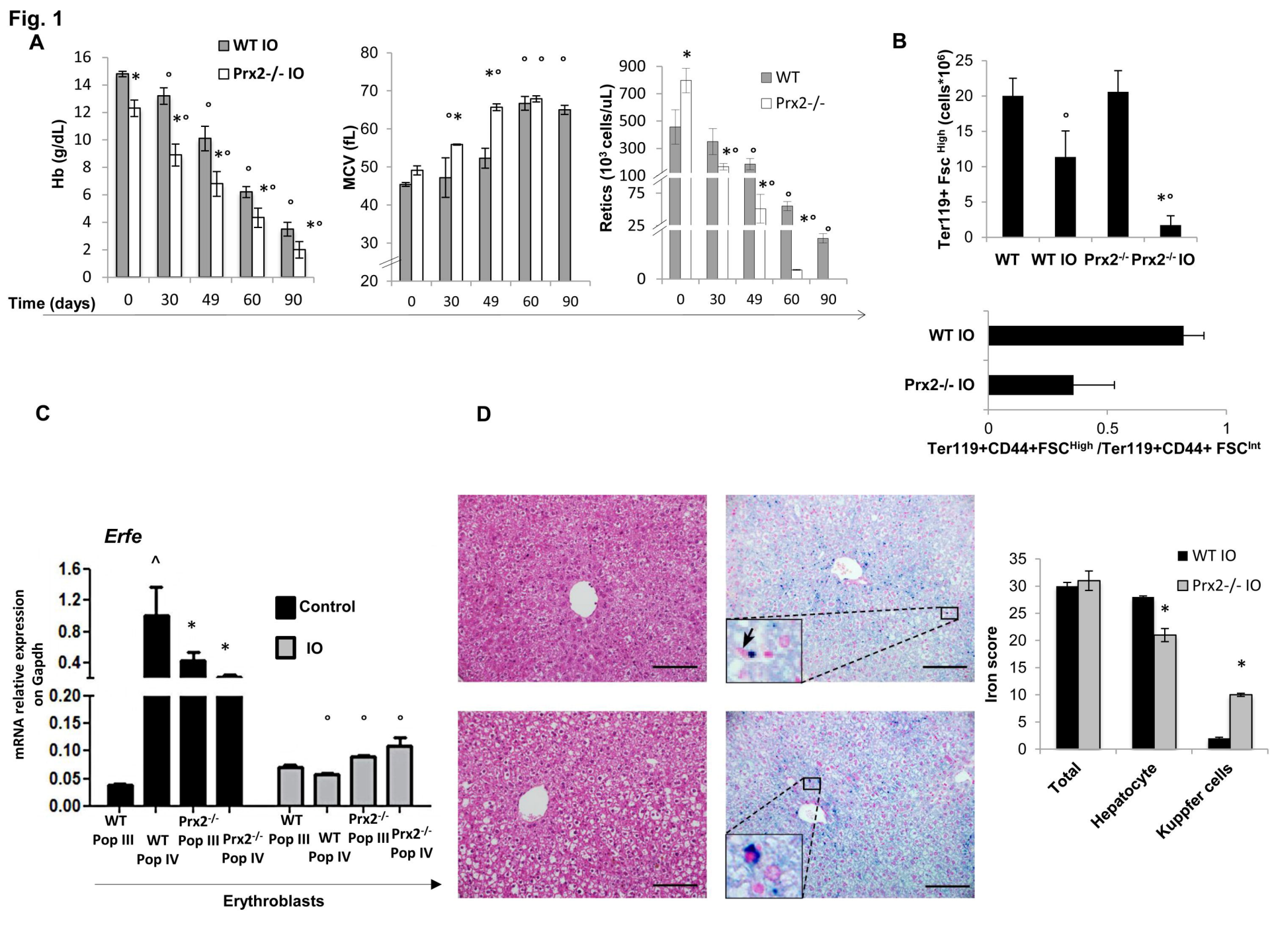
A
WT IO
Prx2-/- IO
Hb (g/dL)
MCV (fL)
Reticulocytes (10³ cells/uL)
WT
Prx2-/-
Time (days)
0
30
49
60
90
B
Ter119+ Fsc High (cells*10⁶)
WT
WT IO
Prx2-/-
Prx2-/- IO
WT IO
Prx2-/- IO
Ter119+CD44+FSCHigh /Ter119+CD44+ FSCInt
C
Erfe
mRNA relative expression on Gapdh
Control
IO
WT Pop III
WT Pop IV
Prx2-/- Pop III
Prx2-/- Pop IV
Erythroblasts
D
Iron score
Total
Hepatocyte
Kuppfer cells

Fig. 2

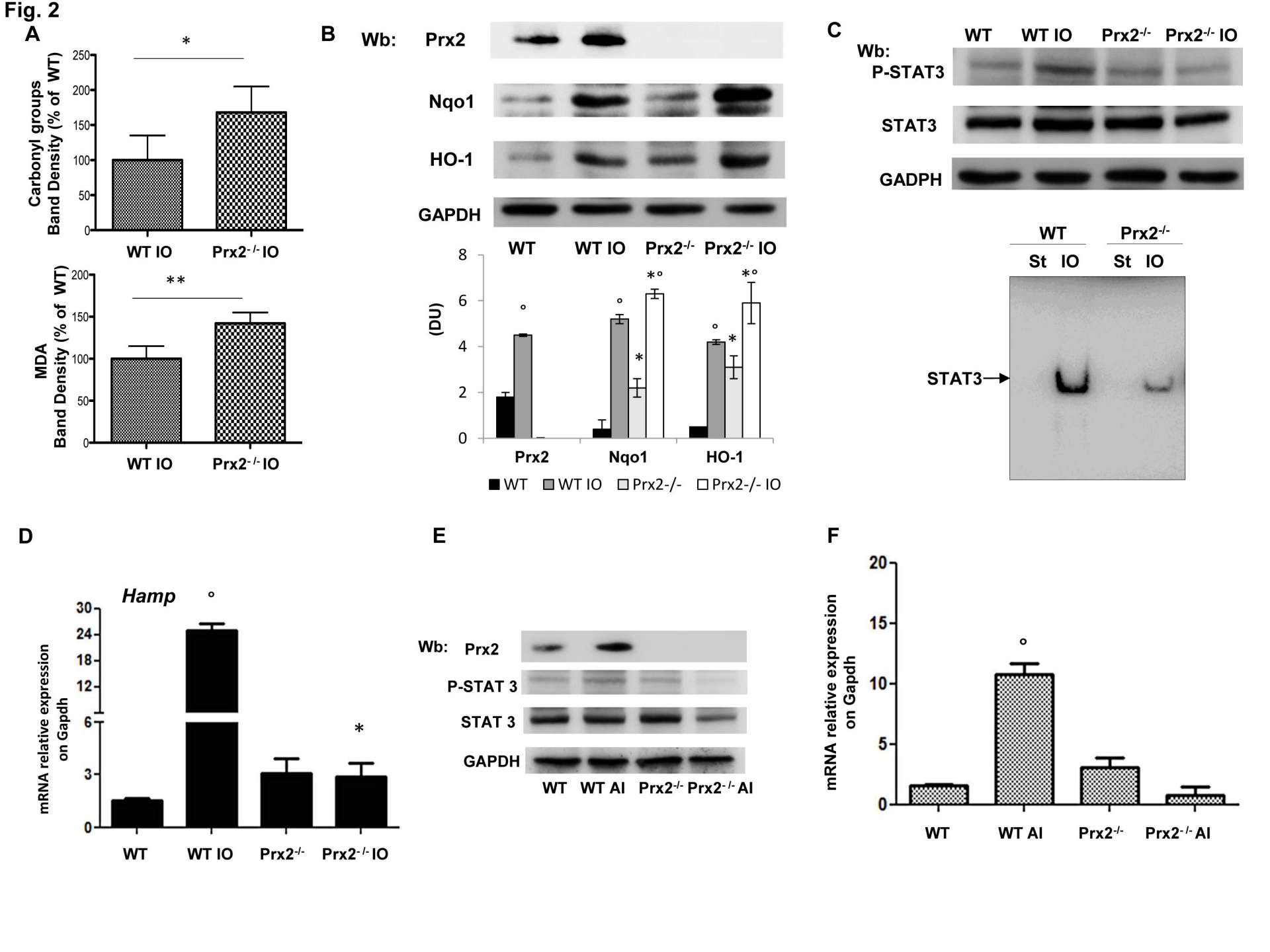
A
Carbonyl groups Band Density (% of WT)
WT IO
Prx2-/- IO
MDA Band Density (% of WT)
B
Wb:
Prx2
Nqo1
HO-1
GAPDH
WT
WT IO
Prx2-/-
Prx2-/- IO
(DU)
Prx2
Nqo1
HO-1
C
Wb:
P-STAT3
STAT3
GADPH
St
IO
STAT3
D
Hamp
mRNA relative expression on Gapdh
E
Wb:
Prx2
P-STAT 3
STAT 3
GAPDH
WT AI
Prx2-/- AI
F
mRNA relative expression on Gapdh

Fig. 3

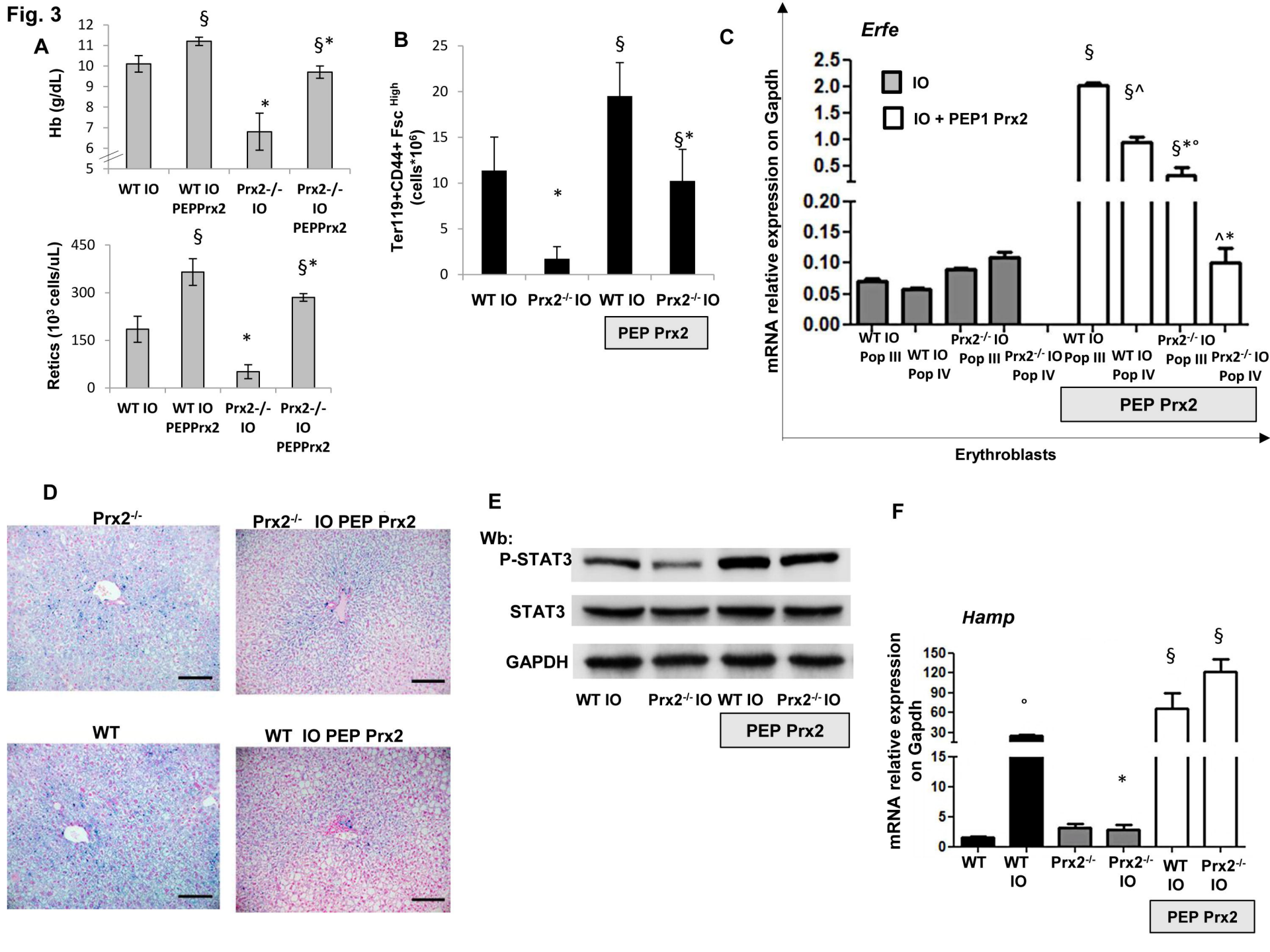
A
Hb (g/dL)
WT IO
WT IO PEPPrx2
Prx2-/- IO
Prx2-/- IO PEPPrx2
Retics (10³ cells/uL)
B
Ter119+CD44+ Fsc High (cells*10⁶)
WT IO
Prx2-/- IO
PEP Prx2
C
Erfe
IO
IO + PEP1 Prx2
mRNA relative expression on Gapdh
WT IO Pop III
WT IO Pop IV
Prx2-/- IO Pop III
Prx2-/- IO Pop IV
PEP Prx2
Erythroblasts
D
Prx2-/-
Prx2-/- IO PEP Prx2
WT
WT IO PEP Prx2
E
Wb:
P-STAT3
STAT3
GAPDH
F
Hamp
mRNA relative expression on Gapdh
WT
WT IO
Prx2-/-
Prx2-/- IO

Fig. 4

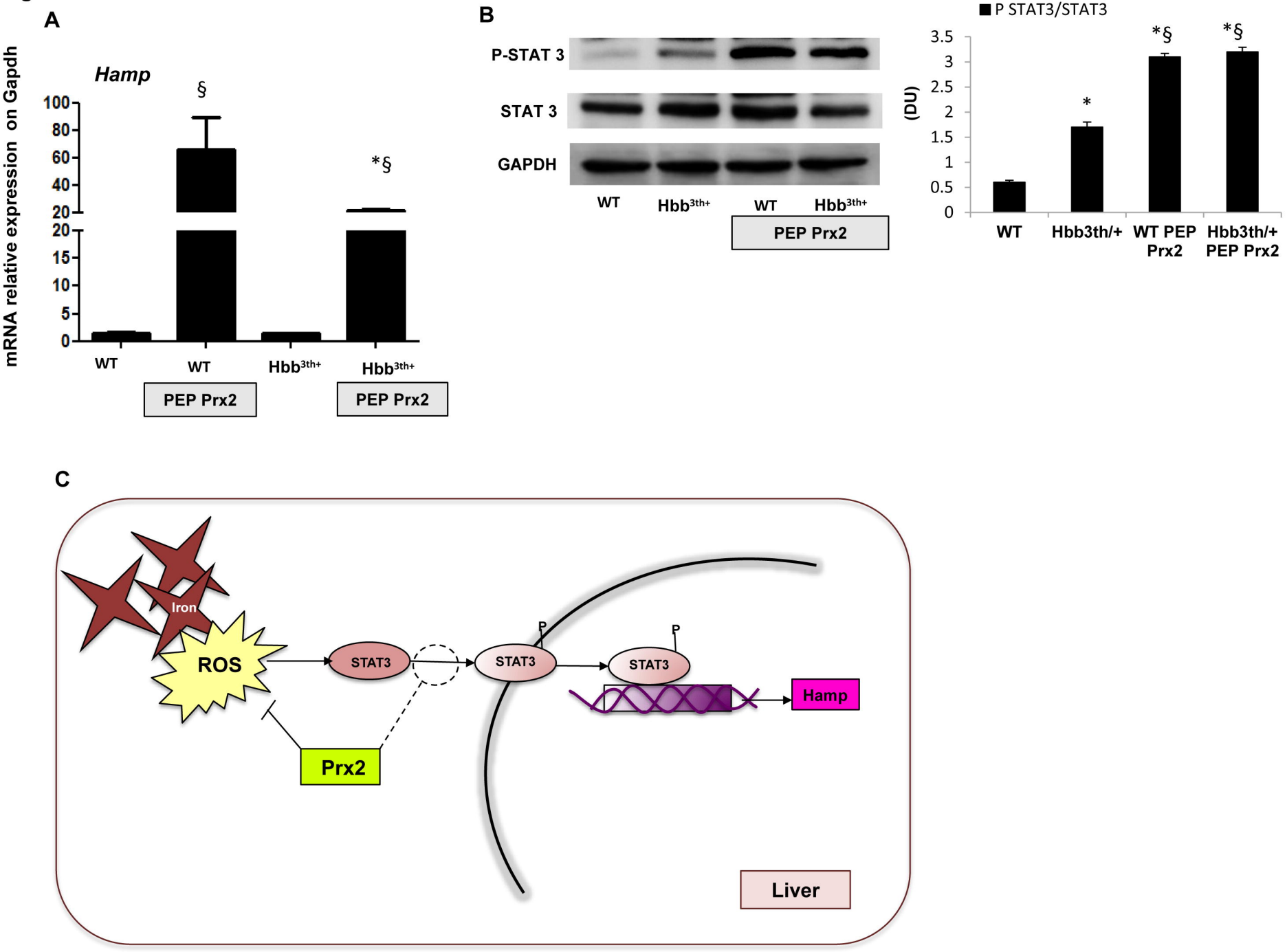
A
Hamp
mRNA relative expression on Gapdh
§
*§
100
80
60
40
20
20
15
10
5
0
WT
WT
Hbb3th+
Hbb3th+
PEP Prx2
PEP Prx2
B
P-STAT 3
STAT 3
GAPDH
WT
Hbb3th+
WT
Hbb3th+
PEP Prx2
P STAT3/STAT3
(DU)
3.5
3
2.5
2
1.5
1
0.5
0
*
*§
*§
WT
Hbb3th/+
WT PEP Prx2
Hbb3th/+ PEP Prx2
C
Iron
ROS
STAT3
STAT3
STAT3
P
P
Hamp
Prx2
Liver

Section 3

Dietary ω-3 fatty acids protect against vasculopathy in a transgenic mouse model of sickle cell disease

EF author contributions: EF has carried out experiments and contributed to data analysis.

Dietary ω-3 fatty acids protect against vasculopathy in a transgenic mouse model of sickle cell disease

Brian T. Kalish,[1]* Alessandro Matte,[2]* Immacolata Andolfo,[3] Achille Iolascon,[3] Olga Weinberg,[4] Alessandra Ghigo,[5] James Cimino,[5] Angela Siciliano,[2] Emilio Hirsch,[5] Enrica Federti,[2] Mark Puder,[1] Carlo Brugnara,[4] and Lucia De Franceschi[2]

[1]Department of Surgery and The Vascular Biology Program, Boston Children's Hospital, Harvard Medical School, Boston, MA, USA; [2]Department of Medicine, University of Verona-AOUI Verona, Policlinico GB Rossi, Verona, Italy; [3]Department of Biochemistry, University Federico II, Naples, Italy; [4]Departments of Pathology and Laboratory Medicine, Boston Children's Hospital, Harvard Medical School, Boston, MA, USA; and [5]Molecular Biotechnology Center and Department of Molecular Biotechology and Health Science, University of Turin, Italy

*These authors contributed equally to this work.

ABSTRACT

The anemia of sickle cell disease is associated with a severe inflammatory vasculopathy and endothelial dysfunction, which leads to painful and life-threatening clinical complications. Growing evidence supports the anti-inflammatory properties of ω-3 fatty acids in clinical models of endothelial dysfunction. Promising but limited studies show potential therapeutic effects of ω-3 fatty acid supplementation in sickle cell disease. Here, we treated humanized healthy and sickle cell mice for 6 weeks with ω-3 fatty acid diet (fish-oil diet). We found that a ω-3 fatty acid diet: (i) normalizes red cell membrane ω-6/ ω-3 ratio; (ii) reduces neutrophil count; (iii) decreases endothelial activation by targeting endothelin-1 and (iv) improves left ventricular outflow tract dimensions. In a hypoxia-reoxygenation model of acute vaso-occlusive crisis, a ω-3 fatty acid diet reduced systemic and local inflammation and protected against sickle cell-related end-organ injury. Using isolated aortas from sickle cell mice exposed to hypoxia-reoxygenation, we demonstrated a direct impact of a ω-3 fatty acid diet on vascular activation, inflammation, and anti-oxidant systems. Our data provide the rationale for ω-3 dietary supplementation as a therapeutic intervention to reduce vascular dysfunction in sickle cell disease.

Introduction

Sickle cell disease (SCD) is a worldwide hereditary red cell disorder caused by a point mutation in the β-globin gene resulting in the synthesis of pathological hemoglobin S (HbS), and abnormal HbS polymerization in hypoxic conditions.[1] The two main clinical manifestations of SCD are chronic hemolytic anemia and acute vaso-occlusive crises (VOC), which are the principal causes of hospitalization of SCD patients. Recent studies have underscored the central role of sickle vasculopathy in the generation of sickle cell-related acute events and chronic organ complications.[2-4] The pathophysiology of these complications is based on intravascular sickling in capillaries and small vessels leading to vaso-occlusion, impaired blood flow, vascular inflammation, and thrombosis with ischemic cell damage.[2-4] Studies in various models of vasculopathy, including those with ischemia and inflammation, have shown protective effects of ω-3 polyunsaturated fatty acid (PUFA) supplementation.[5] This is supported by several mechanisms: (i) favorable changes in cell membrane lipid composition;[6] (ii) modulation of soluble and cellular inflammatory responses;[7] (iii) modulation of the coagulation cascade,[8] and (iv) production of nitric oxide.[9]

The fatty acid profile of the red cell membrane from SCD patients is intrinsically different from that of healthy controls, with a relative increase in the ratio of ω-6 to ω-3 PUFA.[10,11] Sickle erythrocytes have increased ω-6-derived arachidonic acid (20:4n6) and decreased eicosapentaenoic acid (20:5n3) and docosahexaenoic acid (22:6n3).[10,11] Recently, human studies have demonstrated that supplementation of SCD subjects with fish oil containing ω-3 fatty acids reduces VOC, pain episodes, and blood transfusions.[12-14] To date, however, there are insufficient clinical and molecular data to support routine dietary supplementation with fish oil for SCD patients.

In the present study, we studied the effects of an ω-3 diet (fish oil diet, FD) on the vasculopathy of a humanized mouse model for SCD. The evaluation of the impact of FD supplementation on SCD is relevant since the typical Western diet has a 15:1 ratio of ω-6 to ω-3 PUFA.[15]

We found that in SCD mice, the FD modified sickle red cell membrane lipid composition and was associated with a reduction in vascular activation and an improvement of cardiovascular dysfunction. In a model of acute VOC induced by exposure to hypoxia-reoxygenation (H/R) stress, we showed that FD decreases vascular activation, modulates the inflammatory response, and reduces sickle cell-related organ damage. Thus, our findings shed new light on the significance of PUFA in SCD and VOC and support a therapeutic role of ω-3 PUFA supplementation in SCD.

Methods

Mice and study design

Experiments were performed on 4- to 6-week old healthy control (*Hba*$^{tm1(HBA)Tow}$ *Hbb*$^{tm3(HBG1,HBB)Tow}$) and SCD (*Hba*$^{tm1(HBA)Tow}$ *Hbb*$^{tm2(HBG1,HBB*)Tow}$)

 doi:10.3324/haematol.2015.124586
The online version of this article has a Supplementary Appendix.
Manuscript received on February 2, 2015. Manuscript accepted on April 27, 2015.
Correspondence: carlo.brugnara@childrens.harvard.edu

mice.[16,17] The animal protocol was approved by the Animal Care and Use Committee of the University of Verona (CIRSAL). Two-month old animals were fed for 6 weeks with either the standard AIN-93M purified rodent diet (soy-diet with n6/n3 ratio of 8:1 - Dyets Inc., Bethlehem, PA, USA), containing 140 g/kg casein, 1.8 g/kg L-cystine, 100 g/kg sucrose, 465.9 g/kg cornstarch, 155 g/kg dextrose, 40 g/kg soybean oil, 0.8 mg/kg t-butylhydroquinone, 50 g/kg cellulose, 35 g/kg mineral mix, 10 g/kg vitamin mix, and 2.5 g/kg choline bitartrate[18] or the ω-3 FD, an AIN-93M-based purified rodent diet in which all of the calories provided by fat (10%) are replaced by 7.9% from HCO and 2.1% from ω-3 oil (Dyets Inc., Bethlehem, PA, USA). At the end of the 6 weeks of FD supplementation, animals were anesthetized with isofluorane, and whole blood was collected from each mouse via retro-orbital venipuncture by heparinized microcapillaries. Mice were euthanized and organs removed immediately. The organs were divided into two and either frozen immediately in liquid nitrogen or fixed in 10% formalin and embedded in paraffin for histology. Whenever indicated, 6-week old mice were exposed to hypoxia (8% oxygen for 10 h) followed by 3 h of reoxygenation (21% oxygen) (H/R stress) to mimic an acute VOC, as previously described.[19]

Hematologic parameters and red cell indices

Hematologic parameters and red cell indices were measured as previously described.[19-21] Details are reported in the *Online Supplementary Materials and Methods*.

Red cell fatty acid composition

Red cell membrane total lipids were extracted as previously reported[22] and determined by gas liquid chromatography using a Hewlett Packard 6890 equipped with a flame ionization detector. Peaks were identified by comparison of retention times with external fatty acid methyl ester standard mixtures from NuCheck Prep (Elysian, MN, USA). The fatty acid profiles were expressed as percentage of the total fatty acid (weight percent).

Blood pressure and echocardiographic measurements

Heart rate, systolic, diastolic, and mean blood pressures were measured in conscious mice with a non-invasive computerized tail cuff system (CODA, Kent Scientific Corp) as previously reported.[16] Transthoracic echocardiography was performed with a Vevo 2100 echocardiograph (Visual Sonics, Toronto, Canada) equipped with a 22-55 MHz transducer (MicroScan Transducers, MS500D) as previously described.[16] Details are reported in the *Online Supplementary Materials and Methods*.

Histological analysis

Multiple (at least five) three-micron whole mount sections were obtained for each paraffin-embedded liver and stained with hematoxylin & eosin, Masson trichome, and May-Grünwald-Giemsa. The lung and liver pathology were analyzed and the liver pathological score, inflammatory cell infiltrate and presence of thrombi were determined by blinded pathologists as previously described.[19,23] Details on the histological analysis are provided in the *Online Supplementary Materials and Methods*.

Tissue molecular analysis

Total RNA was extracted from mouse tissues using Trizol reagent (Life Technologies). cDNA was synthesized from total RNA (2 μg) using Super Script II First Strand kits (Life Technologies). Quantitative reverse transcriptase polymerase chain reaction (qRT-PCR) was performed using the SYBR-green method as previously reported.[24] Primers used are reported in *Online Supplementary Table S1*. For the immunoblot analysis, frozen lungs, livers, and aortas from each studied group were homogenized and lysed with iced lysis buffer (LB containing: 150 mM NaCl, 25 mM bicine, 0.1% SDS, Triton 2%, EDTA 1 mM, protease inhibitor cocktail tablets (Roche), 1 mM Na_3VO_4 final concentration) then centrifuged at 12,000 for 10 min at 4°C g.[25] Proteins were quantified and analyzed by one-dimensional sodium dodecylsulfate polyacrylamide gel electrophoresis. Gels were transferred to nitrocellulose membranes for immunoblot analysis with specific antibodies. Detailed information on the antibodies used is provided in the *Online Supplementary Materials and Methods*.

Bronchoalveolar lavage measurements

Bronchoalveolar lavage (BAL) fluids were collected and cellular contents were recovered by centrifugation and counted by microcytometry as previously reported.[19,26] The percentage of neutrophils was determined on cytospin centrifugation. The remaining BAL samples were centrifuged at 1,500 x g for 10 min at 4°C. The supernatant fluids were used for determination of total protein content.[19,26]

Statistical analysis

The two-way ANOVA algorithm for repeated measures combined with Bonferroni correction was used for data analysis. Differences with $P<0.005$ were considered statistically significant.

Results

ω-3 polyunsaturated fatty acids modify red cell membrane composition and reduce neutrophil count in mice with sickle cell disease

We analyzed the lipid composition of red cell membranes from healthy (AA) and sickle cell (SS) mice fed with isocaloric diets containing either soy (SD) or fish-oil (FD) for 6 weeks. As shown in Figure 1A and *Online Supplementary Table S2*, red cell membrane ω-6 content was higher in SS-SD mice than in AA-SD mice, similar to that observed in human SCD patients.[13] FD supplementation markedly increased ω-3 membrane content in both AA-FD and SS-FD mice, resulting in a dramatically lower ω-6/ω-3 ratio compared to that in both mouse strains fed SD (Figure 1A, *Online Supplementary Table S2*). In addition, in SS mice, FD resulted in significantly increased mean corpuscular volume and decreased mean cell hemoglobin concentration compared to control mice fed with SD, without significant changes in hemoglobin levels. No differences in hematologic parameters or red cell indices were evident in AA mice based on which of the two dietary interventions they received (Table 1). Interestingly, SS-SD mice showed increased neutrophil counts compared to AA-SD mice, as reported in other mouse models of SCD, a likely indication of elevated chronic systemic inflammation.[27] As shown in Table 1, FD reduced the neutrophil count by 30.4±7.2% (n=6) and 64.6±15.1% (n=6) in AA mice and SS mice, respectively, compared to the counts in SD groups. Since inflammation plays an important role in the pathogenesis of vasculopathy in SCD,[4] we evaluated the impact of FD on cardiovascular function in SCD mice.

ω-3 polyunsaturated fatty acids beneficially affect the cardiovascular system and endothelial activation in sickle cell mice

Vascular system. As shown in Figure 1B, FD treatment of SS mice resulted in a significantly lower diastolic blood

pressure compared to that in either SS mice or AA mice fed SD. In order to understand the effects of FD on the vascular system in SCD better, we isolated aortas from AA and SS mice and evaluated the expression of endothelin-1 (ET-1) as a key vasoactive and pro-inflammatory cytokine,[28] vascular adhesion molecule 1 (VCAM-1) as a marker of vascular endothelial activation,[29] and heme-oxygenase-1 (HO-1) as an efficient anti-oxidant system interfacing heme overload and vascular inflammation in SCD.[16,30] As expected, ET-1, VCAM-1 and HO-1 expression was increased in aortas from SS mice compared to that in AA mice fed the SD (Figure 1C, lanes 1 and 3). In SS mice, FD significantly reduced the expression of all three markers compared to their levels in SS control mice, reaching values similar to those observed in AA mice (Figure 1C, see also *Online Supplementary Figure S1A* for densitometric analysis).

Cardiac system. Echocardiographic measurements were carried out in both mouse strains fed either SD or FD diet. In SS-SD mice, we observed left ventricular hypertrophy, as measured by the ratio of heart weight to body weight, as well as a significant increase in left ventricular outflow tract diameter compared to that in AA-SD mice (Figure 1D). FD significantly reduced left ventricular outflow tract diameter in SS mice, without causing changes in the heart weight to body weight ratio (Figure 1D). No major differences were present in AA mice. Heart VCAM-1 and HO-1 expression was significantly higher in SS mice than in AA mice fed the SD (Figure 1D, lower panel). FD supplementation significantly reduced VCAM-1 and HO-1 in SS mice compared to levels in both SS and AA-SD groups (Figure 1D lower panel, *Online Supplementary Figure S1B* for densitometric analysis). No major differences were observed in ET-1 expression in either AA or SS mouse strains (Figure 1D, see also *Online Supplementary Figure S1B* for densitometric analysis).

These data suggest that in SS mice, FD reduces biochemical markers of vascular/oxidant damage and decreases evidence of ventricular loading.

ω-3 polyunsaturated fatty acids reduce pulmonary vascular permeability and endothelin-1 expression in mice with sickle cell disease

Abnormal vascular activation plays an important role in pulmonary complications of SCD.[4,19] ω-3 PUFA has previ-

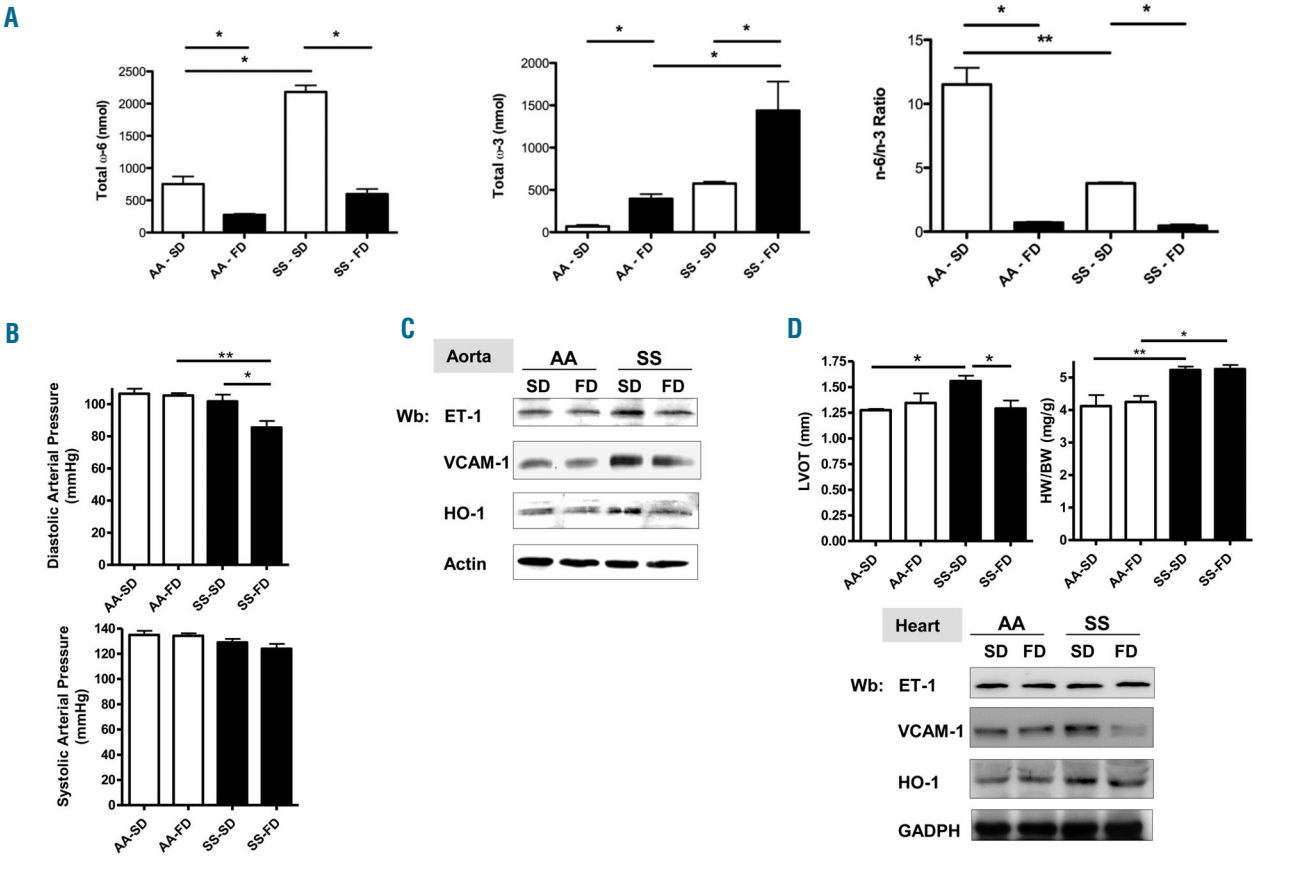

Figure 1. FD modified red cell membrane fatty acid composition and beneficially affects cardiovascular system in sickle cell mice. (A) Total ω-6 fatty acids (n-6) and ω-3 fatty acid/ ω-6 fatty acid ratio (n3/n6 ratio) red cell membrane content as determined by mass spectroscopy in AA and SS mice under a soy-diet (SD) or fish-oil diet (FD). (B) Measurements of diastolic and systolic blood pressure (upper panel) in AA and SS mice under a SD or FD. (C) Immunoblot analysis with specific antibodies against endothelin-1 (ET-1), vascular adhesion molecule-1 (VCAM-1) and heme oxygenase-1 (HO-1) of isolated aortas from AA and SS mice under a SD or FD. One representative gel from six with similar results is presented. Densitometric analysis of anti- ET-1, VCAM-1 and HO-1 immunoblots is shown in *Online Supplementary Figure S1A*. (D) Upper panel. Left ventricular outflow tract (LVOT) diameter and left ventricular hypertrophy expressed as heart weight/body weight (HW/BW[61]) in AA and SS mice under a SD or FD. Lower panel. Immunoblot analysis with specific antibodies against ET-1, VCAM-1, and HO-1 of hearts from AA and SS mice under a SD or FD. One representative gel from six with similar results is presented. Densitometric analysis of immunoblots is shown in *Online Supplementary Figure S1B.*

ously been shown to be protective in several models of lung injury.[31,32] We evaluated pulmonary vascular leakage by measuring protein content and leukocyte counts in BAL fluid from AA and SS mice. As shown in Figure 2A, SS mice fed the SD had higher BAL protein and leukocyte levels compared to healthy mice, indicating accumulation of proteins and inflammatory cells in the alveolar space. FD significantly reduced both the leukocyte and protein content in the BAL fluid of the SS mice, suggesting an amelioration of vascular permeability compared to that in animals fed the SD (Figure 2A).

Since ET-1 plays a key role in clearance of alveolar fluid, local inflammatory response[33] and in SCD vasculopathy,[28,34] we evaluated the expression of ET-1 in lungs from SS and AA mice. Pulmonary ET-1 expression at both molecular and protein levels was significantly increased in SS-SD mice compared to that in AA-SD (Figure 2B, *Online Supplementary Figure S2A* for densitometric analysis). FD significantly reduced lung ET-1 expression in SS mice (Figure 2B, *Online Supplementary Figures S2A and S3*), in agreement with the observed improvement of pulmonary vascular leakage (Figure 2A). VCAM-1 levels were similar in both AA and SS mice, without modulation by ω-3 PUFA supplementation (Figure 2B, *Online Supplementary Figure S2A*). The increased pulmonary inflammatory state was associated with higher expression of HO-1 in SS mice than in AA mice, without significant changes in FD-treated groups (Figure 2B, *Online Supplementary Figure S2B*). These data suggest that ω-3 PUFA supplementation significantly reduces lung ET-1 expression, thereby resolving

Table 1. Hematologic parameters in wild-type (AA) and sickle cell mice (SS) treated with ω−3 fatty acid supplementation.

	AA-SD (n=12)	AA-FD (n=12)	SS-SD (n=12)	SS-FD (n=14)
Hematocrit (%)	46.6±1.5	47.3±0.7	37.3±3.3°	38.2±1.7
Hemoglobin (g/dL)	13.2±0.2	13.6±0.3	8.3±0.3°	8.7±0.1
MCV (fL)	38.4±0.4	38.6±0.4	51.4±1.5°	55.1±2.33*
MCH (g/dL)	12.3±0.3	12.2±0.5	12.2±0.2	12.2±0.6
CHCM (g/dL)	24.8±0.2	24.1±0.3	25.8±0.2°	23.9±0.2*
HDW (g/dL)	2.87.±0.05	3.01±0.02	4.98±0.09°	4.46±0.1
Reticulocytes (%)	8.67±1.0	9.0±0.7	42.1±12°	40±8.69
Neutrophils (cells/ μL)	961±229	682±120*	6241±1421°	1520±371*

*AA: HbA homozygous control mice or wild-type mice; SS: HbS homozygous mice or sickle cell mice; SD: soy-diet; FD: fish-oil diet; MCV: mean corpuscular volume; MCH: mean corpuscular hemoglobin; CHCM: cell hemoglobin concentration; HDW: heterogeneity of red cell distribution; *P<0.002 compared to untreated mice; °P< 0.005 compared to AA mice.*

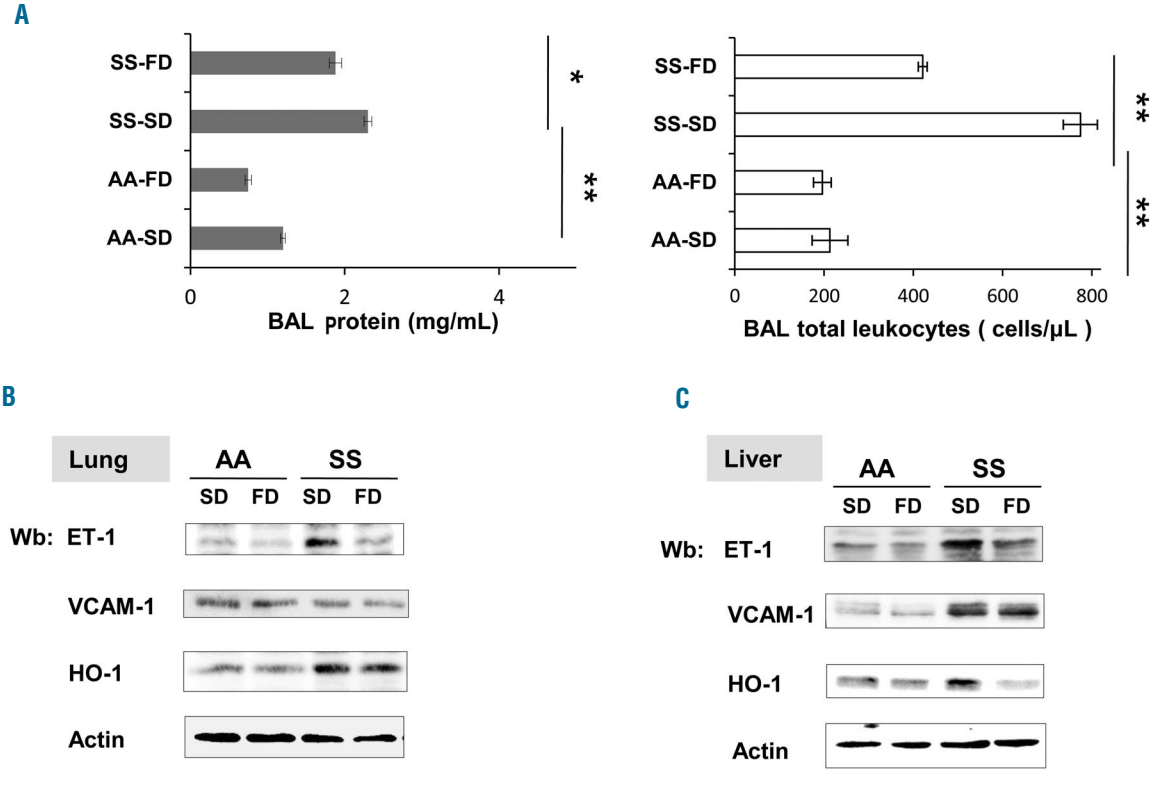

Figure 2. FD ameliorates vascular dysfunction in lung and liver from SS mice. (A) Left panel. Bronchoalveolar (BAL) fluid protein content from AA and SS mice under a soy-diet (SD) or fish-oil diet (FD). Right panel. BAL fluid leukocyte content from AA and SS mice under a SD or FD. (B) Immunoblot analysis with specific antibodies against endothelin-1 (ET-1); vascular adhesion molecule-1 (VCAM-1) and heme-oxygenase-1 (HO-1) of lungs from AA and SS mice under a SD or FD. One representative gel from six with similar results is presented. Densitometric analysis of ET-1, VCAM-1 and HO-1 immunoblots is shown in *Online Supplementary Figure S2A*. (C) Immunoblot analysis with specific antibodies against ET-1, VCAM-1, and HO-1 of livers from AA and SS mice under a SD or FD. One representative gel from six with similar results is presented. Densitometric analysis of ET-1, VCAM-1 and HO-1 immunoblots is shown in *Online Supplementary Figure S2B*.

pulmonary vascular permeability and local inflammation in SCD mice.

ω-3 polyunsaturated fatty acids modulate hepatic inflammation and endothelin-1 expression in mice with sickle cell disease

Studies in models of liver injury have shown an important role of ET-1 on hepatic microvasculature, specifically related to local ischemic/reperfusion injury and inflammatory response.[35,36] Although the liver is not a target organ for SCD, we have previously demonstrated that its functional anatomy, its high metabolic rate and the fine regulation of its microcirculation make the liver an interesting window-organ to explore the pathogenesis of SCD vasculopathy and the effects of new therapeutic tools.[23] Here, we found increased inflammatory cell infiltrates in the liver portal space of SS mice compared to AA mice fed SD (*data not shown*). This was associated with increased expression of ET-1 at both the molecular and protein levels in livers from SS mice (Figure 2C, see also *Online Supplementary Figure S2B* for densitometric analysis and *Online Supplementary Figure S3* for molecular analysis), suggesting a role of ET-1 as both a pro-inflammatory and a potent vasoconstrictor cytokine in the portal vascular system. The levels of VCAM-1 were significantly higher in livers from SS mice than AA mice, which argues for the presence of abnormal vascular activation and local inflammation.[37] This is in agreement with the increased expression of HO-1 as a vaso-protective anti-oxidant.[16,38] FD significantly reduced hepatic expression of ET-1 and HO-1 in SS mice compared to SS-SD mice, but it did not affect expression of VCAM-1 in the liver (Figure 2C, *Online Supplementary Figure S2B*).

Hypoxia/reoxygenation stress mimics acute sickle cell-related lung and liver damage

To evaluate the impact of FD on acute sickle cell-related events, we developed a model of acute VOC based on the exposure of mice to H/R stress.[19,23,28] The H/R conditions were chosen based on previous models of acute VOC with related tissue injury and preliminary experiments to identify the time course of H/R that would recapitulate sickle cell acute organ damage in the present mouse model of SCD.[19,23,28] We selected an experimental protocol of H/R in which AA and SS mice were exposed to hypoxia (8% oxygen) for 10 h followed by 3 h of re-oxygenation (21% oxygen, room air).[19,23,28] In SS mice, H/R induced significant reductions in hematocrit and hemoglobin and a marked increase in hemoglobin distribution width, an index of the amount of dense red cells[39] (Figure 3A,B). In H/R mice fed the SD we observed a significant increase in neutrophil count in both AA (SD: 257±23.2%; n=6) and SS mice (176.8±12%; n=6) compared to counts in normoxic mice, indicating a sustained systemic inflammatory response to H/R stress (Figure 3C). No major changes were observed in reticulocyte count comparing SS mice subjected to H/R stress or normoxic conditions (*data not shown*).

Histological analysis revealed that H/R stress induced a severe sickle cell-related tissue injury in both the lungs and livers of SS mice (Table 2; Figures 4 and 5). In the lung, H/R induced inflammatory cell infiltration, as well as bronchial mucus secretion and thrombi in 80% of the SS mice (Table 2). In AA mice, H/R induced modest inflammatory cell infiltration with mucus production, but without thrombi formation (Table 2). Livers from SS mice exposed to H/R demonstrated severe hepatic injury characterized by the loss of hepatic architecture, coagulative necrosis, inflammatory cell infiltrates and thrombi (Table 2). Livers from AA mice exposed to H/R demonstrated a modest inflammatory cell infiltrate with mild liver damage (Table 2).

ω-3 polyunsaturated fatty acids prevent hypoxia/reoxygenation-induced formation of dense red cells and neutrophilic response

In SS mice, FD: (i) significantly mitigated the H/R-induced reductions in hematocrit and hemoglobin Hb levels; and (ii) significantly reduced the fraction of H/R-generated dense red cells, as supported by the decrease in high distribution width of red cells in these animals compared with SS mice (Figure 3A,B). In addition, we observed a significant reduction in the H/R-induced increased neutrophil count in both AA-FD (41.9±3.7%; n=6) and SS-FD (46.6%±23%; n=6) mice compared to the SD groups of mice (Figure 3C). These findings suggest that ω-3 PUFA supplementation causes a shift towards an anti-inflammatory phenotype in SS mice during acute VOC.

Hypoxia/reoxygenation-induced sickle cell lung injury is attenuated by ω-3 polyunsaturated fatty acids via the endothelin-1 pathway

The lungs of SS-FD mice exposed to H/R stress showed reduced inflammatory cell infiltrates (Figure 4B, Table 2), no mucus filling the bronchi, and fewer thrombotic events (Figure 4D, Table 2) compared to those of SS-SD mice (Table 2). Both the protein content and leukocyte counts of BAL fluid were significantly reduced in SS-FD mice compared to SS-SD animals (Figure 4E). A reduction in BAL fluid protein content was also observed in AA-FD mice exposed to H/R stress (Figure 4E). These findings indicate a protective role of ω-3 PUFA against the H/R-induced pulmonary vascular permeability and local inflammatory cellular response, suggesting a possible modulation of the H/R-induced ET-1 pathway.[28]

In SS mice, FD promoted a significant reduction in H/R-induced ET-1 molecular and protein expression compared to levels in SS-SD mice (Figure 4F, see also *Online Supplementary Figure S4A,B* for densitometric analysis), which was paralleled by a decrease in endothelin-1B receptor (ETBR) expression (*Online Supplementary Figure S5A*). The ability of FD to blunt the cytokine storm in H/R stress was also supported by significant reductions in interleukin-1β and interleukin-10 expression in the lungs of SS-FD mice compared to SS-SD ones (*Online Supplementary Figure S5B*). VCAM-1 expression was increased in H/R SS mice compared with AA mice, with no significant differences between FD- and SD-fed SS mice (Figure 4F, see also *Online Supplementary Figure S4B* for densitometric analysis). The absence of effects of FD on H/R-induced VCAM-1 lung expression in SS mice is not surprising given that H/R stress promotes a redistribution of extracellular VCAM-1 towards the alveolar compartment, as shown in asthma models.[40] This is also supported by the significant down-regulation of lung VCAM-1 gene expression in SS-FD and AA-FD mice compared to SD groups (*Online Supplementary Figure S4A*). Thus, VCAM-1 lung expression reflects only one of the functional components of VCAM-1 involved in H/R lung injury. H/R induced a significant up-regulation of HO-1 in SS mice compared to AA mice, which was prevented in SS-

FD mice (Figure 4F, *Online Supplementary Figure S4B*). These data suggest that FD efficiently protects SS mice from acute H/R lung injury through the reduction of ET-1 expression and the modulation of the inflammatory response, as supported by the reduction in inflammatory cell infiltrates, BAL fluid leukocyte content, and the decreased expression of HO-1.

ω-3 polyunsaturated fatty acids blunt the hypoxia/reoxygenation-induced inflammatory response and decrease vascular activation in the livers of sickle cell mice

The histological analysis of livers from SCD mice exposed to H/R stress showed that FD markedly reduced inflammatory cellular infiltrates and thrombi formation compared to the SD (Figure 5B,D; Table 2). This was in agreement with a reduced pathologic severity score in H/R-exposed SS-FD mice compared with SS-SD mice (Table 2). Serum levels of alananine and aspartate transaminases were significantly lower in both AA-FD and SS-FD mice than in the groups fed the SD (*Online Supplementary Table S3*). No significant changes in liver ET-1 expression were observed in SS-SD mice compared to SS-FD mice (Figure 5E). We found a marked increase in VCAM-1 expression in SS mice, compared to AA mice, in response to H/R stress (Figure 5E, see also *Online Supplementary Figure S6A* for densitometric analysis). FD reduced the H/R-related VCAM-1 up-regulation compared to that in SS-SD mice (Figure 5). HO-1 expression in response to H/R was higher in livers of SS mice than in AA mice, but it was unaffected by ω-3 PUFA supplementation (SS-FD and AA-FD; Figure 5). Interestingly, HO-1 mRNA levels were down-regulated in SS-FD mice compared to SS-SD mice (*Online Supplementary Figure S6B*). Since HO-1 also

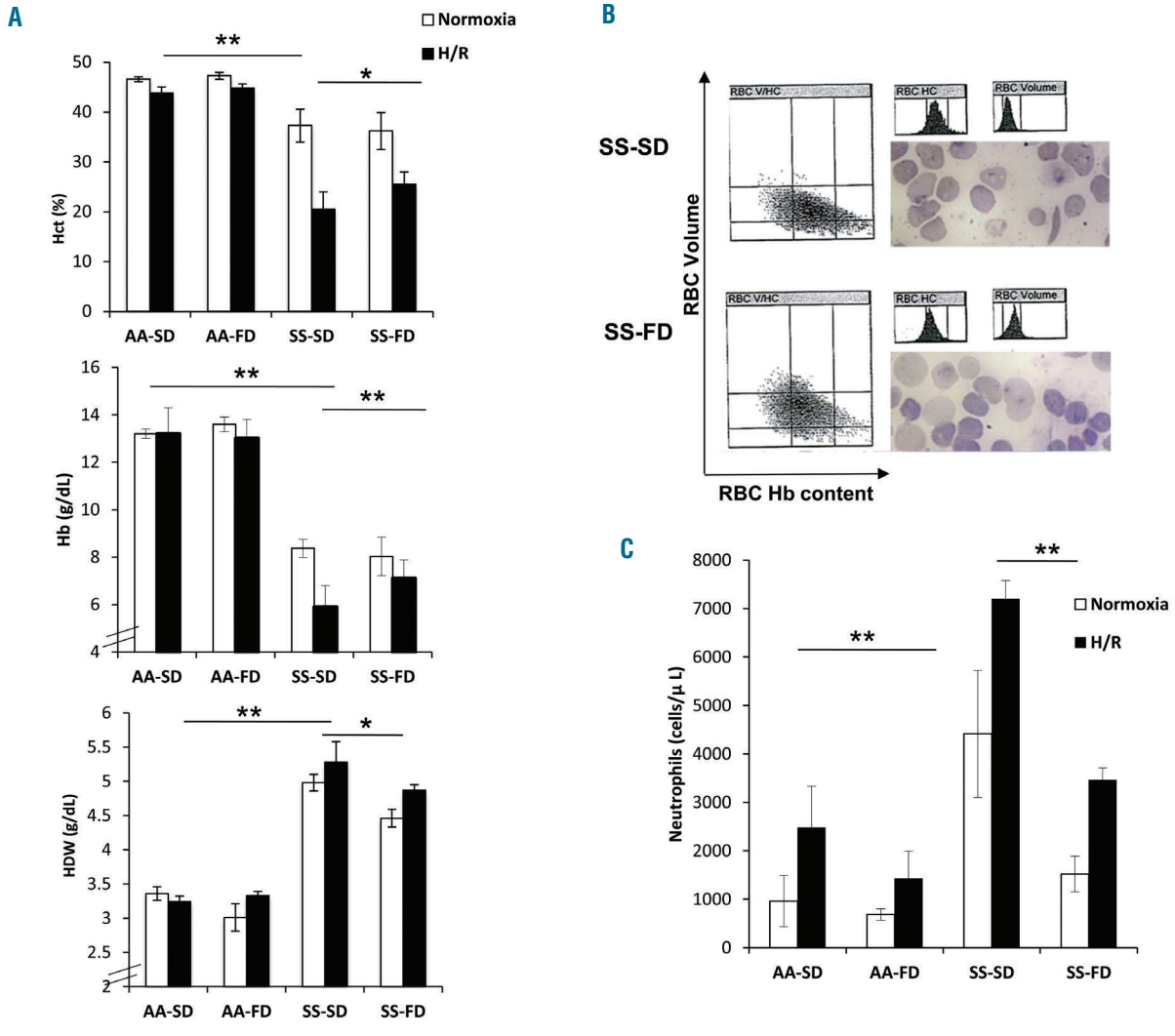

Figure 3. FD prevents H/R-induced dense cell formation and increased neutrophil counts in SS mice. (A) Hematocrit (Hct), hemoglobin (Hb), and red cell distribution width (HDW) of AA and SS mice under a soy-diet (SD) or fish-oil diet (FD) under normoxia (white bars) and exposed to hypoxia (black bars) (8% oxygen; 10 h) followed by reoxygenation (21% oxygen; 3 h) (H/R). (B) Red cell distribution histograms generated for erythrocyte cell volume (RBC Volume) and cell hemoglobin concentration (RBC-HC). Red cell morphology is shown for each condition. (C) Neutrophil counts in AA and SS mice treated as in (A) under normoxia (white bars) and exposed to hypoxia (black bars) (8% oxygen; 10 h) followed by reoxygenation (21% oxygen; 3 h) (H/R). All statistical data are presented as means ± standard deviation (n=6; *P<0.005; **P<0.002).

Table 2. Effects of ω−3 supplementation on lung and liver pathology of wild-type (AA) and sickle cell (SS) mice under normoxia and exposed to hypoxia/reoxygenation stress

	AA-SD		AA -FD		SS-SD		SS-FD	
	Normoxia	H/R	Normoxia	H/R	Normoxia	H/R	Normoxia	H/R
Lung	(n=3)	(n=6)	(n=3)	(n=5)	(n=3)	(n=5)	(n=3)	(n=5)
Inflammatory cell infiltrates	+ (1/3)	+ (2/6)	+ (1/3)	+ (2/5)	+(2/3)	+ (2/5) ++ (3/5)	+(2/3)	+ (3/5)
Edema	0	0	0	0	0	0	0	0
Mucus	0	+ (3/6)	0	+ (1/5)	0	+ (1/5)	0	0
Thrombi	-	-	-	-	-	+ (4/5)	-	+(2/5)
Liver	(n=3)	(n=6)	(n=3)	(n=5)	(n=3)	(n=5)	(n=3)	(n=6)
Inflammatory cell infiltrates	0	+ (3/6)	+(1/3)	+ (1/5)	+ (1/3), ++(1/3); +++ (1/3)	+ (1/5) ++ (4/5)	+(2/3) ++(1/3)	+ (3/6) ++(1/6)
Thrombi	-	-	-	-	-	+ (2/5)	-	-
Score	2-2-0	2-2-1-0-0-0	1-1-0	1-1-0-0-0	3-3-3	3-3-3-4-4	2-3-3	2-2-3-3-4-4-

SD: soy-diet; FD: fish-oil diet; H/R: hypoxia/reoxygenation. Lungs:Thrombi: 0: no thrombi, + presence of thrombus per field at the magnification x250. Mucus: 0: no mucus, +: mucus filling < 25 % of the area of the bronchus circumference; ++ mucus filling 25-50% of the area of the bronchus circumference; +++: 50-100% of the area of the bronchus circumference at magnification x400. Inflammatory cell infiltrate: + 1-10 cells per field at magnification of x250; ++: 10-50 cells per field at magnification of x250; +++: > 50 cells per field at magnification x250 Liver: + : 1-10 cells per field at magnification x 400; ++: 10-50 cells per field at magnification x 400; +++: >50 cells per field at magnification x 400; Liver score; 0: no hepatocellular damage. 1: mild injury characterized by cytoplasmic vacuolization and focal nuclear pyknosis. 2: moderate injury with dilated sinusoids, cytosolic vacuolization, and blurring of intercellular borders. 3: moderate to severe injury with coagulative necrosis, abundant sinusoidal dilatation, red blood extravasation into hepatic chords, hypereosinophilia and migration of neutrophils. 4: severe necrosis with loss of hepatic architecture, disintegration of hepatic chords, hemorrhage and neutrophil infiltration.

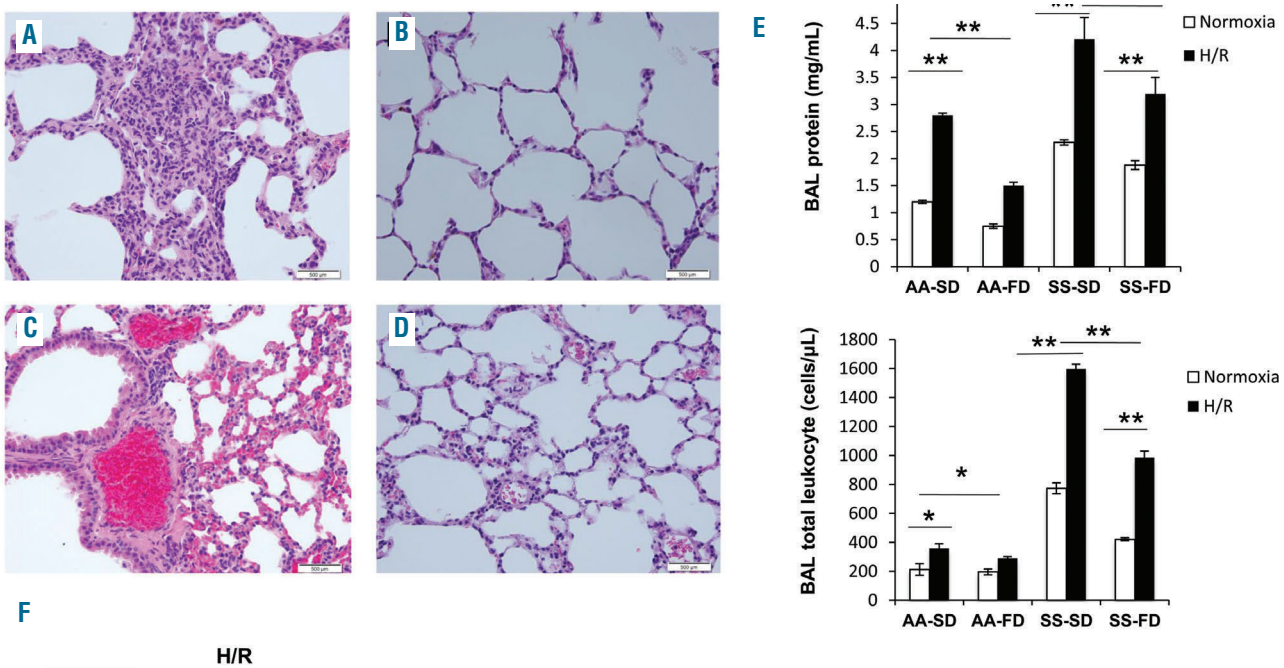

Figure 4. FD reduces H/R-induced lung damage and prevents H/R-induced ET-1 up-regulation. (A-D) Hematoxylin and eosin-stained sections of lung tissue at 400x magnification from SS mice under a SD (A and C) or supplemented with FD (B and D) exposed to hypoxia (8% oxygen; 10 h) followed by reoxygenation (21% oxygen; 3 h) (H/R). Lungs from SS mice given a FD have less inflammatory cellular infiltrate (B) and thrombi (D) than SS mice not fed FD (A and C). (E) Upper panel. BAL protein content from AA and SS mice treated as in (A-E). Lower panel. BAL leukocyte content from AA and SS mice treated as in (A-E). White bars show data from mice under normoxia and black bars show data from mice under H/R. (F) Immunoblot analysis with specific antibodies against ET-1, VCAM-1, and HO-1 of lung from AA and SS mice treated as in (A-E). One representative gel from six with similar results is presented. Densitometric analysis of ET-1, VCAM-1 and HO-1 immunoblots is shown in *Online Supplementary Figure S4B*.

plays a role as a heat shock protein (HSP32) in other animal models, such as the rat,[41] we evaluated the hepatic expression of HSP27, which is known to be important in H/R liver injury.[23,42] FD attenuated the H/R-induced HSP27 expression in SS mice compared to SS-SD animals (Figure 5E, *Online Supplementary Figure S6B*), supporting the anti-inflammatory effects of ω-3 PUFA following H/R stress. These findings align with data from other models of H/R liver injury[35,43] and confirm that VCAM-1 mediates adhesion events in the hepatic microvasculature and contributes to amplified inflammatory liver disease in SCD mice. In livers from SS mice, FD prevented vascular activation and reduced inflammation, improving endothelial dysfunction and reducing organ damage.

Vascular protective effects of ω-3 polyunsaturated fatty acids during acute vaso-occlusive crises in sickle cell mice

We isolated aortic tissue from AA and SS mice exposed to H/R stress. As shown in Figure 6A, in SS mice, FD reduced H/R-induced ET-1 and VCAM-1 expression compared to SS-SD. This finding was associated with reduced expression of acute inflammatory response-related proteins such as HO-1, SOD-1 and peroxiredoxin-2 (Prx2) (Figure 6A, see also *Online Supplementary Figure S7* for densitometric analysis). These effects were also evident in AA-FD mice exposed to H/R compared to AA-SD mice (Figure 6A). These results support the hypothesis that FD attenuates endothelial dysfunction in SCD by reducing vascular activation, vasoconstriction, inflammation and oxidative stress.

Discussion

The effects of ω-3 fatty acid supplementation have been widely studied in cardiovascular diseases and in other disorders characterized by acute or chronic vascular damage and an amplified inflammatory response.[44,45] In SCD, vasculopathy, inflammation and intravascular oxidative stress are crucial in the pathogenesis of acute and chronic clinical complications. Recent reports on the beneficial effects of ω-3 fatty acid supplementation on the human hematologic phenotype of SCD suggest a possible therapeutic effect of ω-3 fatty acids in SCD.[12-14] The present work provides evidence for several relevant mechanisms underlying this potential benefit. We propose that the beneficial role of ω-3 PUFA on SCD vascular dysfunction might be exerted: (i) directly through the reduction of ET-1 expression, which is involved in adaptive inflammation, expression of adhesion molecules such as VCAM-1, and neutrophil chemotaxis;[46] and (ii) indirectly through reduced inflammation and oxidative stress. Importantly, the ω-3 PUFA supplementation in our study is comparable to that achieved in recent human studies.[47]

In SS mice, ω-3 PUFA consistently modulate ET-1, a potent vasoconstrictor, in agreement with recent meta-analyses demonstrating a significant improvement in flow-mediated dilation in subjects supplemented with FD.[45,48] This is of particular interest in the context of SCD, in which ET-1 has been implicated in severe clinical complications of SCD.[28,49] The positive impact of FD on ET-1 is not limited to the aorta but also involves the pulmonary vascular bed, where we observed a decrease in the abnor-

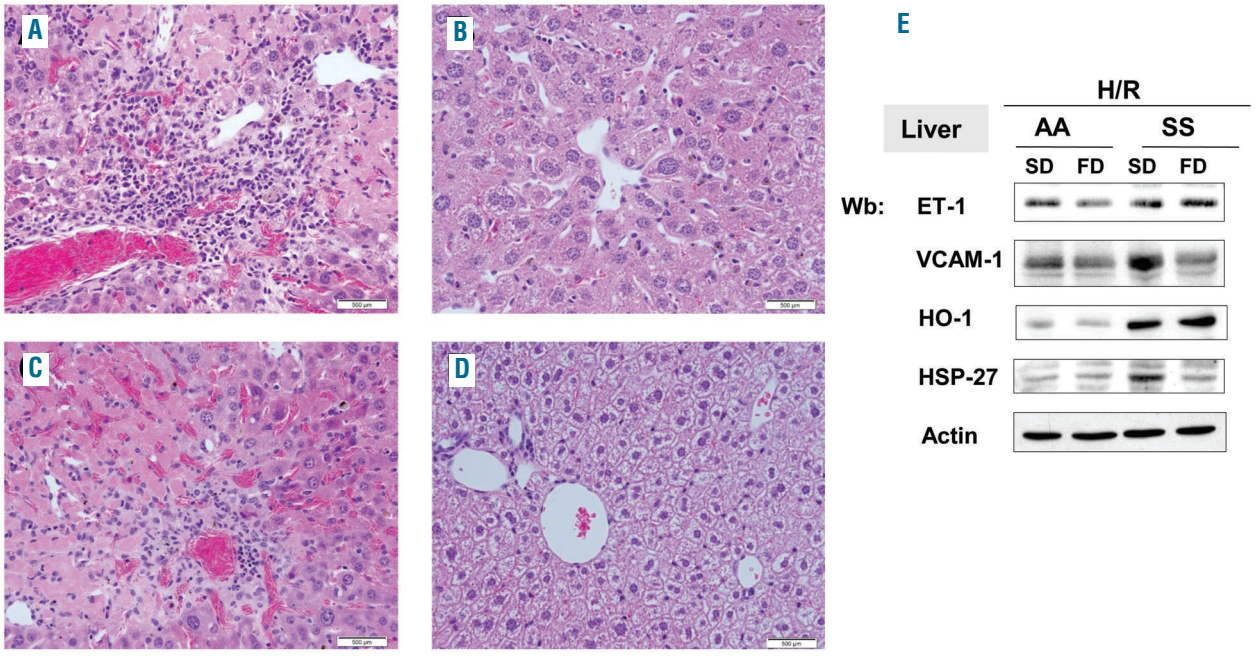

Figure 5. FD reduces H/R-induced liver damage and vascular activation. (A-D) Hematoxylin and eosin-stained sections of liver tissue at 400x magnification from SS mice under a SD (A and C) or FD supplementation (B and D) exposed to H/R. Livers from mice given FD have less inflammatory cellular infiltrate (B) and thrombi (D) than livers from SS mice fed a SD. The infiltrate shown best in (B) is composed mostly of lymphocytes. Scattered hemosiderin deposits and areas of necrosis are also present. (E) Immunoblot analysis with specific antibodies against ET-1, VCAM-1, HO-1, and heat shock protein-27 (HSP27) of liver from AA and SS mice treated as in (A-D). One representative gel from six with similar results is presented. Densitometric analysis of ET-1, VCAM-1, HO-1 and HSP27 immunoblots is shown in *Online Supplementary Figure S5.*

mal pulmonary vascular leakage and a decrease in the accumulation of protein and inflammatory cells in the alveolar space (Figure 2A,B).

To explore the critical balance between vascular tone and endothelial activation in SCD, we used a H/R stress model, which mimics the acute organ damage observed in SCD VOC (Figures 4 and 5; Table 2).[19,50] Compared to SD, FD significantly reduced H/R-related ET-1 expression in the aorta (Figure 6). This was accompanied by a significant reduction in both ET-1 and ET-1BR expression in lungs from SS-FD mice (Fig. 4F, *Online Supplementary 5SA*), suggesting that the beneficial effects of FD treatment on H/R-induced pulmonary vascular permeability might be related to the combination of both ligand and target reduction in the ET-1 system.[33,51] No significant changes in ET-1 expression were observed between livers from H/R-exposed SS-FD and SS-SD mice (Figure 5), most likely because of the peculiar organization of liver vasculature or because of the organ's sensitivity in the context of H/R stress used in the present study.

We then evaluated the effects of FD on VCAM-1 expression, since elevated VCAM-1 has been associated with a severe SCD phenotype and increased risk of early death.[49,52,53] In conditions of normoxia, FD significantly reduced VCAM-1 expression in aortas and hearts of SS mice compared to SS-SD mice (Figure 1B,C). This was associated with improved left ventricular outflow tract dimensions, suggesting a possible contribution of FD in delaying the progression of SCD cardiovascular disease.[54-56] We demonstrated a synergistic effect of ω-3 PUFA on both ET-1-mediated endothelial dysfunction and VCAM-1-mediated endothelial activation on aortas following H/R (Figure 6A). Notably, FD also significantly reduced VCAM-1 expression in livers of SS mice exposed to H/R stress compared to the expression in SS-SD mice (Figure 5). These data support a multimodal therapeutic action of FD on both arterial and microvascular sites, preventing vascular activation and possible amplification of local pro-inflammatory events during acute VOC.

HO-1 is a key cytoprotector interfacing between vascular dysfunction and oxidative stress in SCD.[23,30] Under normoxia, ω-3 PUFA significantly reduced HO-1 expression in the aorta, heart and liver of SS mice (Figure 1B and 2C). Interestingly, FD did not affect lung HO-1 expression in SS mice, even though a pulmonary anti-inflammatory effect for FD supplementation was observed (i.e. reduced neutrophil counts in BAL fluid and reduced pulmonary cell infiltrates) (Figures 2 and 4). This suggests that, under steady state conditions, the anti-inflammatory effects of FD on lungs of SCD mice may be more related to down-regulation of ET-1. During acute VOC mimicked by H/R stress, FD reduced HO-1 expression, indicating a stronger role of ω-3 PUFA in acute events involving the lung than in the steady state condition. This is in agreement with recent studies on the protective role of ω-3-derived pro-resolving mediators in models of acute lung injury.[57,58] The pro-resolving effects of FD supplementation during H/R stress were also evident in aortas of SS-FD mice, in which we observed a marked reduction in H/R-induced HO-1 expression and prevention of the H/R-induced expression of anti-oxidant systems such as SOD-1 and Prx2 (Figure 6A).

In livers from SCD mice exposed to H/R stress, FD was associated with HO-1 mRNA down-regulation and a marked decrease in the expression of HSP27, which is a crucial liver cytoprotector against H/R stress.[42] This finding supports the anti-inflammatory activity of FD in reducing liver injury during H/R stress in SCD mice.

Finally, we observed a reduction in dense red cell formation in SS-FD mice exposed to H/R compared to SS-SD mice, which may contribute to the multimodal action of

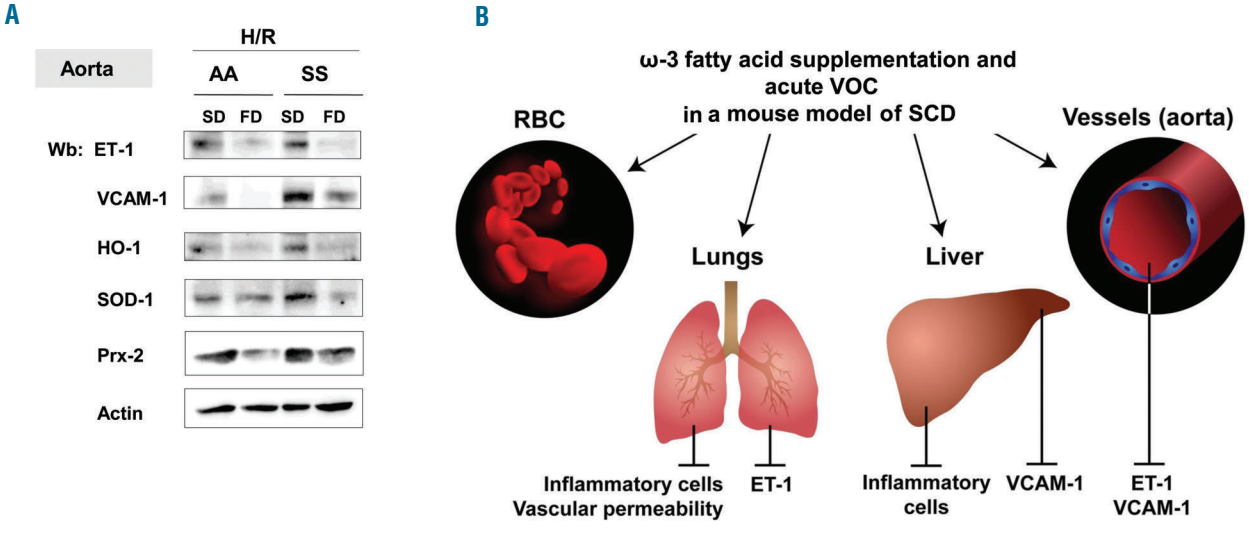

Figure 6. FD prevents H/R-induced ET-1 expression, vascular activation and modulates anti-oxidant systems. (A) Immunoblot analysis with specific antibodies against ET-1, VCAM-1, HO-1, SOD-1, and peroxiredoxin-2 (Prx-2) of isolated aortas from AA and SS under a SD or FD and exposed to H/R. One representative gel from six with similar results is presented. Densitometric analysis of ET-1, VCAM-1 and HO-1 immunoblots is shown in *Online Supplementary Figure S7*. (B) Schematic diagram of effects of ω-3 fatty supplementation on acute vaso-occlusive crises (VOC) in a mouse model of SCD. ω-3 fatty supplementation (i) beneficially affects sickle red cell membrane composition, with a shift towards an anti-inflammatory substrate (ii) has potent anti-inflammatory action in target organs for SCD such as lung and liver; (iii) improves vascular dysfunction through either a reduction of ET-1 (lung) or VCAM-1 (liver) or the synergizing decrease of both molecules in aorta.

ω-3 PUFA on SCD vasculopathy. Changes in membrane lipid composition might affect red cell deformability, as recently shown in a mouse model supplemented with ω-3 PUFA (docosahexaenoic acid),[59] as well as variations in pro-inflammatory arachidonic acid incorporated into sickle erythrocytes.[60] These red cell changes may play a role in reducing the systemic pro-inflammatory environment, which contributes to the pathogenesis of vasculopathy in SCD.[6]

In summary, we propose that ω-3 PUFA may limit sickle cell-related acute damage by: (i) shifting the sickle red cell membrane towards an anti-inflammatory substrate; (ii) exerting local anti-inflammatory effects in target organs for SCD (lung, liver); (iii) improving vascular dysfunction through the reduction of VCAM-1 or ET-1 or the synergistic decrease of both molecules. This functional model supports the preliminary results of a clinical trial with ω-3 PUFA supplementation in SCD patients, which showed a reduction in the rate and severity of painful crises.[13] Taken together, our data add significant new elements to the mechanism of action of ω-3 PUFA in SCD, and generate a rationale for future studies focused on the bioactive metabolites of ω-3 PUFA.

Funding

This work was supported by PRIN (LDF: 201228PNX83_003) and FUR_UNIVR (LDF). The authors would like to thank Amy Pan for her help in isolating RBC fatty acids for membrane analysis. The authors would also like to thank Marykate O'Malley and Kristin Johnson for their help with the figures.

Authorship and Disclosures

Information on authorship, contributions, and financial & other disclosures was provided by the authors and is available with the online version of this article at www.haematologica.org.

References

1. Bunn HF. Pathogenesis and treatment of sickle cell disease. N Engl J Med. 1997;337(11):762-769.
2. Sparkenbaugh E, Pawlinski R. Interplay between coagulation and vascular inflammation in sickle cell disease. Br J Haematol. 2013;162(1):3-14.
3. De Franceschi L, Cappellini MD, Olivieri O. Thrombosis and sickle cell disease. Semin Thromb Hemost. 2011;37(3):226-236.
4. Hebbel RP, Vercellotti G, Nath KA. A systems biology consideration of the vasculopathy of sickle cell anemia: the need for multi-modality chemo-prophylaxsis. Cardiovasc Hematol Disord Drug Targets. 2009;9(4):271-292.
5. Massaro M, Scoditti E, Carluccio MA, De Caterina R. Basic mechanisms behind the effects of n-3 fatty acids on cardiovascular disease. Prostaglandins Leukot Essent Fatty Acids. 2008;79(3-5):109-115.
6. Calder PC. Omega-3 fatty acids and inflammatory processes. Nutrients. 2010;2(3):355-374.
7. Rangel-Huerta OD, Aguilera CM, Mesa MD, Gil A. Omega-3 long-chain polyunsaturated fatty acids supplementation on inflammatory biomakers: a systematic review of randomised clinical trials. Br J Nutr. 2012;107 (Suppl 2):S159-170.
8. Wachira JK, Larson MK, Harris WS. n-3 Fatty acids affect haemostasis but do not increase the risk of bleeding: clinical observations and mechanistic insights. Br J Nutr. 2014;111(9):1652-1662.
9. Chen J, Shearer GC, Chen Q, et al. Omega-3 fatty acids prevent pressure overload-induced cardiac fibrosis through activation of cyclic GMP/protein kinase G signaling in cardiac fibroblasts. Circulation. 2011;123(6):584-593.
10. Ren H, Ghebremeskel K, Okpala I, et al. Abnormality of erythrocyte membrane n-3 long chain polyunsaturated fatty acids in sickle cell haemoglobin C (HbSC) disease is not as remarkable as in sickle cell anaemia (HbSS). Prostaglandins Leukot Essent Fatty Acids. 2006;74(1):1-6.
11. Ren H, Obike I, Okpala I, et al. Steady-state haemoglobin level in sickle cell anaemia increases with an increase in erythrocyte membrane n-3 fatty acids. Prostaglandins Leukot Essent Fatty Acids. 2005;72(6):415-421.
12. Okpala I, Ibegbulam O, Duru A, et al. Pilot study of omega-3 fatty acid supplements in sickle cell disease. APMIS. 2011;119(7):442-448.
13. Daak AA, Ghebremeskel K, Hassan Z, et al. Effect of omega-3 (n-3) fatty acid supplementation in patients with sickle cell anemia: randomized, double-blind, placebo-controlled trial. Am J Clin Nutr. 2013;97(1):37-44.
14. Tomer A, Kasey S, Connor WE, et al. Reduction of pain episodes and prothrombotic activity in sickle cell disease by dietary n-3 fatty acids. Thromb Haemost. 2001; 85(6):966-974.
15. Simopoulos AP. Omega-3 fatty acids in health and disease and in growth and development. Am J Clin Nutr. 1991;54(3):438-463.
16. Vinchi F, De Franceschi L, Ghigo A, et al. Hemopexin therapy improves cardiovascular function by preventing heme-induced endothelial toxicity in mouse models of hemolytic diseases. Circulation. 2013;127(12):1317-1329.
17. Wu LC, Sun CW, Ryan TM, et al. Correction of sickle cell disease by homologous recombination in embryonic stem cells. Blood. 2006;108(4):1183-1188.
18. Reeves PG, Nielsen FH, Fahey GC Jr. AIN-93 purified diets for laboratory rodents: final report of the American Institute of Nutrition ad hoc writing committee on the reformulation of the AIN-76A rodent diet. J Nutr. 1993;123(11):1939-1951.
19. de Franceschi L, Baron A, Scarpa A, et al. Inhaled nitric oxide protects transgenic SAD mice from sickle cell disease-specific lung injury induced by hypoxia/reoxygenation. Blood. 2003;102(3):1087-1096.
20. Stocker JW, De Franceschi L, McNaughton-Smith GA, et al. ICA-17043, a novel Gardos channel blocker, prevents sickled red blood cell dehydration in vitro and in vivo in SAD mice. Blood. 2003;101(6):2412-2418.
21. De Franceschi L, Saadane N, Trudel M, et al. Treatment with oral clotrimazole blocks Ca(2+)-activated K+ transport and reverses erythrocyte dehydration in transgenic SAD mice. A model for therapy of sickle cell disease. J Clin Invest. 1994;93(4):1670-1676.
22. Folch J, Lees M, Sloane Stanley GH. A simple method for the isolation and purification of total lipides from animal tissues. J Biol Chem. 1957;226(1):497-509.
23. Siciliano A, Malpeli G, Platt OS, et al. Abnormal modulation of cell protective systems in response to ischemic/reperfusion injury is important in the development of mouse sickle cell hepatopathy. Haematologica. 2011;96(1):24-32.
24. Andolfo I, Alper SL, De Franceschi L, et al. Multiple clinical forms of dehydrated hereditary stomatocytosis arise from mutations in PIEZO1. Blood. 2013;121(19):3925-3935.
25. De Franceschi L, Platt OS, Malpeli G, et al. Protective effects of phosphodiesterase-4 (PDE-4) inhibition in the early phase of pulmonary arterial hypertension in transgenic sickle cell mice. FASEB J. 2008;22(6):1849-1860.
26. de Franceschi L, Malpeli G, Scarpa A, et al. Protective effects of S-nitrosoalbumin on lung injury induced by hypoxia-reoxygenation in mouse model of sickle cell disease. Am J Physiol Lung Cell Mol Physiol. 2006;291(3):457-465.
27. Kaul DK, Hebbel RP. Hypoxia/reoxygenation causes inflammatory response in transgenic sickle mice but not in normal mice. J Clin Invest. 2000;106(3):411-420.
28. Sabaa N, de Franceschi L, Bonnin P, et al. Endothelin receptor antagonism prevents hypoxia-induced mortality and morbidity in a mouse model of sickle-cell disease. J Clin Invest. 2008;118(5):1924-1933.
29. Osborn L, Hession C, Tizard R, et al. Direct expression cloning of vascular cell adhesion molecule 1, a cytokine-induced endothelial protein that binds to lymphocytes. Cell. 1989;59(6):1203-1211.
30. Belcher JD, Mahaseth H, Welch TE, et al. Heme oxygenase-1 is a modulator of inflammation and vaso-occlusion in transgenic sickle mice. J Clin Invest. 2006;116(3):808-816.
31. Sharma S, Chhibber S, Mohan H, Sharma S. Dietary supplementation with omega-3 polyunsaturated fatty acids ameliorates

acute pneumonia induced by Klebsiella pneumoniae in BALB/c mice. Can J Microbiol. 2013;59(7):503-510.
32. Umar S, Nadadur RD, Li J, et al. Intralipid prevents and rescues fatal pulmonary arterial hypertension and right ventricular failure in rats. Hypertension. 2011;58(3):512-518.
33. Berger MM, Rozendal CS, Schieber C, et al. The effect of endothelin-1 on alveolar fluid clearance and pulmonary edema formation in the rat. Anest Analg. 2009;108(1):225-231.
34. Rybicki AC, Benjamin LJ. Increased levels of endothelin-1 in plasma of sickle cell anemia patients. Blood. 1998;92(7):2594-2596.
35. Kitagawa T, Yokoyama Y, Kokuryo T, Nagino M. Protective effects of branched-chain amino acids on hepatic ischemia-reperfusion-induced liver injury in rats: a direct attenuation of Küpffer cell activation. Am J Physiol Gastrointest Liver Physiol. 2013;304(4):346-355.
36. Shetty S, Lalor PF, Adams DH. Lymphocyte recruitment to the liver: molecular insights into the pathogenesis of liver injury and hepatitis. Toxicology. 2008;254(3):136-146.
37. Volpes R, Van Den Oord JJ, Desmet VJ. Vascular adhesion molecules in acute and chronic liver inflammation. Hepatology. 1992;15(2):269-275.
38. Vercellotti GM, Khan FB, Nguyen J, et al. H-ferritin ferroxidase induces cytoprotective pathways and inhibits microvascular stasis in transgenic sickle mice. Front Pharmacol. 2014;5:79.
39. Billett HH, Fabry ME, Nagel RL. Hemoglobin distribution width: a rapid assessment of dense red cells in the steady state and during painful crisis in sickle cell anemia. J Lab Clin Med. 1988;112(3):339-344.
40. Chihara J, Yamamoto T, Kurachi D, Nakajima S. Soluble ICAM-1 in sputum of patients with bronchial asthma. Lancet. 1994;343(8905):1108.
41. Shibahara S, Muller RM, Taguchi H. Transcriptional control of rat heme oxygenase by heat shock. J Biol Chem. 1987;262(27):12889-12892.
42. Chen SW, Park SW, Kim M, et al. Human heat shock protein 27 overexpressing mice are protected against hepatic ischemia and reperfusion injury. Transplantation. 2009;87 (10):1478-1487.
43. Hafez T, Moussa M, Nesim I, et al. The effect of intraportal prostaglandin E1 on adhesion molecule expression, inflammatory modulator function, and histology in canine hepatic ischemia/reperfusion injury. J Surg Res. 2007;138(1):88-99.
44. De Caterina R. n-3 fatty acids in cardiovascular disease. N Engl J Med. 2011;364(25): 2439-2450.
45. Wang Q, Liang X, Wang L, et al. Effect of omega-3 fatty acids supplementation on endothelial function: a meta-analysis of randomized controlled trials. Atherosclerosis. 2012;221(2):536-543.
46. Sampaio AL, Rae GA, Henriques MG. Participation of endogenous endothelins in delayed eosinophil and neutrophil recruitment in mouse pleurisy. Inflamm Res. 2000;49(4):170-176.
47. Scorletti E, Bhatia L, McCormick KG, et al. Effects of purified eicosapentaenoic and docosahexaenoic acids in non-alcoholic fatty liver disease: results from the *WELCOME study. Hepatology. 2014;60(4):1211-1221.
48. Xin W, Wei W, Li X. Effect of fish oil supplementation on fasting vascular endothelial function in humans: a meta-analysis of randomized controlled trials. PloS One. 2012;7(9):e46028.
49. Hatzipantelis ES, Pana ZD, Gombakis N, et al. Endothelial activation and inflammation biomarkers in children and adolescents with sickle cell disease. Int J Hematol. 2013;98(2):158-163.
50. Belcher JD, Mahaseth H, Welch TE, et al. Critical role of endothelial cell activation in hypoxia-induced vasoocclusion in transgenic sickle mice. Am J Physiol Heart Circ Physiol. 2005;288(6):H2715-2725.
51. Ott J, Hiesgen C, Mayer K. Lipids in critical care medicine. Prostaglandins Leukot Essent Fatty Acids. 2011;85(5):267-273.
52. Kato GJ, Martyr S, Blackwelder WC, et al. Levels of soluble endothelium-derived adhesion molecules in patients with sickle cell disease are associated with pulmonary hypertension, organ dysfunction, and mortality. Br J Haematol. 2005;130(6):943-953.
53. Elmariah H, Garrett ME, De Castro LM, et al. Factors associated with survival in a contemporary adult sickle cell disease cohort. Am J Hematol. 2014;89(5):530-535.
54. Desai AA, Patel AR, Ahmad H, et al. Mechanistic insights and characterization of sickle cell disease-associated cardiomyopathy. Circ Cardiovasc Imaging. 2014;7(3):430-437.
55. Junqueira FP, Fernandes JL, Cunha GM, et al. Right and left ventricular function and myocardial scarring in adult patients with sickle cell disease: a comprehensive magnetic resonance assessment of hepatic and myocardial iron overload. J Cardiovasc Magn Reson. 2013;15:83.
56. Dimitrow PP, Undas A, Wolkow P, Tracz W, Dubiel JS. Enhanced oxidative stress in hypertrophic cardiomyopathy. Pharmacol Rep. 2009;61(3):491-495.
57. Wang Q, Zheng X, Cheng Y, et al. Resolvin D1 stimulates alveolar fluid clearance through alveolar epithelial sodium channel, Na,K-ATPase via ALX/cAMP/PI3K pathway in lipopolysaccharide-induced acute lung injury. J Immunol. 2014;192(8):3765-3777.
58. El Kebir D, Gjorstrup P, Filep JG. Resolvin E1 promotes phagocytosis-induced neutrophil apoptosis and accelerates resolution of pulmonary inflammation. Proc Nat Acad Sci USA. 2012;109(37):14983-14988.
59. Wandersee NJ HM, Maciaszek JL, Larson MC, et al. Dietary supplememntation with Docosahexanoic acid (DHA) improves RBC flexibility and reduces cold hypersensitivity in mice with sickle cell disease. ASH; 2012; 2012:2116.
60. Setty BN, Chen D, Stuart MJ. Sickle red blood cells stimulate endothelial cell production of eicosanoids and diacylglycerol. J Lab Clin Med. 1996;128(3):313-321.
61. Ha T, Li Y, Hua F, Ma J, Gao X, Kelley J, et al. Reduced cardiac hypertrophy in toll-like receptor 4-deficient mice following pressure overload. Cardiovasc Res. 2005;68(2):224-234.